HOLOGRAPHIC LEED: A DIRECT METHOD FOR SURFACE CRYSTALLOGRAPHY

By

John Athanasios Vamvakas

A DISSERTATION SUBMITTED IN
PARTIAL FULFILLMENT OF THE
REQUIREMENTS FOR THE DEGREE OF

DOCTOR OF PHILOSOPHY

IN

PHYSICS

at

The University of Wisconsin-Milwaukee

May 1998

HOLOGRAPHIC LEED: A DIRECT METHOD FOR SURFACE CRYSTALLOGRAPHY

By

John Athanasios Vamvakas

A DISSERTATION SUBMITTED IN

PARTIAL FULFILLMENT OF THE

REQUIREMENTS FOR THE DEGREE OF

DOCTOR OF PHILOSOPHY

IN

PHYSICS

at

The University of Wisconsin-Milwaukee

May 1998

_____

Dilano Kerzaman Saldin   Date

_____

Graduate School Approval   Date

ii

HOLOGRAPHIC LEED: A DIRECT METHOD FOR SURFACE CRYSTALLOGRAPHY

By

John Athanasios Vamvakas

The University of Wisconsin-Milwaukee, 2002
Under the Supervision of Professor Dilano Kerzaman Saldin

ABSTRACT

Since 1960's Low Energy Electron Diffraction (LEED) has been one of the most reliable methods for surface crystallography. It has solved hundreds of structures over the past 20–25 years and continues to be a powerful tool in the hands of crystallographers. Yet, the main disadvantage of the method is the fact that it is very time consuming. The programs that do the multiple scattering calculations can run literally for days! The key part of the method is the initial "guess" of a structure that will be close the one being sought. A wrong guess would lead to huge amounts of wasted time and effort.

We suggest a direct method that can give us a pretty good idea of the structure under determination. We call this method of ours: **Holographic LEED (h-LEED)** because it is based on the ideas of Dennis Gabor, the inventor of holography. The 3D images h-LEED reconstructs from LEED diffraction patterns can be reliably used to initialize LEED thus reducing the annoying computation time as well as the effort required by the crystallographer.

iii

We show that h-LEED produces good images for $p(2 \times 2)$ reconstruction of adsorbed atoms by testing it on two adsorption systems: O/Ni(001) and K/Ni(001). The images were reconstructed from both diffuse LEED patterns from disordered adsorbates and superstructure Bragg spots from ordered adsorbates.

Dilano Kerzaman Saldin   Date

Acknowledgements

In the name of the Holy and Consubstantial and Undivided Trinity.
Thank you my God for giving me the strength to complete this thesis.

UWM and its Physics Department was my first experience as far as the American educational system is concerned. It was Tuesday, August 17, 1988 around 10:30 in the morning, when I was knocking on the door of Donald Beck, the graduate students advisor then. His warm welcoming to the department was the beginning of a great friendship with all the members of it. The next person I met was the Chairman, back then, the late Nicholas Papastamatiou whose great character made me long for the life that I was about to start among my fellow students and my professors. And it was the same friendly environment that welcomed me back after my three-year absence from the department due to my service at the Greek Armed Forces.

It was upon my return to the department that I encountered Dilano Saldin and his work in Surface Physics. His warm, kind behavior along with his profound knowledge and instinct in Physics, convinced me to choose him as my advisor. And I was rewarded for my choice. Over the years we have been working together, at the meetings, at the conferences or during our discussions for the preparation of a new paper, I had the feeling that he created such an environment that the graduate student or the co-worker wanted to give his best towards the common task. Even when the research was going bad, when things looked disappointing, he never lost his sense of humor and never stopped encouraging me to try one more time, to consider something else, always full of new ideas. This seems the proper space for the author to share a joke that Dr. Saldin told during one of the meetings when things were looking bad:

> When Albert Einstein was making the rounds of the speaker's circuit, he usually found himself eagerly longing to get back to his laboratory work. One night

as they were driving to yet another rubber-chicken dinner, Einstein mentioned to his chauffeur (a man who somewhat resembled Einstein in looks and manner) that he was tired of speechmaking. "I have an idea, boss," his chauffeur said. "I've heard you give this speech so many times. I'll bet I could give it for you." Einstein laughed loudly and said, "Why not? Let's do it!"

When they arrived at the dinner, Eistein donned the chauffeur's cap and jacket and sat in the back of the room. The chauffeur gave a beautiful rendition of Einstein's speech and even answered a few questions expertly. Then a supremely pompous professor ask an extremely esoteric question about anti-matter formation, digressing here and there to let everyone in the audience know that he was nobody's fool. Without missing a beat, the chauffeur fixed the professor with a steely stare and said, "Sir, the answer to that question is so simple that I will let my chauffeur, who is sitting in the back, answer it for me."

I would also like to thank here the four other people of my PhD committee, Maria Gajdardiska-Josifovska, Jun Nogami, Richard Sorbello and Brian Tonner for their support and constructive suggestions to the thesis draft.

I would like to thank the members of Dr. Saldin's group, Dr. Valentin Shneyerson and Ross Harder for their friendship and support. Dr. Xiang Chen, the first member of our group I met when I joined, was always supportive and helpful and has been a very good friend of mine.

The last six months of 1997 I had the opportunity to meet and collaborate with Karsten Reuter, member of Dr. Klauss Heinz' group in Lehrstuhl für Festkörperphysik of Universität Erlangen-Nürnberg, Germany, who impressed me with his suggestions and understanding of our method and of Physics in general. My thanks go to him too.

I do not wish to forget other people from the Physics department, like Jon C. Glueckstein, always a good friend, and of course Eric A. Hagedorn, roommate for two years and brotherly friend to me. The people I worked for as a Teaching Assistant, like Elihu Lubkin, Yutze Chow, Robert Wood, William Walters, Dewayne Johnson and Moises Levy, were always very helpful during the performance of my duties.

Besides the staff and the graduate students, the Physics Department is a work place for a number of other people. I believe it would have been an oversight on my behalf if I omitted them since they facilitated my everyday life in the department. First of all I would like to mention our retired secretary Joyce McDade who always was very helpful to everybody; our new secretary, Barbara Duchow, has been an equally able

Dedication

To Angela and to Krinio
Στὴν ᾿Αγγελικὴ καὶ στὴν Κρινιώ

Contents

List of Tables

List of Figures

xvi

Chapter 1

Introduction

The short inelastic scattering length of the low energy electrons makes them ideal tools for surface crystallography. This important feature of them has made Low Energy Electron Diffraction (LEED) one of the most commonly used methods for the exploration of a surface. Although the dual behavior of the electrons, that was verified in the late 19th century, inspired experiments in which the electrons were used as probes of the crystal structure, thus being the precursors of LEED experiments, yet only with the design of Ultra High Vacuum pumps did LEED find its way to the world of surface physics. The decades of 1960, 1970 and 1980 were the most productive ones since during those years a large number of structures were solved succesfully bestowing LEED the reputation of one of the most reliable surface methods. The development of the new generation of fast supercomputers has partially solved the problem that people working with LEED had been trying to cope with since the beginning; the computation time. Figure 1 shows schematically the LEED cycle. The whole proccess is based upon
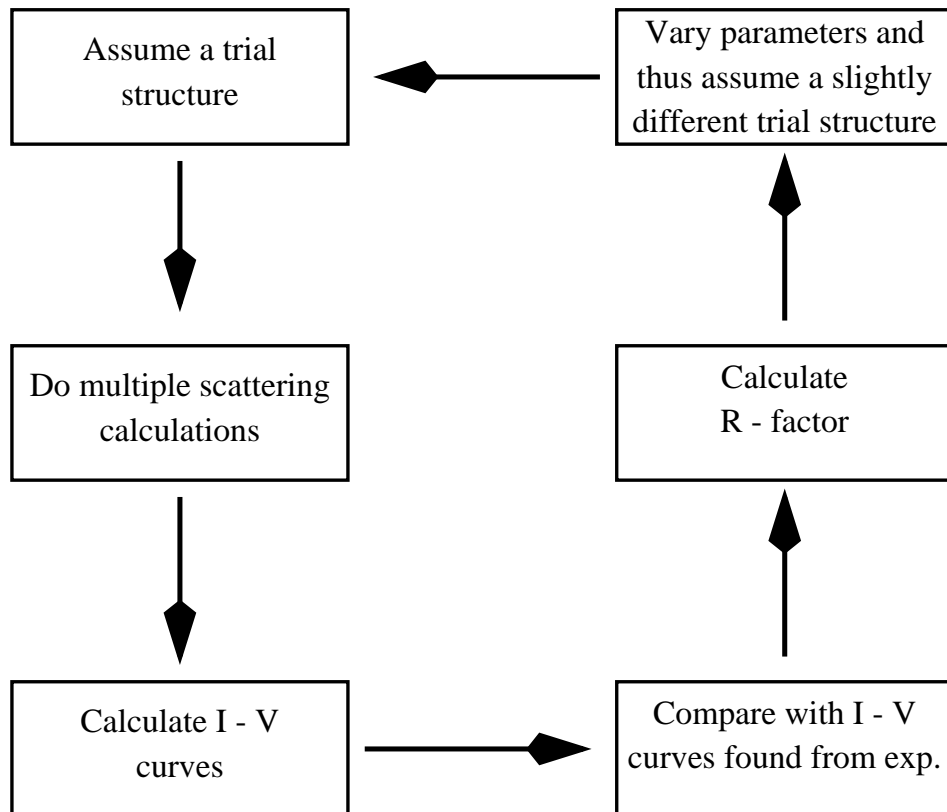
Figure 1: The LEED cycle

a trial-and-error search scheme. One of the key parts in the LEED procedures is the initialization of this cycle, that is, guessing a structure as close to the one being sought (the real one) as possible. Years of experience and intuition are the basic characteristics for some one who works with LEED while trying to guess a starting structure. Following this is the multiple scattering calculations step. The time for those culculations depend on the availabilty of fast computer systems. Let us try to get a rough idea of this time. Suppose we need to determine the 3 Cartesian coordinates of N symmetry inequivalent atoms, and for this purpose we consider models with 10 values of each coordinate. The time required for an exhaustive search amongst these parameters is $T = S \times 10^{3N}$, where S is the time required to calculate the LEED spectra from each model. Taking $S = 1$ second and $N = 3$ we find $T = 30$ years. Just doubling the number of atoms to $N = 6$ results in a time T of the order of the age of the universe. In the latter case, increases in computer speeds by even a million-fold would only bring T down to a few millenia! In the next steps we calculate the I-V curves which we compare with their experimental sisters and finally we calculate a R factor. In the case that this factor is less than some generally accepted value, we stop there having solved the structure. But this scenario is rather rare. We will have to vary the initial parameters and thus get a slightly different structure which will initialize the second iteration of the cycle. The reader understands that this may continue for some time. Everything depends on the original structure assumption. Obviously some alternative to an exhaustive trial-and-error search is needed. So, on the one hand procedures applying a directed search in the multidimensional parameter space were developed. In this context the testing of

simulated annealing-like and genetic algorithms[?] are certainly steps in a most promising direction. Also, quasidirect methods were developed allowing a search-free optimization of structural parameters once a model near the correct structure had been found or guessed[?]. The other approach that has shown considerable promise for LEED in recent years has been the holographic method[?]. This thesis describes exactly this approach. The author shows how it was created, almost ten years ago, with partial but promising success and how succesful it has become, chiefly from the work done by the groups of K. Heinz at the University of Erlangen-Nuremberg, Germany and of D.K. Saldin at the University of Wisconsin-Milwaukee in whose group the author did this research.

The thesis is divided into seven chapters.

1. Chapter 1 contains this introduction.

2. In the second chapter a general discussion of LEED theory and experiment is given that helps the reader follow the rest of the thesis. This discussion is far from being exhaustive and the interested reader should go to the two classical books on LEED, of J.B. Pendry[?] and of M.A. van Hove *et al.*[?].

3. In the first part of chapter 3 the ideas of electron holography are discussed and their application to surface crystallography, and especially to diffuse LEED (DLEED) are explained. A reconstruction algorithm is developed in the second part and reconstructed images of O/Ni(001) and K/Ni(001) from both experimental and theoretically calculated DLEED patterns are shown.

4. Chapter 4 continues the discussion started in the previous chapter on DLEED

with further investigation the author did towards the improvement of the reconstructed images, and an exploration of the limits of validity of the holographic reconstruction algorithm.

5. A simple program that simulates a DLEED experiment is the theme of the fourth chapter. The program was developed by the author and is schematically presented in the chapter whereas its complete code can be found in the appendix B. This program, which, exactly because of each simplicity, is fast, enabled the author to do a speedy investigation of the reconstruction algorithm developed in chapters 3 and 4 towards its application to an ordered adsorption.

6. The success of the investigation in the previous chapter with the model program gave the signal for the development of the initially proposed algorithm and its application to both experimental and theoretically calculated LEED patterns. This is the content of the sixth chapter. Reconstructed images from such patterns are also shown to establish the reliability of the method.

7. A general summary is the content of the seventh chapter.

Chapter 2

Elements of LEED

2.1 Introduction

The story of LEED goes back to 1897 when J. J. Thomson measured the ratio of charge to mass of the electron (e/m) thus establishing its particle nature. Then, in 1924, L. de Broglie[?] in his PhD thesis proposed that the electron behaved as a wave as well, with a wavelength given by h/p, where h is Planck's constant and p its momentum. Possessing this duality property, the electron can be diffracted following the diffraction laws conventional waves do. Thus, an electron with a low kinetic energy (let us say of the order of $100\,eV$) will have momentum $p = (2mE)^{1/2} = 5.59 \times 10^{-24}\,m\,kg/s$ and wavelength $\lambda = h/p = 1.18\,\text{Å}$. This short wavelength will enable it to diffract from a crystal, since it (the crystal) is a grating with periodicity of the order of atomic dimensions. And indeed, the first experiments performed by Davisson and Germer[?, ?, ?] in 1927 made use of a Ni(111) crystal surface. But all these were nothing more than
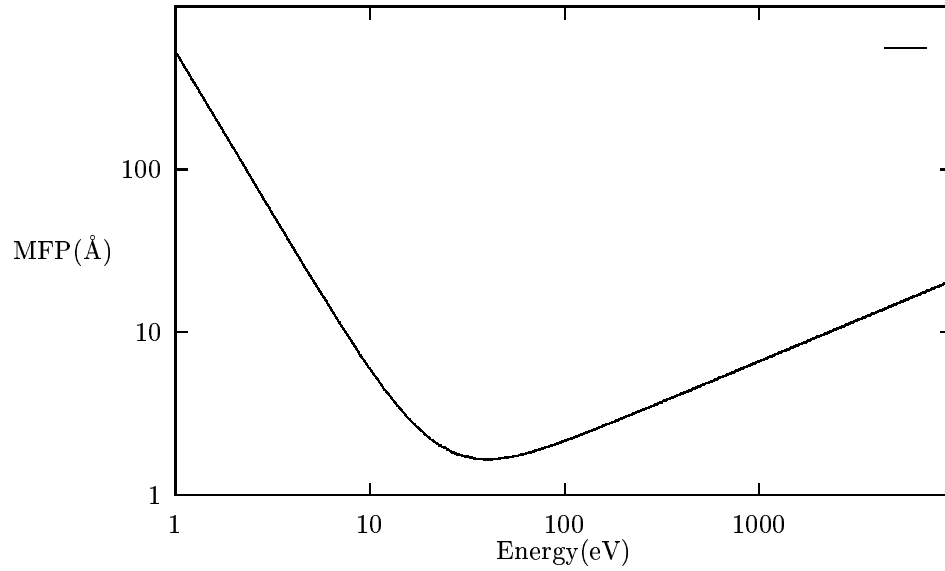
Figure 2: Universal curve of electron inelastic mean free path

Low Energy Electron Diffraction (LEED) experiments at their primitive stage. LEED knew its peak development almost 40 years later when Ultra High Vacuum pumps were in commercial usage. Only under these conditions of vacuum (of the order of $10^{-10}\,Torr$) can a LEED experiment give reliable results, since then we are sure that our sample crystal is free from impurities during the course of the experiment.

1960's and 1970's were the two decades that saw LEED being developed to its maximum degree. Nowadays, Low Energy Electron Diffraction is a powerful tool for surface exploration.

2.2 The LEED experiment

We would like to start this section by answering the question: Why use electrons to do the scattering? Figure 2 shows the so-called *universal curve* of the electron inelastic

mean free path[?]. By looking at this curve we will make a very important observation; that electrons with kinetic energy in the range $15 - 1000\,eV$ have very short mean free path (less than $10\,\text{Å}$). If we consider that a typical crystal surface is not deeper that a few layers, or about $10\,\text{Å}$, then the answer is easy. This interesting trait of the electrons makes them powerful probes for surface exploration. We see from figure 2 that in the above energy range the electrons are an ideal tool for surface studies.

As we said in the introduction, LEED was greatly developed after UHV pumps became commercially available. This is because the crystal sample will have to be as free from impurities as possible at least during the course of the experiment which lasts about an hour. To put it in other words, the rate of the arrival of the surrounding gas molecules must be kept very low. To quantify that we can say that we do not want to have more than a few per cent of an atomic layer of impurities to be attached to the surface of the sample over the time that the experiment lasts. A rough calculation, using the kinetic theory of gases justifies the use of UHV pumps which can keep a vacuum in the order of $10^{-10}\,Torr$.

Looking at the figure 3(a) we see that only the atoms or molecules that are contained within the cylindrical volume shown will be arriving at the surface. The total number of particles with speeds between v and $v + dv$ at polar angles θ and $\theta + d\theta$ incident on the surface area A will be given by:

$$N\frac{Av\cos\theta}{V}\frac{d\Omega}{4\pi}f(v)dv \tag{1}$$

where, N is the total number of particles, $Av\cos\theta/V$ is the fraction of all the particles that are contained in the culinder, $d\Omega/4\pi$ is the fraction of the particles moving in
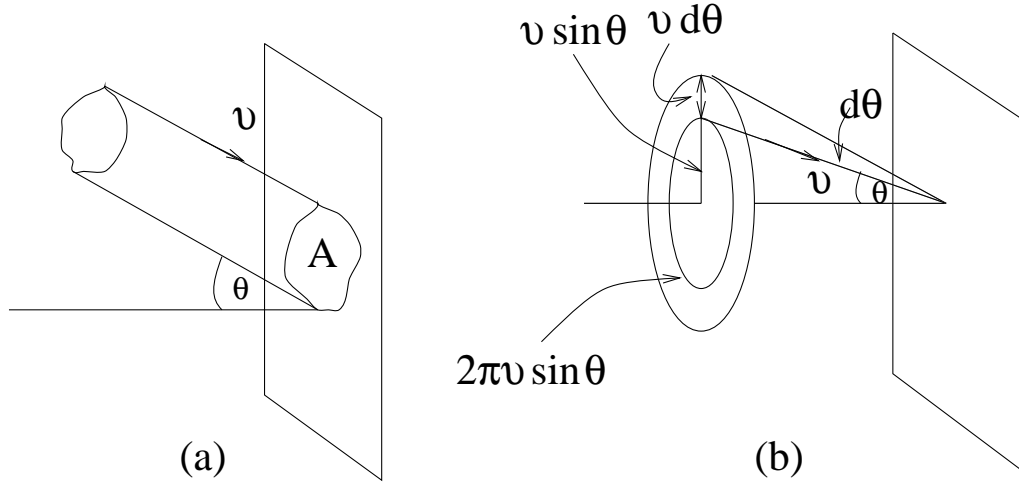
Figure 3: Evaluation of molecule arrival rate

directions between θ and $\theta + d\theta$ and $f(v)dv$ is the probability that one particle has speed between v and $v + dv$, $f(v)$ being the Maxwell-Boltzmann distribution of the speeds. Seeing from figure 3(b) that $d\Omega = 2\pi v^2 \sin\theta d\theta / v^2 = 2\pi \sin\theta d\theta$, makes (1):

$$\frac{NA}{V}v\frac{\sin\theta\cos\theta}{2}d\theta f(v)dv \tag{2}$$

Defining R to be the number of molecules arriving at the unit area of the surface in the unit time and integrating over all speeds and possible angles, we obtain:

$$
\begin{aligned}
R &= \int_{v=0}^{\infty}\int_{\theta=0}^{\pi/2}\frac{NA}{V}v\frac{\sin\theta\cos\theta}{2}d\theta f(v)dv \\
&= \frac{NA}{4V}\int_{\theta=0}^{\pi/2}\sin 2\theta d\theta \int_{v=0}^{\infty}f(v)v dv \\
&= \frac{NA}{4V}\left[-\frac{\cos 2\theta}{2}\right]_{0}^{\pi/2}v_a \\
&= \frac{1}{4}\frac{NA}{V}v_a \\
&= \frac{1}{4}nv_a
\end{aligned}
\tag{3}
$$

where, $v_a = \int_0^{\infty}f(v)dv$, the average speed, and n their density ($n = N/V$). The

Maxwell-Boltzmann distribution of the momenta (since $p = mv$) is given by:

$$f(p) = C \exp(-Ap^2), \tag{4}$$

where, $C = n/(2\pi m k_B T)^{3/2}$ and $A = 1/2mk_B T$, and m is the mass of the atom or molecule, $k_B = 1.38 \times 10^{-23} \, JK^{-1}$, the Boltzmann constant. This distribution will give an average velocity:

$$v_a = \frac{\int d^3 p v f(p)}{\int d^3 p f(p)} = (\frac{8k_B T}{m\pi})^{1/2} \tag{5}$$

Now, since the pressure for ideal gases is given by:

$$P = nk_B T \tag{6}$$

we can substitute n and v_a in (3) from (6) and (5) respectively to take the following expression:

$$R = P[\frac{1}{2\pi k_B T m}]^{1/2} \tag{7}$$

If we express the pressure P in $Torr$ $(1 \, Torr = 133.416 \, Pa)$ and substitute the mass m by the molecular weight M multiplied by the atomic mass unit $amu = 1.66 \times 10^{-27} \, Kg$, we will get a convenient formula for the rate in units of molecules per cm^2 per s, or

$$R = 3.51 \times 10^{22} \frac{P}{(TM)^{1/2}} \tag{8}$$

Let us assume that we have nitrogen molecules (N_2) with molecular weight $M = 28$. Then at room temperature $T = 293 \, K$ and pressure $1 \, Torr$ the arrival rate at the surface will be, using formula (8), 3.88×10^{20} molecules $cm^{-2} s^{-1}$. If we assume that a typical monolayer consists of about 10^{15} atoms per cm^2 and that all the molecules arriving at the surface stick on it, then we see that at pressure $1 \, Torr$ one monolayer of impurities

needs about $3 \times 10^{-6}\, s$ to be formed. For pressure $10^{-6}\, Torr$ it will take $3\, s$. The modern UHV pumps create a vacuum of the order of $10^{-10}\, Torr$ which gives us a time of $3 \times 10^4\, s$ or about $8\, hours$ for a monolayer of impurities to be stuck on the surface. From this rough estimation we conlclude that our sample's surface remains completely impurity-free over the period of the experiment.

2.2.1 Preparation of the sample

We discussed above the effectiveness of a UHV chamber in trying to keep our sample impurity-free during the course of the experiment. Next we will go through the procedure we follow to prepare our sample for the experiment. The first thing we need is to get its surface cut along a desired orientation. Good materials for this kind of proccess are those that cleave easily (like, oxides or alkali halides). A proccess of mechanical polishing with carbide powders and chemical etching makes the surface smooth. In order to render it as clean as possible we use the method of annealing. This causes a desorpion of gases having adsorbed on it. Sputtering (usually bombardment of the surface with ions of Ar) is another method that helps remove layers of impurities from the surface. One undesired side effect of the bombardment is that it leaves the surface heavily damaged with Ar atoms embedded. So we usually anneal it one more time to remove those atoms and to re-crystalline the surface. Finally, we may wish to have atoms or molecules adsorbed on the surface. To do that we will have to introduce gases into the vacuum champer where the sample sits (*in-situ* procedure) at pressures of about $10^{-6}\, Torr$ or less. Decomposition of the molecules produces atoms that get adsorbed

onto the surface. We can have two kinds of adsorption. If the atoms are held to the surface only by van der Waals' forces, the adsorption is called *physisorption* and creates weak bonds with the surface atoms (of the order of $0.6\,eV$ per atom). This kind of adsorbed atoms can be readily desorbed at temperatures around $200\,K$. On the other hand, if the adsorption changes the electronic structure of the ad-atom, then it is called *chemisorption* and produces strong bonds.

2.2.2 Performing the experiment

Figure 4 shows schematically the main parts of the apparatus for the LEED experiment. As one can see, the apparatus consists of a hemispherical fluorescent screen along with an array of four also hemispherical and concentric grids. All four grids and the display screen have a central hole through which the electron gun is inserted. The electron gun can shoot electrons with energy range between $30\,eV$ and $1000\,eV$ at the sample which is mounted at the center of the system and which, along with the first grid, is grounded. We do this in order to provide a field-free enviroment between them. The second and third grids (suppressor grids) are charged negatively to make sure that only elastically scattered electrons and only a fraction of them will reach the fluorescent screen. The fourth grid is also grounded to reduce penetration of the field by the suppresor grids into the region close to the screen which is charged positively with a potential of a few kV in order to make the electrons visible. Thus, what essentially happens is that a cathode supplies a steady current and heats up a tungsten filament, as seen in figure 5. The electrons extracted by the filament make up a beam that has diameter of the order of

Electron gun

Diffraced beam

Sample

Fluorescent Screen

Incident beam

1st

Grids

4th
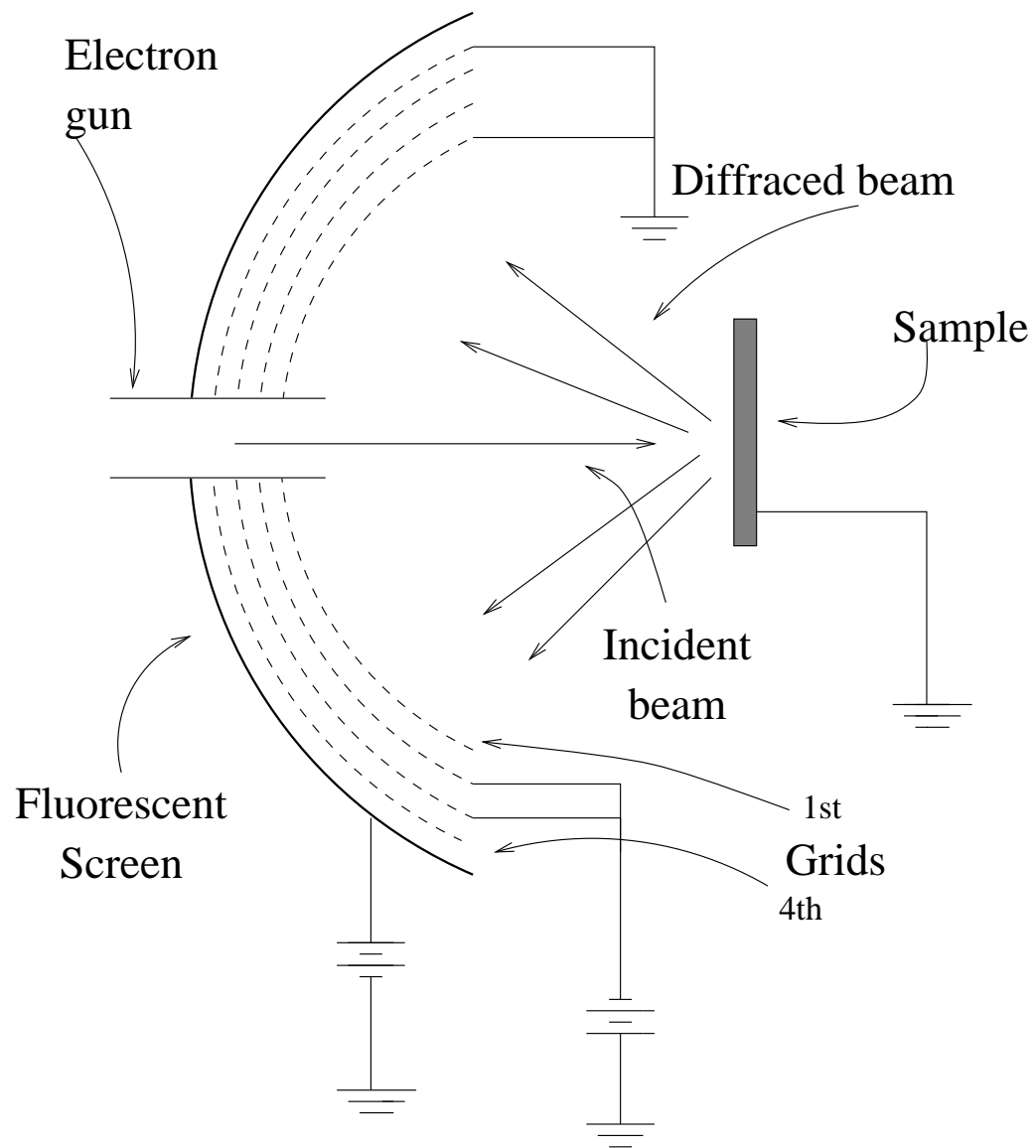
Figure 4: The LEED experiment
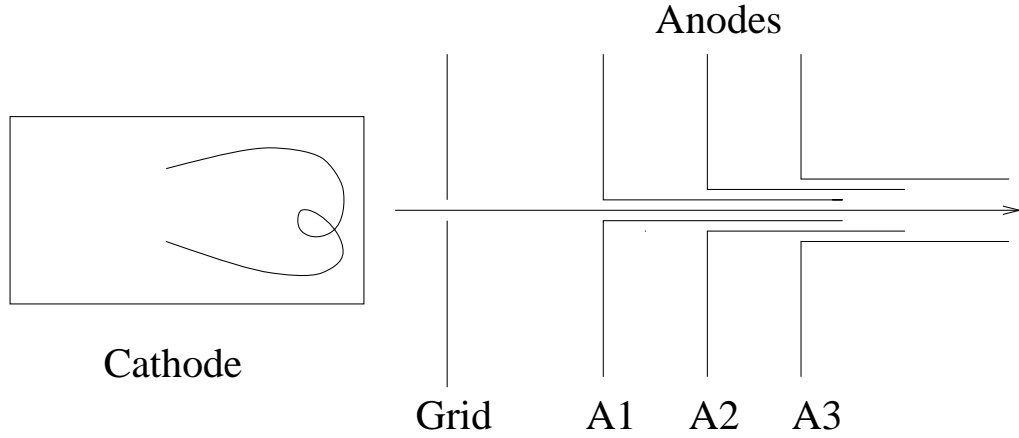
Figure 5: The electron gun

$0.1\,cm$ and carries a current of the order of $1\,\mu A$. The potential between the cathode and the array of anodes controls the final kinetic energy of the electrons. This beam of electrons is shot upon the specimen. The diffracted particles travel within the field-free ambient towards the screen. If they are elastically scattered they make it through the two suppressor grids and eventually end they trip on the fluorescent screen where they can be traced by the spots they leave upon collision.

2.2.3 Coherence length

An ideal beam would be described by a simple plane wave of the form, $A \exp(\imath \vec{k} \cdot \vec{r})$, with kinetic energy, $E = \hbar k^2/2m$ and a well defined direction given by the wave vector $\vec{k}$. If that was the case a wave normally incident on a surface would have the same phase everywhere on it. In general two points on the surface separated by a distance ℓ that receive the incident wave would differ by a phase difference $\vec{\ell} \cdot \vec{k}$. In reality we have to deal not with one wave but with a set of them having slightly different

directions and, hence, kinetic energies. This means that the electron waves scattered by two different points of the surface will not have phase difference always the same exactly because of the uncertainty of $\vec{k}$. This is very important when these waves are involved in diffraction where the amplitudes are simply added to take the known diffraction patterns. If two waves that interfere have different phases then this interference will give neither a maximum nor a minimum. Fortunately, we can define a characteristic length on the surface, within which these variations of $\vec{k}$ are not so important. Outside this length the phase difference of the scattered waves are completely arbitrary. This length is called *coherence length*. In order that we get an approximate idea of the size order of the coherence length we should account for both perpendicular and parallel variations of the wave vector. Change in $\vec{k}$ along its direction results in a change of the kinetic energy, as follows:

$$\Delta E = \frac{\hbar^2}{2m} 2\Delta\vec{k}_{\parallel} \cdot \vec{k} \tag{9}$$

Writting $\hbar^2/2m = E/k^2$, substituting in the expression above and squaring both sides we will see:

$$k^4 \frac{(\Delta E)^2}{E^2} = 4(\vec{k} \cdot \Delta\vec{k}_{\parallel})^2 \tag{10}$$

Taking the average of both parts we end up to:

$$k^2 \frac{\overline{(\Delta E)^2}}{4E^2} = \frac{\overline{(\Delta\vec{k}_{\parallel} \cdot \vec{k})^2}}{k^2} \tag{11}$$

On the other hand, perpendicular variations in $\vec{k}$ result in an angular spread of the beam. Figure 6(a) helps us evaluate that. A perpendicular change of $\vec{k}$ by $\Delta\vec{k}_{\perp}$ results in making the wave vector $\vec{k} + \Delta\vec{k}_{\perp}$. Assuming that $\Delta\theta$ is the angle between $\vec{k}$ and

(a)   (b)
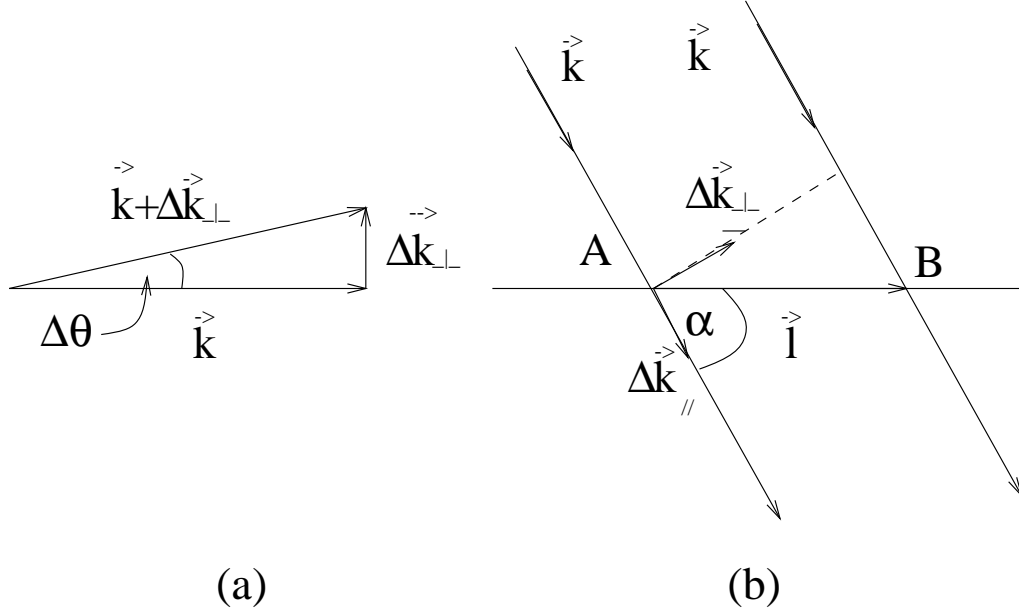
Figure 6: Coherence length

$\vec{k} + \Delta\vec{k}_\perp$ we will have:

$$|\vec{k} \times (\Delta\vec{k}_\perp + \vec{k})| = k|\vec{k} + \Delta\vec{k}|\sin(\Delta\theta) \tag{12}$$

But also:

$$|\vec{k} \times (\Delta\vec{k}_\perp + \vec{k})| = |\vec{k} \times \vec{k} + \Delta\vec{k}_\perp \times \vec{k}| = |\Delta\vec{k}_\perp \times \vec{k}| \tag{13}$$

Equating the right hand side of (12) and (13) and squaring both sides, we get:

$$|\Delta\vec{k}_\perp \times \vec{k}|^2 = k^2[k^2 + |\Delta\vec{k}_\perp|^2 + 2\vec{k} \cdot \Delta\vec{k}_\perp]\sin^2(\Delta\theta) \tag{14}$$

Taking into account that $\Delta\vec{k}$ and $\Delta\theta$ are infinitesimal quantities, we average both sides and we finally have:

$$\frac{\overline{|\Delta\vec{k}_\perp \times \vec{k}|^2}}{k^2} = k^2\overline{(\Delta\theta)^2} \tag{15}$$

From figure 6(b) we see that the phase difference of the wave scattered by the points A and B separated by a distance ℓ in the surface, will be:

$$
\begin{aligned}
\Delta\phi &= \vec{\ell} \cdot \Delta\vec{k} \\
&= \vec{\ell} \cdot (\Delta\vec{k}_{\parallel} + \Delta\vec{k}_{\perp}) \\
&= \vec{\ell} \cdot (\Delta\vec{k}_{\parallel}) + \vec{\ell} \cdot (\Delta\vec{k}_{\perp}) \\
&= \ell(\Delta k_{\parallel})\cos\alpha + \ell(\Delta k_{\perp})\sin\alpha
\end{aligned}
\tag{16}
$$

Squaring both sides of (16), taking the average, using (11) and (15) and thinking that $\Delta k_{\parallel}$ and $\Delta k_{\perp}$ are small quantities, we find:

$$
\begin{aligned}
\overline{(\Delta\phi)^2} &= \ell^2 \overline{(\Delta k_{\parallel})^2}\cos^2\alpha + \ell^2 \overline{(\Delta k_{\perp})^2}\sin^2\alpha \\
&= \frac{1}{2}\overline{(\Delta\theta)^2}k^2\ell^2\sin^2\alpha + \frac{\overline{(\Delta E)^2}}{4E^2}k^2\ell^2\cos^2\alpha
\end{aligned}
\tag{17}
$$

In defining the coherence length we argue that when the average phase change becomes of the order of π, then the two waves emanating from the two points will be completely independent having no relation between them. Seting $\overline{(\Delta\phi)^2} = \pi^2$ in (17) and solving for ℓ_c we will have:

$$
\ell_c = \frac{2\pi|\vec{k}|^{-1}}{[2\sin^2\alpha\overline{(\Delta\theta)^2} + \cos^2\alpha\overline{(\Delta E/E)^2}]^{1/2}}
\tag{18}
$$

For an estimation let us take $\Delta\theta \approx 0.0001\,rad$, $\Delta E \approx 0.2\,eV$ at $E = 150\,eV$ and $\alpha = 45°$. Then, (18) gives, $\ell_c \approx 500\,\text{Å}$. In other words, within $500\,\text{Å}$ or, to put it in another way, within 100 surface atoms the scattered beams are coherent.

2.2.4   Data aquisition and interpretation

Before he actually tries to interpret the results of the experiment the experimentalist will have to estimate the angle of incidence of the electron beam. A fairly simple method to do this is the one developed by Cunningham and Weinberg[?]. What makes it so simple is that we do not need any particular equipment. All we use is a camera to take a picture of the LEED pattern and a computer to run a simple ForTran program[?]. We will not enter into any details here but the interested reader should look for a detailed description of the method in Low Energy Electron Diffraction book by M.A. van Hove et at.[?].

The result of the LEED experiment is a circular region on the fluorescent screen that contains spots; the traces left by the electrons scattered by the sample after their collision with the surface of the screen. The job of the experimentalist is to take this nicely ordered array of spots and attempt to decrypt it and find what kind of atom array on the specimen surface would produce this design of spots.

Before we start our attempt to decipher such a pattern we should say a few things about a clean surface. This should be characterized be two fundamental concepts: the *Bravais lattice* and the *basis*. The former is a two-dimensional array of points that have translational symmetry, meaning that we can use the combination of two fundamental vectors, $\vec{a}$ and $\vec{b}$ (figure 7(a)), like $\ell\vec{a}+m\vec{b}$, where ℓ and m are integers, and go to any point of the lattice we choose. The two fundamental vectors $\vec{a}$ and $\vec{b}$ make what we call, the *unit cell* of the two-dimensional surface. In two dimensions we can have only five different kinds of such lattices shown in figure 7: (b) Oblique, with $|\vec{a}| \neq |\vec{b}|$, (c) Hexagonal,
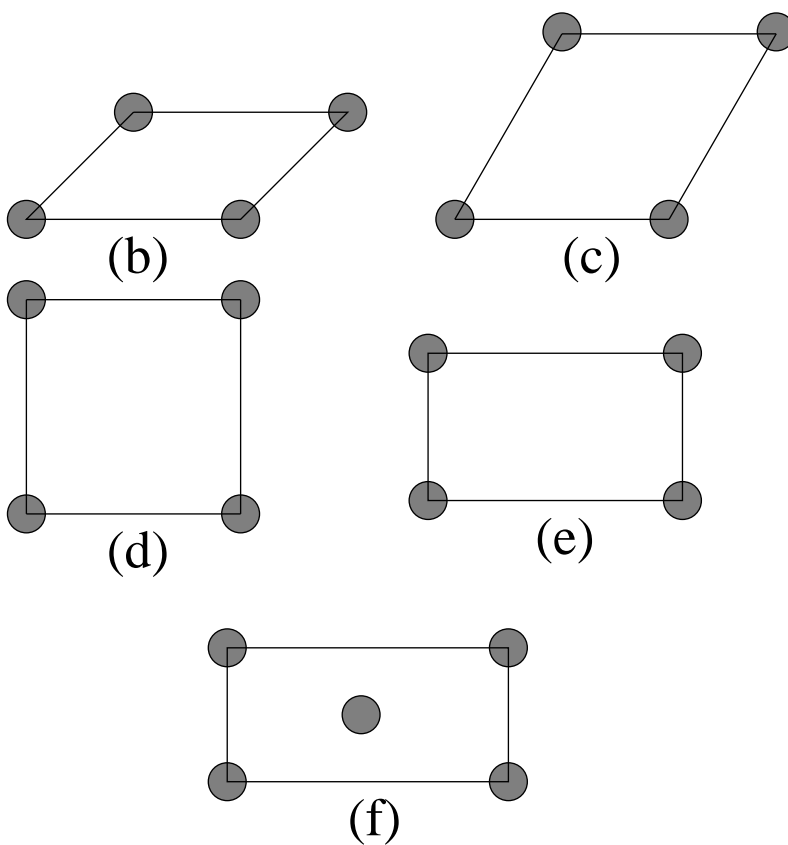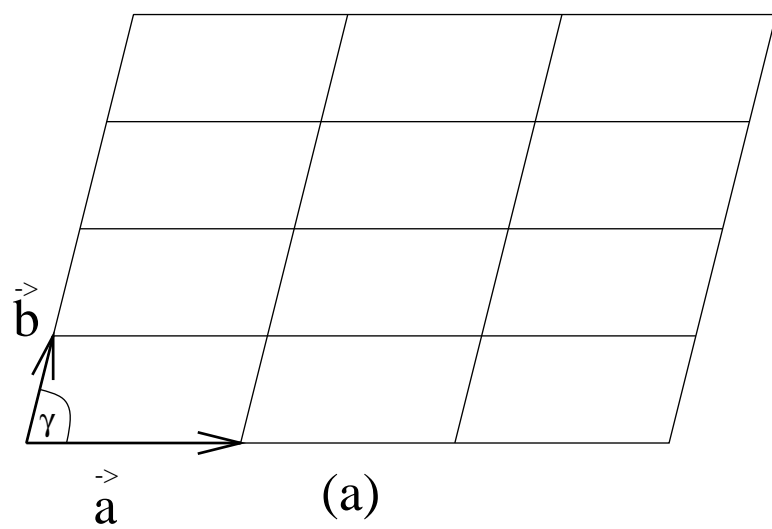
Figure 7: The two-dimensional Bravais lattice

with $|\vec{a}| = |\vec{b}|, \gamma = 60°$, (d) Square, with $|\vec{a}| = |\vec{b}|, \gamma = 90°$, (e) Rectangular, with $|\vec{a}| \neq |\vec{b}|, \gamma = 90°$ and (f) Centered Rectangular, with $|\vec{a}| \neq |\vec{b}|, \gamma = 90°$. The basis can be atom or cluster of atoms with respect to the lattice points. Together the lattice and the basis make up the structure.

After this short remind of the basic concepts of a clean two-dimensional surface we will attempt to examine the scattering proccess of an electron by the surface. Since here we have to deal with a periodic situation with period $\ell\vec{a} + m\vec{b}$, as we said previously, the potential, $V(\vec{r})$, that the electrons face upon entering the surface must be a periodic one having the same period, that is, it must satisfy the relation:

$$V(\vec{r} + \ell\vec{a} + m\vec{b}) = V(\vec{r}) \tag{19}$$

Before we continue with our analysis it would be useful to mention that in theoretical physics in general and in LEED particularly we use the so-called *atomic units*. For convenience and to avoid typing quantities like $\hbar$ or the mass and the charge of the electron we set them all equal to one, $\hbar^2 = m_e = e^2 = 1$. By doing that we take new units for the energy, the so-called *Hartrees*, with $1H = 27.2\,eV$, the length unit being the Bohr radius, with $1a.u. = 0.5291\,\text{Å}$.

If $\psi_i(\vec{r})$ is the wavefunction of the incident electron with total energy $E = k_i^2/2$ and wavevector $\vec{k}_i$ and $\psi_s(\vec{r})$ the wavefunction of the scattered one and since the sum of the two is the total wavefunction of the system, then the Schrödinger's equation will be:

$$-\frac{\nabla^2}{2}[\psi_i(\vec{r}) + \psi_s(\vec{r})] + V(\vec{r})[\psi_i(\vec{r}) + \psi_s(\vec{r})] = E[\psi_i(\vec{r}) + \psi_s(\vec{r})] \tag{20}$$

Contemplating (19) we substitute for:

$$\vec{r} = \vec{r}' + \ell\vec{a} + m\vec{b} \tag{21}$$

Making use of the above substitution in (20), (19) and seeing that $\nabla^2 = \nabla'^2$ we will have:

$$
\begin{aligned}
&- \frac{\nabla'^2}{2} \left[\psi_i(\vec{r}' + \ell\vec{a} + m\vec{b}) + \psi_s(\vec{r}' + \ell\vec{a} + m\vec{b}) \right] \\
&+ V(\vec{r}') \left[\psi_i(\vec{r}' + \ell\vec{a} + m\vec{b}) + \psi_s(\vec{r}' + \ell\vec{a} + m\vec{b}) \right] \\
&= E \left[\psi_i(\vec{r}' + \ell\vec{a} + m\vec{b}) + \psi_s(\vec{r}' + \ell\vec{a} + m\vec{b}) \right]
\end{aligned}
\tag{22}
$$

Comparing (20) and (22) we see that the total wavefunction of the system satisfies the same equation at two points of the surface that differ by a lattice translation. The wavefunction of the incident electron will be:

$$\psi_i(\vec{r}) = A e^{i\vec{k}_i \cdot \vec{r}} \tag{23}$$

Using (21), (23) can be written as:

$$
\begin{aligned}
\psi_i(\vec{r}' + \ell\vec{a} + m\vec{b}) &= A e^{i\vec{k}_i \cdot \vec{r}'} e^{i\vec{k}_i \cdot (\ell\vec{a} + m\vec{b})} \\
&= \psi_i(\vec{r}') e^{i\ell\vec{k}_i \cdot \vec{a}} e^{im\vec{k}_i \cdot \vec{b}}
\end{aligned}
\tag{24}
$$

We do not know the analytical form of the wavefunction of the scattering electron but we can see that if the wavefunction of the incident electron at two different points differing by $\ell\vec{a} + m\vec{b}$ is given by equation (24) then in order that (22) reduces to (20) when we go from point $\vec{r}' + \ell\vec{a} + m\vec{b}$ to point $\vec{r}'$ the wavefunction of the scattered electron must satisfy the following relation:

$$\psi_s(\vec{r}' + \ell\vec{a} + m\vec{b}) = \psi_s(\vec{r}') e^{i\ell\vec{k}_{i\parallel} \cdot \vec{a}} e^{im\vec{k}_{i\parallel} \cdot \vec{b}} \tag{25}$$

where, because $\vec{a}$ and $\vec{b}$ are vectors in the plane of the surface, we have used $\vec{k}_{i\parallel}$ to denote the parallel to the surface components of the wave vector. Since $\psi_s(\vec{r})$ does not satisfy an equation like (19), or in other words, does not have the periodicity of the crystal, we see that if we write it as:

$$\psi_s(\vec{r}) = e^{i\vec{k}_{i\parallel}\cdot\vec{r}_\parallel}\chi_s(\vec{r}) \tag{26}$$

and substitute (26) into (25), we will have:

$$\chi_s(\vec{r} + \ell\vec{a} + m\vec{b}) = \chi_s(\vec{r}) \tag{27}$$

meaning that the function $\chi_s(\vec{r})$ does have the periodicity of the crystal. So, all we will have to do is to determine $\chi_s(\vec{r})$ and use (26) to get $\psi_s(\vec{r})$. By Fourier expanding $\chi_s(\vec{r})$ we will have:

$$\chi_s(\vec{r}) = \sum_g a_g(z)e^{i\vec{g}\cdot\vec{r}_\parallel} \tag{28}$$

To see what $\vec{g}$ represents we substitute (28) into (27) and we will get:

$$\sum_g a_g(z)e^{i\vec{g}\cdot\vec{r}_\parallel}e^{i\vec{g}\cdot(\ell\vec{a}+m\vec{b})} = \sum_g a_g(z)e^{i\vec{g}\cdot\vec{r}_\parallel} \Rightarrow$$

$$e^{i\vec{g}\cdot(\ell\vec{a}+m\vec{b})} = 1 \Rightarrow$$

$$\ell\vec{g}\cdot\vec{a} + m\vec{g}\cdot\vec{b} = 2\pi \times \text{integer} \tag{29}$$

Eventually, $\vec{g}$'s satisfy:

$$\vec{g}\cdot\vec{a} = 2\pi \times \text{integer} \tag{30}$$

$$\vec{g}\cdot\vec{b} = 2\pi \times \text{integer} \tag{31}$$

These two equations can be satisfied by vectors of the form:

$$\vec{g} = h\vec{A} + k\vec{B} \tag{32}$$

where h and k are integers and,

$$\vec{A} = (A_x, A_y) = \frac{2\pi}{a_x b_y - a_y b_x}(b_y, -b_x) \tag{33}$$

$$\vec{B} = (B_x, B_y) = \frac{2\pi}{a_x b_y - a_y b_x}(-a_y, a_x) \tag{34}$$

Taking a glimpse at the dimensions of $\vec{g}$ we see that are inverse length and so are the dimensions of $\vec{A}$ and $\vec{B}$. What we have seen so far is that those two vectors, that have only x and y components, are associated with $\vec{a}$ and $\vec{b}$ through (33, 34) and that can be combined as in (32) to create another Bravais lattice, akin to the one we started with (created by the vectors $\vec{a}$ and $\vec{b}$). This new lattice is what we have learned from introductory Solid State Physics, the two-dimensional *reciprocal* space or *reciprocal* lattice. Next we will try to show that this concept of the reciprocal lattice explains the diffraction pattern observed in a LEED experiment.

To do this we will first have to determine $\psi_s(\vec{r})$, which means that we will have to determine the Fourier coefficients $a_g(z)$ of (28). Let us substitute $\chi_s(\vec{r})$ from (28) into (26):

$$\psi_s(\vec{r}) = \sum_g a_g e^{i(\vec{g}+\vec{k}_{i\|})\cdot\vec{r}_\|} \tag{35}$$

Substituting $\psi_i(\vec{r})$ and $\psi_s(\vec{r})$ from (23) and (35) respectively into (20) for the region outside the surface (where the potential is zero), we get:

$$-\frac{\nabla^2}{2}(\psi_i(\vec{r}) + \psi_s(\vec{r})) = E(\psi_i(\vec{r}) + \psi_s(\vec{r}))$$

$$\mathrm{LHS} = \mathrm{RHS} \tag{36}$$

Let us start with the LHS and let us drop the subsript i from $\vec{k}_{i\|}$ for convenience. Let us also write for the operator $\nabla^2 = \nabla_\|^2 + \nabla_z^2$, recalling that the z direction has been

chosen to be perpendicular to the surface.

$$
\begin{aligned}
\text{LHS} \; = \; & -(1/2)\nabla^2 \left[A e^{i\vec{k}\cdot\vec{r}} + \sum_g a_g(z) e^{i(\vec{g}+\vec{k}_\parallel)\cdot\vec{r}_\parallel} \right] \\
= \; & -(1/2) \left[A e^{ik_z z}\nabla_\parallel^2 e^{i\vec{k}_\parallel\cdot\vec{r}_\parallel} + \sum_g a_g(z)\nabla_\parallel^2 e^{i(\vec{g}+\vec{k}_\parallel)\cdot\vec{r}_\parallel} \right. \\
+ \; & \left. A e^{i\vec{k}_\parallel\cdot\vec{r}_\parallel}\nabla_z^2 e^{ik_z z} + \sum_g \nabla_z^2 a_g(z) e^{i(\vec{g}+\vec{k}_\parallel)\cdot\vec{r}_\parallel} \right] \\
= \; & -(1/2) \left[A e^{ik_z z}(-k_\parallel^2) e^{i\vec{k}_\parallel\cdot\vec{r}_\parallel} + \sum_g a_g(z)(-|\vec{g}+\vec{k}_\parallel|^2) e^{i(\vec{g}+\vec{k}_\parallel)\cdot\vec{r}_\parallel} \right. \\
+ \; & \left. A e^{i\vec{k}_\parallel\cdot\vec{r}_\parallel}(-k_z^2) e^{ik_z z} + \sum_g \frac{d^2 a_g(z)}{dz^2} e^{i(\vec{g}+\vec{k}_\parallel)\cdot\vec{r}_\parallel} \right] \\
= \; & -(1/2) \left[-A e^{i\vec{k}\cdot r} k_\parallel^2 - \sum_g a_g(z)|\vec{g}+\vec{k}_\parallel|^2 e^{i(\vec{g}+\vec{k}_\parallel)\cdot\vec{r}_\parallel} \right. \\
- \; & \left. A e^{i\vec{k}\cdot\vec{r}} k_z^2 + \sum_g \frac{d^2 a_g(z)}{dz^2} e^{i(\vec{g}+\vec{k}_\parallel)\cdot\vec{r}_\parallel} \right] \\
= \; & (1/2) \left[(k_\parallel^2 + k_z^2) A e^{i\vec{k}\cdot\vec{r}} + \sum_g \left(a_g(z)|\vec{g}+\vec{k}_\parallel|^2 - \frac{d^2 a_g(z)}{dz^2} \right) e^{i(\vec{g}+\vec{k}_\parallel)\cdot\vec{r}_\parallel} \right] \\
= \; & \frac{1}{2}k^2 A e^{i\vec{k}\cdot\vec{r}} + \frac{1}{2}\sum_g \left(a_g(z)|\vec{g}+\vec{k}_\parallel|^2 - \frac{d^2 a_g(z)}{dz^2} \right) e^{i(\vec{g}+\vec{k}_\parallel)\cdot\vec{r}_\parallel} \quad\quad (37)
\end{aligned}
$$

The RHS will have the form:

$$
\text{RHS} = E A e^{i\vec{k}\cdot\vec{r}} + E \sum_g a_g(z) e^{i(\vec{g}+\vec{k}_\parallel)\cdot\vec{r}_\parallel} \tag{38}
$$

Combining the two sides of (36) we get:

$$
\left[\frac{1}{2}k^2 - E\right] A e^{i\vec{k}\cdot\vec{r}} + \sum_g \left[\left(\frac{1}{2}|\vec{g}+\vec{k}_\parallel|^2 - E\right) a_g(z) - \frac{1}{2}\frac{d^2 a_g(z)}{dz^2} \right] e^{i(\vec{g}+\vec{k}_\parallel)\cdot\vec{r}_\parallel} = 0
$$

$$
\left[k^2 - 2E\right] A e^{i\vec{k}\cdot\vec{r}} + \sum_g \left[\left(|\vec{g}+\vec{k}_\parallel|^2 - 2E\right) a_g(z) - \frac{d^2 a_g(z)}{dz^2} \right] e^{i(\vec{g}+\vec{k}_\parallel)\cdot\vec{r}_\parallel} = 0 \tag{39}
$$

The first term of (39) is by default zero. Thus at last we have:

$$
\sum_g \left[\left(|\vec{g}+\vec{k}_\parallel|^2 - 2E\right) a_g(z) - \frac{d^2 a_g(z)}{dz^2} \right] e^{i(\vec{g}+\vec{k}_\parallel)\cdot\vec{r}_\parallel} = 0 \tag{40}
$$

Multiplying (40) by $\exp[-\imath(\vec{k}_{\parallel} + \vec{g}') \cdot \vec{r}_{\parallel}]$ and integrating over all two-dimensional space, we get:

$$\sum_g \int \left[\left(|\vec{g} + \vec{k}_{\parallel}|^2 - 2E \right) a_g(z) - \frac{d^2 a_g(z)}{dz^2} \right] e^{\imath(\vec{g} - \vec{g}') \cdot \vec{r}_{\parallel}} dr_{\parallel} = 0 \Rightarrow$$

$$\frac{d^2 a_{g'}(z)}{dz^2} + \left(2E - |\vec{g}' + \vec{k}_{\parallel}|^2 \right) a_{g'}(z) = 0 \qquad (41)$$

Solving this simple differential equation we will get for the Fourier coefficients:

$$a_g(z) = b_g \exp(-\imath \left[2E - |\vec{g} + \vec{k}_{\parallel}|^2 \right]^{1/2} z) \qquad (42)$$

where, b_g is a constant and we have chosen the negative root in the solution since we are dealing with the scattered electron waves traveling out of the surface. Substituting (42) into (28) we will have:

$$\chi_s(\vec{r}) = \sum_g b_g \exp \left[\imath \left(xg_x + yg_y - z \left[2E - |\vec{g} + \vec{k}_{\parallel}|^2 \right]^{1/2} \right) \right] \qquad (43)$$

Finally, substituting (43) into (26) we get:

$$\begin{aligned} \psi_s(\vec{r}) &= \sum_g b_g \exp \imath \left(x(g_x + k_x) + y(g_y + k_y) - z \left[2E - |\vec{g} + \vec{k}_{\parallel}|^2 \right]^{1/2} \right) \\ &= e^{\imath \vec{K}_g^- \cdot \vec{r}} \end{aligned} \qquad (44)$$

where,

$$\vec{K}_g^- = \hat{x}(k_{ix} + g_x) + \hat{y}(k_{iy} + g_y) - \hat{z} \left[2E - |\vec{g} + \vec{k}_{\parallel}|^2 \right]^{1/2} \qquad (45)$$

and the minus sign indicates, as we said before, that the waves travel out of the surface.

The previous result is very important because, as we can see, the outgoing waves depend on the kinetic energy of the incident electrons, their wavevectors components parallel to the surface and the reciprocal lattice vector $\vec{g}$. This means that these waves do

not travel arbitrarily towards every directions but rather selectively towards directions that depend on $\vec{g}$. But these electrons end up finishing their trip on the fluorescent screen, leaving a spot to indicate their trace. For every $\vec{g}$ we get a different spot displayed on the screen. So, we understand that the surface lattice, through this proccess of the scattering of the electrons by its atoms, is mapped out on the screen. The electrons act as probes or scouts (to use an anthropomorphic term) that carry with them the information they have gotten by having come in contact, during the course of the scattering, with the atoms. On the screen they "report" with their trace what they saw and learned! The truth is, of course, (like in any military expedition) that we have losses. Not all ingoing electrons do manage to get back to the fluorescent screen; only the elastically scattered that will make it through the suppressor grids. But besides those two factors that ban electrons from completing their trip there is one more, purely mathematical. If we take a look at equation (45) we will see that $\vec{K}_g^-$ depends on the energy of the incoming electrons only through its z component. Looking at $[2E - |\vec{g} + \vec{k}_{\parallel}|^2]^{1/2}$ we realize that for a given energy E and wave vector $\vec{k}$, the larger $\vec{g}$ becomes the smaller the expression in the brackets gets. If $\vec{g}$ keeps growing, or in other words, if we look at the surface further and further away from its center, there will come one moment that the expression will become very close to zero. In that case the outgoing waves will travel parallel to the surface. In the case that the expression becomes negative we will have the waves entering the surface again, dying exponentially inside it, since the square root of the expression will be an imaginary number. This schematically can be seen in figure 8. The characteristic reciprocal lattice vector for which the beams travel parallel to the surface is called *critical*, $\vec{g}_c$. There is

$$|\vec{g}_1| < |\vec{g}_2|$$

$$\vec{K}_g$$

Sample

+z

$$(2E-|\vec{k}_{//} + \vec{g}_2|^2)^{1/2}$$

$$(2E-|\vec{k}_{//} + \vec{g}_1|^2)^{1/2}$$
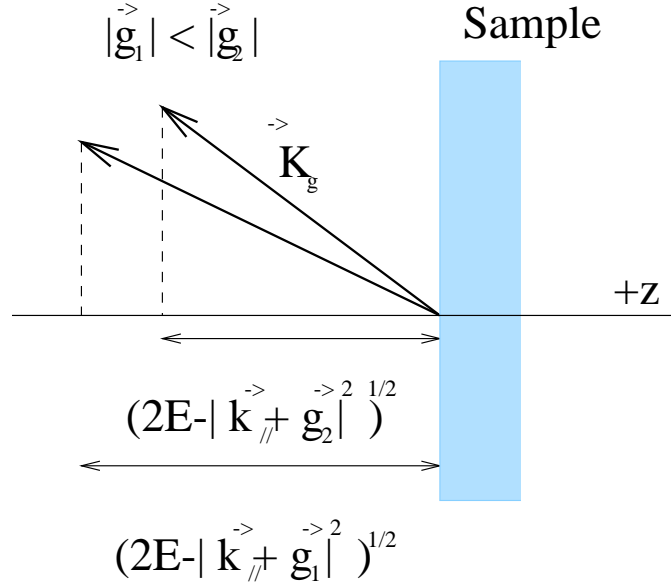
Figure 8: Dependence of beams from $\vec{g}$

one more observation one can make. Looking at figure 9 we can see that for given wave vector of the incident electrons and given reciprocal lattice vector, the larger the energy the closer to the center of the fluorescent screen the electrons land. In other words, for small energies the density of Bragg spots is lower than for higher ones.

From the previous treatment we have realized that the diffraction pattern we get by performing a LEED experiment on a crystal surface is a map of the reciprocal lattice of that surface. Our next task will be to try to "see" the cluster of the atoms that give this icon as they are in real space. Theoretically, this is easy. As we said before, each spot on the pattern is associated with a different reciprocal lattice vector $\vec{g}$ or with two integer numbers h and k through relation (32). The central spot, called the *specular*, is the (00). The rest are numbered in a way similar to the one figure 10 shows. Thus, through each spot we get the reciprocal vectors $\vec{A}$ and $\vec{B}$, or A_x, A_y, B_x, B_y. If we invert
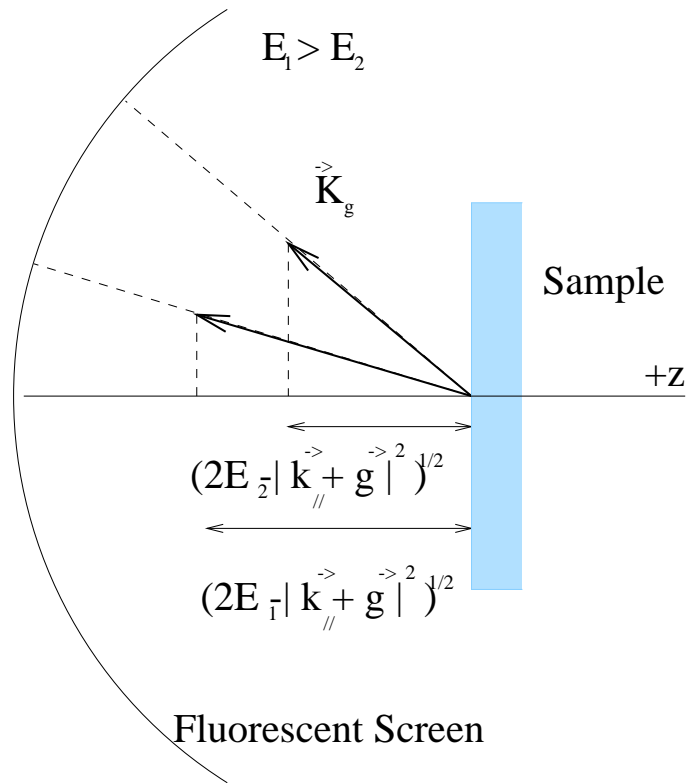
Figure 9: Dependence of beams from the energy
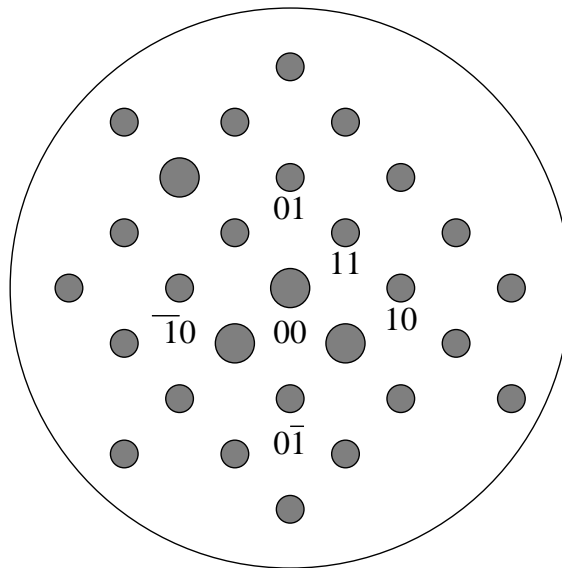
Figure 10: Numbering the beams

(33,34) and solve for the real lattice vecors a_x, a_y, b_x, b_y, we will have:

$$\vec{a} = (a_x, a_y) = \frac{2\pi}{A_x B_y - A_y B_x}(B_y, -B_x) \tag{46}$$

$$\vec{b} = (b_x, b_y) = \frac{2\pi}{A_x B_y - A_y B_x}(-A_y, A_x) \tag{47}$$

As we saw above, each diffracted beam is associated with two integer numbers h and k that actually name it; we speak of the hk beam. But, beyond the integer numbered beams there are cases that we find on the pattern *fractional-order* beams, *i.e.*, beams that are associated with non-integer numbers. We can have three different cases that justify their appearances: (a) Reconstruction of the clean surface, (b) Adsorbed overlayer of atoms, and (c) Adsorbed overlayer of molecules.

At this point it would be useful to dedicate a few lines to the notation we use to indicate an ordered overlayer. If the fundamendal vectors of the unit cell of the substrate are: $\vec{a}$ and $\vec{b}$ with Cartesian components S_{ij}, and those of the unit cell of the overlayer are $\vec{\alpha}$ and $\vec{\beta}$ with components O_{ij} respectively, then these componets are related through the following matrix equation:

$$\boldsymbol{M = OA^{-1}} \tag{48}$$

If the elements M_{ij} are all integers then there exists a simple relation between substrate and overlayer unit cell and we call the latter *simple*. If the elements are rational numbers then we say that we have a *comensurate* superlattice, whereas when M_{ij} are irrational numbers we have a *incommensurate* superlattice. We use two notations to describe the overlayer[?]:

The matrix notation In this case if K is the chemical composition of the substrate, (hkl)

the orientation of it, M the above matrix, Λ the chemical formula of the atomic or molecular overlayer and η the number of ad-species per unit cell, then we have:

$$K(hkl) - M - \eta\Lambda \tag{49}$$

The Wood notation In this case, if α/a and β/b are the ratios of the magnitudes of the two unit cell vectors and ϕ is the angle between $\vec{a}$ and $\vec{\alpha}$, then we have:

$$K(hkl) - i\left(\frac{\alpha}{a} \times \frac{\beta}{b}\right) R\phi - \eta\Lambda \tag{50}$$

with i being p (primitive) or c (centered).

With the discussion we had had above we saw how we can get information about the real lattice unit cell. We can find out if the surface underwent any reconstruction or we can extract information about the unit cell of both the overlayer and the substrate if we had adsorption on the surface. This is all the arrangement of the spots on a diffraction pattern is able to give us. We cannot know the distances between the adsorbate and the substrate atoms, or, we are not able to learn anything about the distances between the different layers of the clean surface. Looking at figure 10 we will see that the different spots have different sizes, and the different spots correspond to elastically scattered electron beams with different intensities. This is the key observation to make, because this difference in the intensities containes all the information we cannot get just by looking at their arrangement. There are three kinds of information one can get out of the intensities, depending on the manner of their measurement.

I-θ **curves** By measuring the intensities I as a function of the emergence angle of the scattered beams, we can determine the so-called *instrumental response function.*
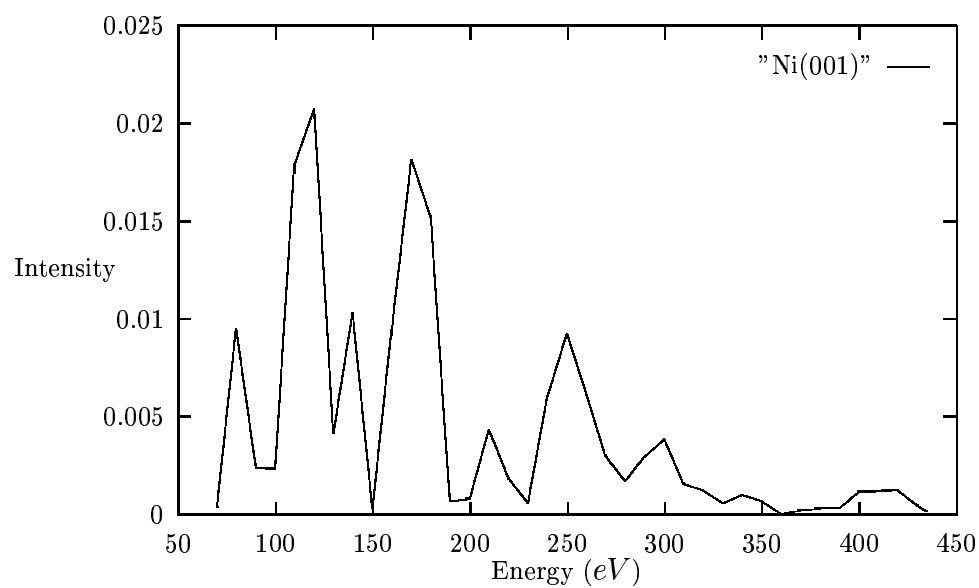
Figure 11: *I-V* curve of the 00 beam from Ni(001) surface
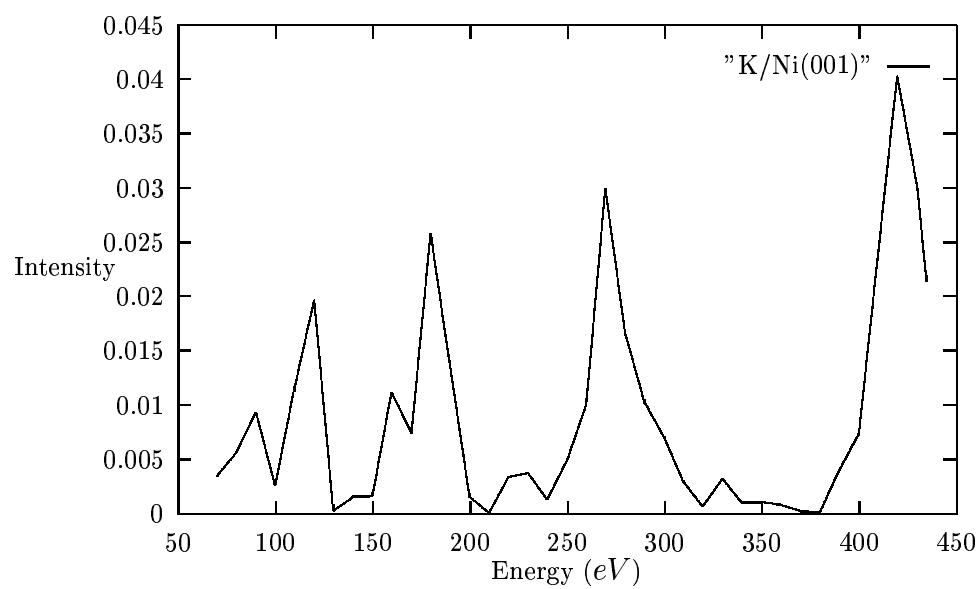
Figure 12: *I-V* curve of the 00 beam from K/Ni(001) surface

Exactly because we use instruments for the experiment that they are not perfect and because we deal with specimen surfaces that are not also perfect, rigid and infinite, we need a tool to calculate how much we are off the perfect conditions. This tool is the instrumental response function.

I-T **curves** Here the intensity of the beams is measured as a function of the temperature of the sample. We make use of these diagrams (curves) in the case that we need to measure the Debye temperature of the used crystal.

I-V **curves** These are the curves that contain all the information we described a few lines above. They are the most important and can be seen in any LEED paper. Here, we measure the intensity of the beams with respect to the energy of the incident electrons (actually, with respect to the accelerating voltage). Two examples of theoretically calculated *I-V* curves can be seen in figure 11 where we see the behavior of the specular (00) beam diffracted off a nickel sample with orientation (001) and in figure 12 where we look at the same beam diffracted off the same surface on which we had disordered adsorption of potasium.

2.3   Theory of LEED

Thus far we have seen how we perform a typical LEED experiment. We discussed what kind of information the experimentalist can get out of the diffraction pattern, that is, the kind of unit cell or whether reconstruction of the substrate atoms or of the adsorbate atoms or molecules took place. We also emphasized on the fact that by

just the appearance of the pattern we are unable to find out about the distances of the atoms in the different layers, or those between the substrate and overlayer atoms. This information can be extracted out of the study of the scattered beams intensity as a function of the kinetic energy of the incident electrons. Next we are going to examine the theory of LEED. We need a model that will be able to predict the *I-V* curves the experiment gives us. We will have to follow the path an incident electron takes before and after its scattering with a surface atom. There are two approaches we will explore. The so-called *kinematic* or *single scattering* approximation, according to which an electron gets scattered by only one surface atom and then travels toward the detector and the *dynamical* or *multiple scattering* approximation according to which the electron undergoes more than one scattering from the surface atoms before it emerges from the surface on its way to the fluorescent screen.

Before we immerse ourselves into examining those two approximations we will look at an important approximation of conventional LEED theory; the *muffin-tin potential*.

2.3.1 The muffin-tin potential

On entering the surface region the electron feels the presense of the inner potential. This is created by the core electrons and the nucleus of its surface atoms, as well as the valence and the conduction electrons. Of course, this kind of combination should result in an extremely complicated potential that should depend on the form of the unit cell. It would have been inconvenient to employ such a complicated potential in the Schröndiger equation. Thus we implement a simpler form of potential. After years
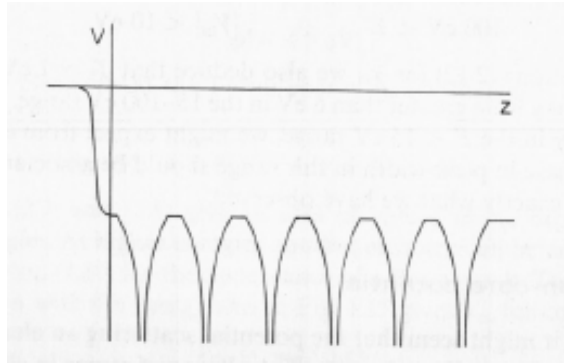
Figure 13: The muffin-tin potential (side view)
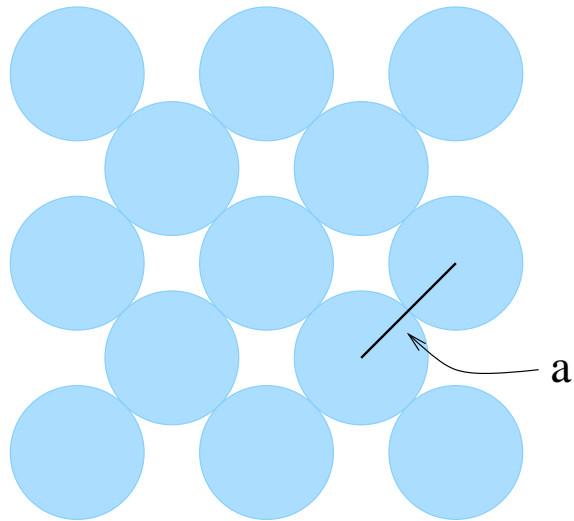
Figure 14: The muffin-tin potential (top view). a is the interatomic distance. The radius of the sphere is $a/2$.

of testing, people have accepted that the potential seen in figure 13 is close to the real one for many materials, especially, the close-packed metals. This potential is called, *the muffin-tin potential* due to its shape. To get a physical realization of the muffin-tin potential let us draw imaginary spheres around each individual surface atom in a manner that they will not overlap with any neighboring spheres, as figure 14 clearly shows (this construction determines the radius of the spheres, being equal to 1/2 of the interatomic distance). Within the spheres the potential is spherically symmetric, but outside it is considered constant. In LEED we measure all energies with respect to this constant value of the inner potential.

2.3.2   The Kinematic Theory

As we said in the introduction of this section, in the kinematic or single scattering approximation we consider that each incident electron undergoes only one elastic scattering with a surface atom and then travels towards the fluorescent screen. This would happen if the absorption of the electrons by the crystal is so strong as to not allow them to be multiply scattered. Then only a small percentage of them undergoes a second scattering. An electron, upon entering the crystal, finds itself immersed in the potential of the conduction and valence electrons; this increases its kinetic energy. Then it finds itself surrounded by the ion cores (or muffin-tin) potential. The flat part of the potential between the muffin-tin spheres can be represented by a constant V_o which has a real part, V_{or}, and an imaginary one, V_{oi}, which is responsible for the dying out of the electron wave as proceeds deeper into the crystal.
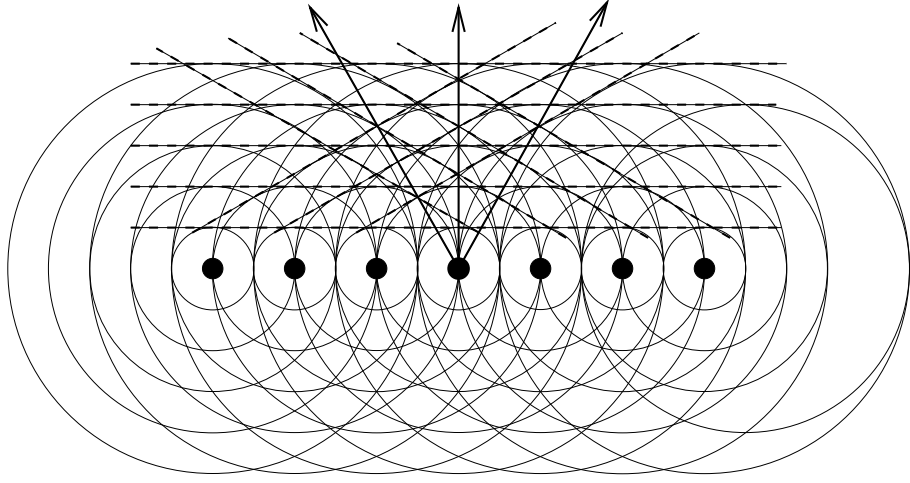
Figure 15: Diffraction of electrons in one-dimension

We will try to calculate the amplitude of the diffracted wave in the one-dimension case

of figure 15, where we have used the Huyghens' construction to visualize the diffraction

proccess.

Let the incident electron be represented by:

$$\phi(\vec{r}) = B e^{i\vec{k}_i \cdot \vec{r}}$$
(1)

its energy being $E = (1/2)k_i^2$. Coming across the inner potential, V_o, it is partially

reflected by and partially transmitted through it. If the coefficient of reflection is R

then the reflected wave will be given by:

$$R B e^{i\vec{k}_s \cdot \vec{r}}$$
(2)

where, $\vec{k}_{s\parallel} = \vec{k}_{i\parallel}$. The transmitted wave will have wave vector $\vec{k}$ with $E - V_o = (1/2)k^2$. Its surface parallel component will remain the same whereas the perpendic-

ular z-component will be complex due to the imaginary part of V_o. Thus, if T^+ is the
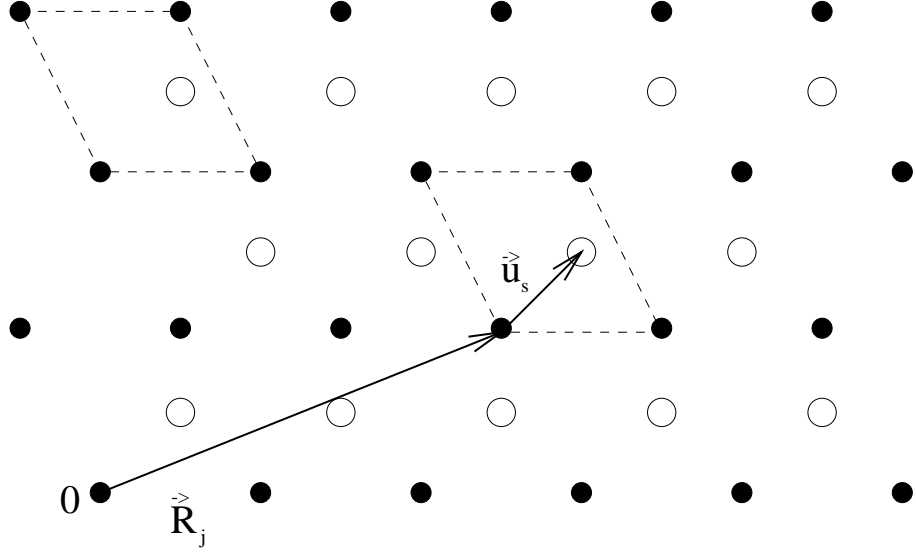
Figure 16: Identifying an atom in a unit cell

transmission coefficient, the plus sign indicating the unchanged direction of traveling, this is represented by:

$$T^+(\vec{k})Be^{i\vec{k}\cdot\vec{r}} \tag{3}$$

with $\vec{k}_{\parallel} = \vec{k}_{i\parallel}$ and $k_z = ((2E - 2V_{or} - k_{i\parallel}^2) - i2V_{oi})^{1/2}$. Let the transmitted wave be incident on the s atom of the jth unit cell of one of the layers that the sample is made up. As it can be seen in figure 16, choosing an origin in this layer we can identify the unit cell with the vector $\vec{R}_j$ and the atom within it with the position vector $\vec{R}_j + \vec{u}_s$. So, the transmitted wave at the atom s will have the form:

$$T^+(\vec{k})Be^{i\vec{k}\cdot(\vec{R}_j+\vec{u}_s)} \tag{4}$$

which will be scattered by it resulting in:

$$T^+(\vec{k})Be^{i\vec{k}\cdot(\vec{R}_j+\vec{u}_s)}\chi[\vec{r} - (\vec{R}_j + \vec{u}_s)] \tag{5}$$

where:

$$\chi(\vec{r}) = \sum_{\ell}(2\ell+1)P_{\ell}(\cos\theta)\sin(\delta_{\ell}(s))e^{i\delta_{\ell}(s)}i^{\ell+1}h_{\ell}^{(1)}(kr) \qquad (6)$$

and:

$$\cos\theta = \frac{\vec{k}\cdot\vec{r}}{kr} \qquad (7)$$

To get (5) and (6) we have employed the theory for scattering from a spherical potential. Summing over all the atoms and all the unit cells we will have for the scattering wave off the layer:

$$\phi_{\text{scatt}} = \sum_{js} T^{+}B e^{i\vec{k}\cdot(\vec{R}_{j}+\vec{u}_{s})}\chi(\vec{r}-\vec{R}_{j}-\vec{u}_{s}) \qquad (8)$$

Since what we observe on the fluorescent screen is beams of scattered electrons we will have to express (8) in this kind of form. Thus, we write the scattering wave as a sum of plane waves:

$$\phi_{\text{scatt}} = \sum_{\vec{k}} b_{k}e^{i\vec{k}\cdot\vec{r}} \qquad (9)$$

with b_k to be coefficients that we will try to determine. Towards this task, let us multiply ϕ_{scatt} with $\exp(-i\vec{k}'\cdot\vec{r})$ and integrate over the entire layer area; thus:

$$\begin{aligned}
\int \phi_{\text{scatt}}e^{-i\vec{k}'\cdot\vec{r}}d\vec{r}_{\|} &= \int\sum_{\vec{k}}b_{k}e^{i(\vec{k}-\vec{k}')\cdot\vec{r}}d\vec{r}_{\|}\\
&= \sum_{\vec{k}}b_{k}e^{i(k_{z}-k'_{z})z}\int e^{i(\vec{k}_{\|}-\vec{k}'_{\|})\cdot\vec{r}_{\|}}d\vec{r}_{\|}
\end{aligned} \qquad (10)$$

But:

$$\int e^{i(\vec{k}_{\|}-\vec{k}'_{\|})\cdot\vec{r}_{\|}}d\vec{r}_{\|} = \begin{cases} 0 & \text{if } \vec{k}_{\|} \neq \vec{k}'_{\|} \\ N^{2}A & \text{if } \vec{k}_{\|} = \vec{k}'_{\|} \end{cases} \qquad (11)$$

as it can be easily seen, where N^2 is the number of unit cells and A is the area illuminated

by the incident beam. Thus, we obtain from (10):

$$b'_k = \frac{1}{N^2 A} \int \phi_{\text{scatt}} e^{i\vec{k}' \cdot \vec{r}} d\vec{r}_{\|} \tag{12}$$

Substituting (8) into (12) we get:

$$
\begin{aligned}
b'_k &= \frac{1}{N^2 A} \sum_{js} \int T^+ B e^{i\vec{k}\cdot(\vec{R}_j + \vec{u}_s)} \chi(\vec{r} - \vec{R}_j - \vec{u}_s) e^{i\vec{k}'\cdot\vec{r}} d\vec{r}_{\|} \\
&= \frac{T^+ B}{A} \int \sum_{js} e^{i\vec{k}\cdot(\vec{R}_j + \vec{u}_s)} \chi(\vec{r}'') e^{-i\vec{k}'\cdot(\vec{r}'' + \vec{R}_j + \vec{u}_s)} d\vec{r}''_{\|} \\
&= \frac{T^+ B}{A} \left(\frac{1}{N^2} \sum_j e^{i(\vec{k} - \vec{k}')\cdot\vec{R}_j} \right) \left(\sum_s e^{i(\vec{k} - \vec{k}')\cdot\vec{u}_s} \right) \left(\int \chi(\vec{r}'') e^{-i\vec{k}'\cdot\vec{r}''} d\vec{r}''_{\|} \right)
\end{aligned}
\tag{13}
$$

where we have used: $\vec{r}'' = \vec{r} - \vec{R}_j - \vec{u}_s$. $\vec{R}_j$ is a vector always parallel to the surface. Taking account of this, using the fact that any vector identifying a unit cell can be written as an combination of two unit vectors, namely, $\vec{R}_j = \ell\vec{a} + m\vec{b}$, and having seen from the previous section that the parallel components of the wavevectors differ by quanta of the reciprocal vector, that is, $\vec{k}_{\|} - \vec{k}'_{\|} = n\vec{g}$, the first sum becomes:

$$
\begin{aligned}
\frac{1}{N^2} \sum_j e^{i(\vec{k} - \vec{k}')\cdot\vec{R}_j} &= \frac{1}{N^2} \sum_j e^{i(\vec{k}_{\|} - \vec{k}'_{\|})\cdot\vec{R}_j} \\
&= \frac{1}{N^2} \sum_{m\ell} e^{in\vec{q}\cdot(\ell\vec{a} + m\vec{b})} \\
&= \frac{1}{N^2} \sum_{\ell=0}^{N-1} e^{in\ell\vec{q}\cdot\vec{a}} \sum_{m=0}^{N-1} e^{inm\vec{q}\cdot\vec{b}} \\
&= \frac{1}{N^2} \frac{1 - \exp(niN(\vec{q}\cdot\vec{a}))}{1 - \exp(i\vec{q}\cdot\vec{a})} \frac{1 - \exp(iN(n\vec{q}\cdot\vec{b}))}{1 - \exp(i\vec{q}\cdot\vec{b})} \\
&= S(\vec{q})
\end{aligned}
\tag{14}
$$

Of course $S(\vec{q} = \vec{g}) = 1$. In the above calculation we used the identity:

$$\sum_{n=0}^{N-1} e^{na} = \frac{1 - \exp(Na)}{1 - \exp(a)} \tag{15}$$

The integral in (13) is calculated in the Pendry's book on LEED[?] and we can take it from there as:

$$\int \chi(\vec{r}')e^{-\imath \vec{k}'\cdot\vec{r}}d\vec{r}_{\parallel} = \frac{2\pi\imath}{kk_z'}\sum_{\ell}\sin\delta_{\ell}(s)e^{\imath\delta_{\ell}(s)}P_{\ell}\left(\frac{\vec{k}\cdot\vec{k}'}{kk'}\right) \tag{16}$$

Eventually the coefficient b_k take the form:

$$b_k = M(\vec{k},\vec{k}')T^+B \tag{17}$$

with,

$$M(\vec{k},\vec{k}') = S(\vec{q})\frac{2\pi\imath}{Akk_z'}\sum_{s\ell}(2\ell+1)\sin\delta_{\ell}(s)e^{\imath\delta_{\ell}(s)}P_{\ell}\left(\frac{\vec{k}\cdot\vec{k}'}{kk'}\right)e^{\imath(\vec{k}-\vec{k}')\cdot\vec{u}_s} \tag{18}$$

The treatment so far has led us into finding the scattered electron wave from one of the layers of the crystal. Next, we will try to calculate the overall scattering wave from all layers. We will start for simplicity by considering that the crystal is made up of equidistant layers, the distance between them being c. Then the incident wave on the nth layer will have the form:

$$e^{n\imath\vec{k}\cdot\vec{c}}T^+Be^{\imath\vec{k}\cdot(\vec{r}-n\vec{c})} \tag{19}$$

Following the same procedure we did for the one layer case, we can infer that the scattering wave from all layers will be:

$$
\begin{aligned}
\sum_{\vec{k}'}\sum_{n=0}^{\infty}M(\vec{k},\vec{k}')e^{n\imath\vec{k}\cdot\vec{c}}T^+Be^{\imath\vec{k}'\cdot(\vec{r}-n\vec{c})} &= \sum_{\vec{k}'}T^+BM(\vec{k},\vec{k}')e^{\imath\vec{k}'\cdot\vec{r}}\left(\sum_{n=0}^{\infty}e^{n\imath(\vec{k}-\vec{k}')\cdot\vec{c}}\right) \\
&= \sum_{\vec{k}'}T^+BM(\vec{k},\vec{k}') \\
&\times \frac{1}{1-\exp(\imath(\vec{k}-\vec{k}')\cdot\vec{c})}e^{\imath\vec{k}'\cdot\vec{r}} \tag{20}
\end{aligned}
$$

This scattered wave on its way out of the crystal is transmitted one more time through
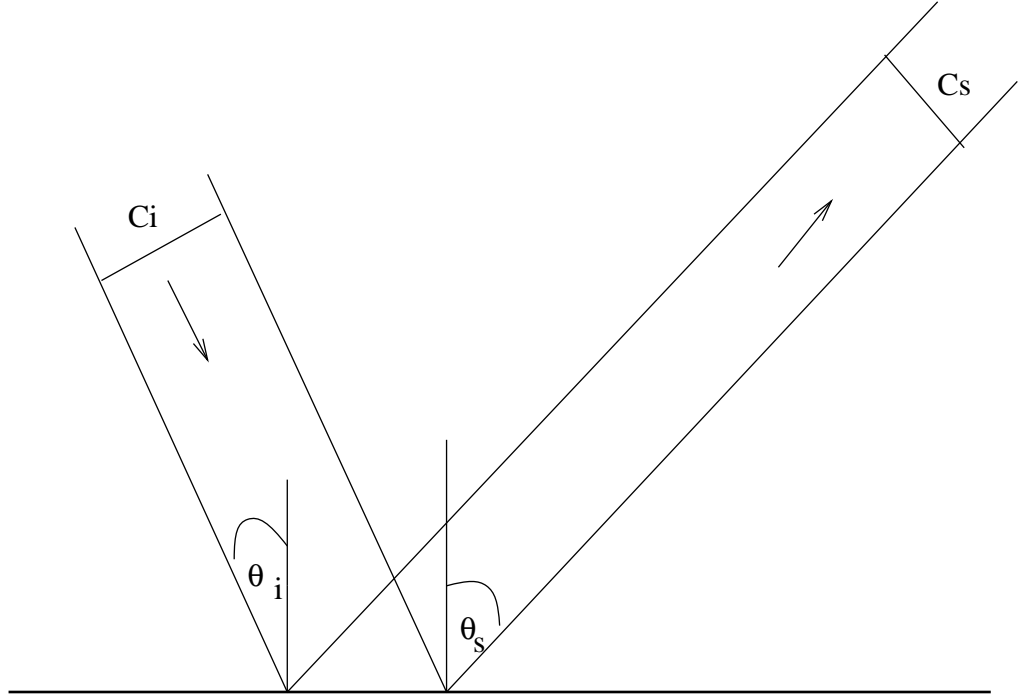
Figure 17: Cross section of incident and diffracted beams

the potential created by the valence/conduction electrons. The coefficient of this transmission is $T^-(\vec{k}')$. This scattered wave along with the one reflected initially will be what we will observe as a spot on the fluorescent screen; this wave will be:

$$\sum_{\vec{k}'} B \left\{ R\delta_{\vec{k}'_\parallel \vec{k}_\parallel} + T^+(\vec{k})T^-(\vec{k}')M(\vec{k},\vec{k}') \frac{1}{1 - \exp(\imath(\vec{k} - \vec{k}') \cdot \vec{c})} \right\} \qquad (21)$$

Equation (21) is the amplitude of the diffracted beam. In the experiment we measure the flux of the electron beam which is propotional to square of the absolute value of the amplitude. We are interested in the ratio of the fluxes for the incident and the diffracted beam, that is: I_i/I_s. This is equal to the ratio of the square of the two amplitudes, $|Inc|^2/|Scat|^2$, which, according to the figure 17 is equal to $\cos\theta_i/\cos\theta_s$. In

other words:

$$\frac{I_i}{I_s} = \frac{|Inc|^2}{|Scat|^2} = \frac{\cos\theta_i}{\cos\theta_s} \tag{22}$$

Let us try to analyze equation (21). First off, $\vec{k} - \vec{k'} = \vec{q}$ is the momentum transfer in the system of the atomic units we are using. Secondly, if $\vec{q}$ were real then the third Bragg condition to which the diffraction of the X-rays from a crystal obeys, that is, $\vec{q}\cdot\vec{c} = 2n\pi$, with n integer, would hold. But that would result in zeroing the denominator in the fraction, and, concequently, in giving very sharp peaks. However, in reality this is not the case, since $\vec{q}$ is complex due to the partial absorption of the beams. Thus we do not observe sharp diffraction beams but smoother ones. The denominator plays a very important role in giving us structure information of the surface, because, although it does not produce the delta-function-like peaks, nevertheless, the ones that we get are still centered on the Bragg conditions. Let us explore this term further. We write:

$$\begin{aligned}
D &= \frac{1}{1 - \exp(\imath\vec{q}\cdot\vec{c})} \\
&= \frac{1}{1 - \exp(\imath(\vec{q}_r + \imath\vec{q}_i)\cdot\vec{c})} \\
&= \frac{1}{1 - \exp(\imath\vec{q}_r\cdot\vec{c})\exp(-\vec{q}_i\cdot\vec{c})}
\end{aligned} \tag{23}$$

and,

$$|D| = \left\{\frac{1}{1 + \exp(-2\vec{q}_i\cdot\vec{c}) - 2\exp(-\vec{q}_i\cdot\vec{c})\cos(\vec{q}_r\cdot\vec{c})}\right\}^{1/2} \tag{24}$$

where, $\vec{q} = \vec{q}_r + \imath\vec{q}_i$ and, since $\vec{k}_{\parallel} = \vec{k'}_{\parallel}$ and $k_z = -k'_z = (2E - 2V_o)^{1/2}$:

$$\vec{q}_r = 2\hat{z}\sqrt{E - V_{or}}\left\{\left[1 + \left(\frac{V_{oi}}{E - V_{or}}\right)^2\right]^{1/2} + 1\right\}^{1/2} \tag{25}$$

$$\vec{q}_i = 2\hat{z}\sqrt{E - V_{or}}\left\{\left[1 + \left(\frac{V_{oi}}{E - V_{or}}\right)^2\right]^{1/2} - 1\right\}^{1/2} \tag{26}$$
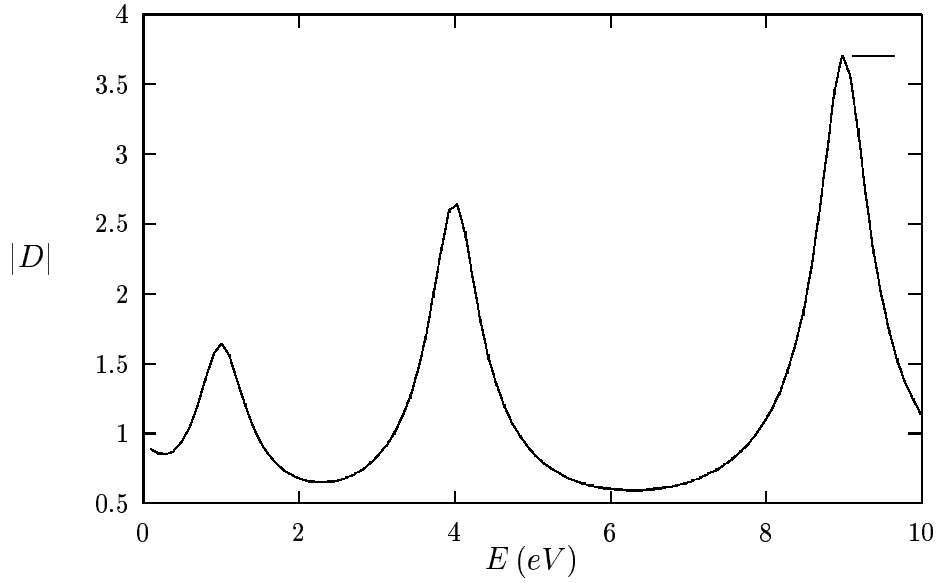
Figure 18: Plot of $|D|$ against energy E

In figure 18 we have plotted $|D|$ as a function of the energy for $V_{or} = -0.5\,a.u., V_{oi} = -0.15\,a.u.$ and $\vec{c} = (0, 0, \pi)\,a.u.$, which, in a way, reminds us a primitive form of the I-V curves of figures 11 and 12.

What we have seen from the discussion above is that in the kinematic theory we should expect I-V curves similar to the ones we would have gotten for X-ray diffraction. Some surfaces behave like that; example of such a case is the (111) surface of fcc xenon crystal[?]. So, for those surfaces, the single scatterning theory suffies to identify them, case that it is not obeyed by the vast majority of them.

2.3.3 The Dynamical Theory

In the previous section we examined the LEED under the light of the kinematic theory. We saw that it is able to help us solve a small number of surface identification problems but rather this is not the rule. The truth is that if we wish to have a thorough picture

of what actually happens during the electron scattering we should migrate into what is called "dynamical or multiple scattering theory". This picture is the realistic one since it is most probable that an electron undergoes more than one scattering from the atoms of the surface.

In this section we will attempt a brief description of this general theory of LEED leaving the reader to look up the details on the two most specialized books of Pendry[?] and van Hove *et al.*[?].

A general introduction

We will go at the simple one-dimensional problem we dealt with in the single scattering case. There we had ended up in a reflected applitude of the form (21). We had emphasized there that in our calculation we would have to take into account a complex inner potential in order to avoid infinite reflection amplitudes, which clearly violates the conservation of the current. Another way to avoid infinite reflected amplitude would be if the incident electron undergoes both a reflection and a transmission. The transmitted electron upon reaching a second layer of atoms will be partially reflected and partially transmitted. The reflected electron, in turn, will be partially transmitted and partially reflected, and this procedure will continue until these byproducts die out. If we wish to be realistic we should take into consideration all reflections in order that we calculate the general reflected electron wave that enters into our detector. We can rewrite (21) as:

$$D^{(1)} = \frac{r}{1 - t^2 \exp(\imath 2kc)} = \frac{r}{1 - |t|^2 \exp(\imath [2kc + \arg(t)])} \tag{27}$$

where r and t are the reflection and transmission coefficients respectively and in (27) we have taken into account that both of them are complex numbers with amplitudes less than 1 and written for t, $t = |t| \exp(\imath \arg(t))$. From (27) we see that in order that we have Bragg scattering $2kc + 2 \arg(t) = 2n\pi$, with n an integer, must hold. What this relation tells us is that the electron's amplitude after having scattered by an atom has been shifted by a phase $\arg(t)$. This is due to the inner potential as well as to the multiple scattering of the electron within the atomic core. This phenomenon makes the peaks in the I-V curves to reduce the intensity they would be expected in the kinematic limit. A simple explanation for that goes as follows. The electron, entering an attractive potential as that of the atom, is accelerated. This shortens its wavelength, since $E + V = 1/2(1/\lambda^2)$. Thus the electron exits the atomic core ahead of its original phase. In order that $2kc + 2 \arg(t) = 2n\pi$ keeps holding, its energy must decrease, causing the shifting to the peaks.

Generalizing the above argument to the three dimensions, we can rewrite (27) as:

$$D^{(3)} = r_{\vec{g}'\vec{g}} \left[1 - t_{\vec{g}'\vec{g}'} t_{\vec{g}\vec{g}} \exp \left(\imath (k_{g'z} + k_{gz})c \right) \right]^{-1} \qquad (28)$$

where now c is the layer separation, $\vec{g}$ is the incident beam and $\vec{g}'$ is the reflected one. In order that we have Bragg scattering,

$$k_{gz}c + \arg(t_{\vec{g}\vec{g}}) + k_{g'z}c + \arg(t_{\vec{g}'\vec{g}'}) = 2n\pi \qquad (29)$$

must hold.

Before we move to a more detailed consideration of the theory we should emphasize on the fact that the diffraction pattern that we get in LEED does not depend on the

way of scattering. No matter whether we use single or multiple scattering to describe the path the electron beams follow, the pattern remains the same. What changes is the intensity of each particular spot and not its position. This happens because the direction of the scattered beams depend only on the relative phases of the reflected waves, which, in turn, depend only on the two dimensional unit cell of the crystal.

The general theory

Before we immerse ourselves into the details of the general theory we should state the steps one has to follow in order to understand the mechanisms involved. The first thing we should do is to remember the way an electron is scattered by a single atom. In this case we saw that the best way to represent the wavefunction of the electron is through spherical waves, since we have assumed that the potential within any atomic core follows spherical variation. After that we should try to describe the scattering between cluster(s) of atoms. In that case the wave function will have the simple form of a plane wave since we deal with the assumed constant potential in the space between the atoms. The last part should include scattering between layers of atoms and stacks of such layers perpendicular to the surface. There the Bloch wave representation is the best mathematical tool to describe the electrons. Besides, this is the general solution to the Schrödinger equation along with the Bloch condition for a periodic potential.

In LEED energies, forward scattering tends to be stronger than backscattering. So, a consistent dynamical theory has to include as many as possible scatterings of the former kind and a small number of the latter one.

As we said in the preamble of this section, we will start describing the scattering of the electrons from the simplest case, that between two atoms, and continue entering into the scene more complicated forms, like, scattering between the atoms of a plane, between two planes, between a layer of planes and finally between a stack of layers, following the KKR (Korringa-Kohn-Rostocker) [**?**, **?**] method and its application to LEED.

Let us start with the simplest case which consists of two atoms. We will attempt to calculate the amplitude of an emerging wave after having multiply scattered between them. Until we specifically mention it we will be making use of the spherical waves. Let us follow a wave, angular momentum $L' = (\ell', m')$ as is incident on the atom 1 at position $\vec{r}_1$. It is scattered towards the atom 2 at position $\vec{r}_2$ with respect to which it acquires angular momentum $L = (\ell, m)$. The amplitude of this new wave will be given by the following Green's function:

$$G^{21}_{LL'} = -4\pi i \frac{2m}{\hbar^2} k \sum_{L_1} i^{\ell_1} a(L, L', L_1) h^{(1)}_{\ell_1}(k|\vec{r}_2 - \vec{r}_1|) Y_{L_1}(\vec{r}_2 - \vec{r}_1) e^{-i\vec{k}_{\text{in}} \cdot (\vec{r}_2 - \vec{r}_1)} \qquad (30)$$

where, $L_1 = (\ell_1, m_1)$ satisfy $|\ell - \ell'| \leq \ell_1 \leq \ell + \ell'$ and $m_1 = m + m'$, whereas:

$$a(L, L', L_1) = \int Y^*_L(\Omega) Y_{L_1}(\Omega) Y^*_{L_1}(\Omega) d\Omega \qquad (31)$$

the Clebsch-Gordan coefficients and the integral in Ω is over all values of solid angle. $h^{(1)}_{\ell_1}$ are the Hankel functions of the first kind, Y_{L_1} are the spherical harmonics and $\exp[-i\vec{k}_{\text{in}} \cdot (\vec{r}_2 - \vec{r}_1)]$ is the phase shift to the amplitude between the two positions. We have seen that the scattering off an atom is characterized by the t-matrix and the product of the Green's function with it, $G^{21}_{LL'} t^1_{\ell'}$, expresses the fact that a wave, L', incident on atom 1 is scatted off it and through the Green's function to a wave L incident on atom
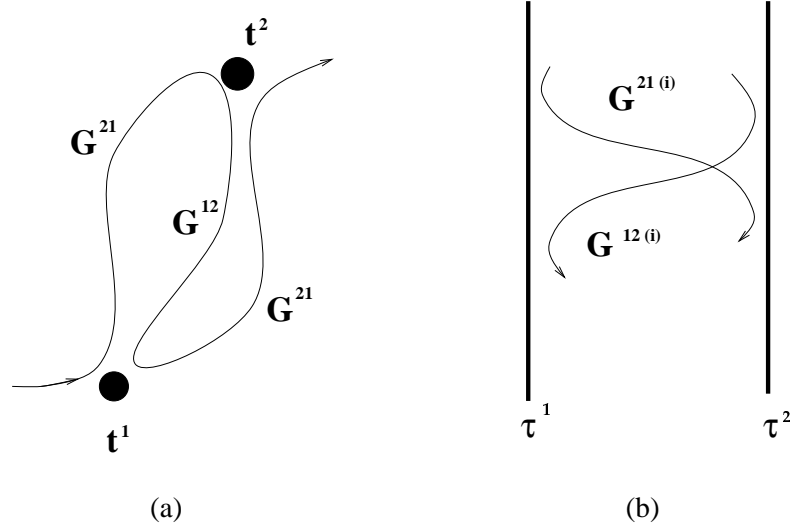
Figure 19: Multiple scattering between two atoms (a) and two planes of atoms (b)

2. Likewise,$G^{12}_{L''L}t^2_\ell$ expresses that fact that wave L incident on atom 2 is scattered by it and is incident in atom 1 with angular momentum L''. Thus, if we combine these two mechanisms we can take into consideration all possible (infinite in number) scatterings between the two atoms. For, example the combination: $t^2 G^{21} t^1 G^{12} t^2 G^{21} t^1$, describes the double scattering of figure 19(a). The reading of such an expression begins from the right to the left where we have summed over all possible angula momenta thus dropping the indices.

Next, let us consider all possible paths that terminate on atom 1 and all possible paths that terminate on atom 2, and let us add them up, separately for each atom. The result will be:

$$T^1 \; = \; t^1 + t^1 G^{12} t^2 + t^1 G^{12} t^2 G^{21} t^1 + t^1 G^{12} t^2 G^{21} t^1 G^{12} t^2 + \dots \tag{32}$$

$$T^2 \; = \; t^2 + t^2 G^{21} t^1 + t^2 G^{21} t^1 G^{12} t^2 + t^2 G^{21} t^1 G^{12} t^2 G^{21} t^1 + \cdots \tag{33}$$

or, as it can be easily seen if in each expression we keep the first and factorize out the part $t^{1,2}G^{12,21}$ of the second term:

$$T^1 = t^1 + t^1 G^{12} T^2 \tag{34}$$

$$T^2 = t^2 + t^2 G^{21} T^1 \tag{35}$$

This system can take the following form:

$$
\left.
\begin{aligned}
T^1 - t^1 G^{12} T^2 &= t^1 \\
-t^2 G^{21} T^1 + T^2 &= t^2
\end{aligned}
\right\}
\Rightarrow
\begin{pmatrix} I & -t^1 G^{12} \\ -t^2 G^{21} & I \end{pmatrix}
\begin{pmatrix} T^1 \\ T^2 \end{pmatrix}
=
\begin{pmatrix} t^1 \\ t^2 \end{pmatrix}
\tag{36}
$$

$$
\begin{pmatrix} T^1 \\ T^2 \end{pmatrix}
=
\begin{pmatrix} I & -t^1 G^{12} \\ -t^2 G^{21} & I \end{pmatrix}^{-1}
\begin{pmatrix} t^1 \\ t^2 \end{pmatrix}
\tag{37}
$$

which can be solved easily with the help of a computer program. The dimensions of the matrices involved, I, G, T and t, are $(\ell_{\max} + 1)^2$, where $\ell_{\max}$ is the maximum value of the angular momentum according to the discussion in appendix A.

Following the above discussion for two atoms we can get a general formula for N atoms. In that case the matrix equation to be solved will be similar to (37) and have the form:

$$
\begin{pmatrix} T^1 \\ T^2 \\ T^3 \\ \vdots \\ T^N \end{pmatrix}
=
\begin{pmatrix}
I & -t^1 G^{12} & -t^1 G^{13} & \cdots & -t^1 G^{1N} \\
-t^2 G^{21} & I & -t^2 G^{23} & \cdots & -t^2 G^{2N} \\
\vdots & \vdots & \vdots & \vdots & \vdots \\
-t^N G^{N1} & -t^N G^{N2} & -t^N G^{N3} & \cdots & I
\end{pmatrix}^{-1}
\begin{pmatrix} t^1 \\ t^2 \\ t^3 \\ \vdots \\ t^N \end{pmatrix}
\tag{38}
$$

The solution of (38) will give us the quantities T^i that will be added together in order to get the general scattering amplitude. If the incident wave had wave number $\vec{k}_{\text{in}}$ then

the multiple scattering of the N atoms will produce an outgoing wave of wave number $\vec{k}_{\text{out}}$ and amplitude:

$$T_{LL'} = \sum_{i=1}^{N} e^{\imath(\vec{k}_{\text{in}} - \vec{k}_{\text{out}}) \cdot \vec{r}_i} T_{LL'}^i \tag{39}$$

So far we have not used the fact that we are dealing with a periodic plane of identical atoms. By taking that into consideration we can simplify our formulae and calculations as follows. Since the atoms are identical they will scatter identically. This means that in the matrix equation produced previously, (38), $t^1 = t^2 = \cdots = t$. If we add to the identity feature of the atoms the periodicity of the Bravais (one atom per unit cell) plane we can argue that the diffraction of a wave incident on one of the atoms is identical to the diffraction of an identical wave incident on a different atom. This second argument will lead us to write: $T^1 = T^2 = \cdots = \tau$. Attempting to write down expressions like (32) or (33) for N atoms per plane and with the aforesaid properties we will get:

$$\tau = t + t \left(\sum_{n}{}' G^{in} \right) \tau \tag{40}$$

where $n = 1, 2, \cdots, i - 1, i + 1, \cdots$, hence the prime on the summation symbol. The Green's function now takes the form:

$$
\begin{aligned}
G_{LL'}^{ii} &= \sum_{n}{}' G_{LL'}^{in} = -4\pi \imath \frac{2m}{\hbar^2} k \\
&\times \sum_{L_1} \sum_{\vec{P}}{}' \imath^{\ell_1} a(L, L', L_1) h_{\ell_1}^{(1)}(k|\vec{P}|) Y_{L_1}(\vec{P}) e^{-\imath \vec{k}_{in} \cdot \vec{P}}
\end{aligned} \tag{41}
$$

with $\vec{P}$ being the position of each atom with respect to an origin at $\vec{P} = 0$ which we do not include in the summation being reminded by the prime on the sum symbol. Thus, the matrix equation (38) is reduced to:

$$\tau = t(1 - G^{ii}t)^{-1} \tag{42}$$

the solution of which will give us the amplitude of the scattered wave $\tau_{LL'}$ with angular momentum L from all the atoms of the Bravais-lattice plane. Again, the matrices involved have dimensions $(\ell_{\max} + 1)^2$.

Working the same way we did in the simple case of the two atoms, we may consider the scattering between two Bravais-lattice planes. And we can go one step further and assume that the atoms of one of the planes are different in kind than those of the other one. In that case we will have τ^1 and τ^2 scattering matrices for the two kinds of atoms. Again, denoting by T^1 the paths ending at an atom of plane 1 and T^2 those teminating at an atom of plane 2, we can write:

$$T^1 = \tau^1 + \tau^1 \sum_{(i)} G^{12(i)} T^2 \tag{43}$$

$$T^2 = \tau^2 + \tau^2 \sum_{(i)} G^{21(i)} T^1 \tag{44}$$

(43), for example, consists of all the multiple scatterings within plane 1 and all the paths that terminate at any atom i of plane 2 and then propagated to any atom of plane 1. We can say something similar about (44); figure 19(b) illustrates schematically the two paths. Then by having:

$$G^{12} = \sum_{(i)} G^{12(i)} \text{ and } G^{21} = \sum_{(i)} G^{21(i)} \tag{45}$$

we can write down an expression similar to (37):

$$\begin{pmatrix} T^1 \\ T^2 \end{pmatrix} = \begin{pmatrix} I & -\tau^1 G^{12} \\ -\tau^2 G^{21} & I \end{pmatrix}^{-1} \begin{pmatrix} \tau^1 \\ \tau^2 \end{pmatrix} \tag{46}$$

The above expression can be generalized for N planes to:

$$
\begin{pmatrix} T^1 \\ T^2 \\ T^3 \\ \vdots \\ T^N \end{pmatrix} = \begin{pmatrix} I & -\tau^1 G^{12} & -\tau^1 G^{13} & \cdots & -\tau^1 G^{1N} \\ -\tau^2 G^{21} & I & -\tau^2 G^{23} & \cdots & -\tau^2 G^{2N} \\ \vdots & \vdots & \vdots & \vdots & \vdots \\ -\tau^N G^{N1} & -\tau^N G^{N2} & -\tau^N G^{N3} & \cdots & I \end{pmatrix}^{-1} \begin{pmatrix} \tau^1 \\ \tau^2 \\ \tau^3 \\ \vdots \\ \tau^N \end{pmatrix}
\tag{47}
$$

Now, the Green's function takes on the form:

$$
\begin{aligned}
G_{LL'}^{ji} &= -4\pi i \frac{2m}{\hbar^2} k \sum_{L_1} \sum_{\vec{P}} {}' i^{\ell_1} a(L, L', L_1) h_{\ell_1}^{(1)}(k|\vec{r}_j - \vec{r}_i + \vec{P}|) \\
&\times Y_{L_1}(\vec{r}_j - \vec{r}_i + \vec{P}) e^{-i\vec{k}_{\text{in}} \cdot \vec{P}}
\end{aligned}
\tag{48}
$$

Solving (47) we will get the $T_{LL'}^i$'s. Then using (39) we will get the amplitude of the electron scattered, from N planes. The number N of the planes that we have to use in our calculations is determined by following the rule: We will include all those planes the last of which is not deeper than a few times the electron mean free path length.

Up until this point we have used spherical waves to calculate the different stages of multiple scattering, from that between two atoms to the one between atoms of different planes. As we mentioned before, the beam that reaches the fluorescent screen can be represented by a simple plane wave. We also said that in the space between the atoms, exactly because of the constant character of the potential, we can keep using plane wave representation. Thus, one of our final tasks would be to tranform the amplitudes of the spherical waves we have calculated so far to that for the plane waves. We have dealt with this problem in the kinematic theory and here we will reproduce the results we found then. So, a plane wave with wave number $\vec{k}_{\text{in}}$ and angular momentum L' is incident on

a sample and is scattered to a wave with wave number $\vec{k}_{out}$ and angular monentum L which has amplitude:

$$M_{\text{out,in}} = -\frac{16\pi^2 m\imath}{Ak_{\text{out}z}\hbar^2} \sum_{LL'} Y_L(\vec{k}_{\text{out}})t_{LL'}Y_{L'}^*(\vec{k}_{\text{in}}) \tag{49}$$

This relation is able to give us an exact solution for the amplitude of the diffracted wave, but the calculations are very tedious even in the case that we use $\ell_{\max} = 4$ and $N = 5$ number of planes rending the dimensions of the matrices to be $N(\ell_{\max} + 1)^2$, or 125. To improve the timing instead of considering a number of planes that will depend on the electron mean free path length we use sets of any number of planes that we call *layers*. This choice improves the calculation time dramatically. In the case of a layer with one only atomic plane and considering any plane wave $\vec{k}_g^{\pm}$ incident on it, in order to determine the matrix $M_{gg'}^{\pm\pm}$ of any diffracted wave $\vec{k}_{g'}^{\pm}$, we will have:

$$M_{gg'}^{\pm\pm} = -\frac{16\imath\pi^2 m}{Ak_{gz}^+\hbar^2} \sum_{LL'} Y_L(\vec{k}_{g'}^{\pm})\tau_{LL'}Y_{L'}^*(\vec{k}_g^{\pm}) \tag{50}$$

In the case of a layer with N planes and hence N atoms at position $\vec{r}_i$ (since each plane is Bravais-lattice plane it will have one atom per unit cell), $M_{gg'}^{\pm\pm}$ takes on the form:

$$\begin{aligned} M_{gg'}^{\pm\pm} &= -\frac{16\imath\pi^2 m}{Ak_{g'z}\hbar^2} \sum_{LL'} Y_L(k_{g'}^{\pm}) \\ &\quad \times \sum_{i=1}^{N} \left\{ e^{\imath(\pm\vec{k}_g^{\pm}\mp\vec{k}_{g'}^{\pm})\cdot\vec{r}_i} T_{LL'}^i \right\} Y_{L'}^*(\vec{k}_g^{\pm}) \end{aligned} \tag{51}$$

All the formulae we have given above may be found slightly different in the bibliography, but all of them are equivalent to each other.

Now we have reached the point we may say that we are able to attempt to solve the general LEED problem. We will discuss in brief three methods or three approaches, that
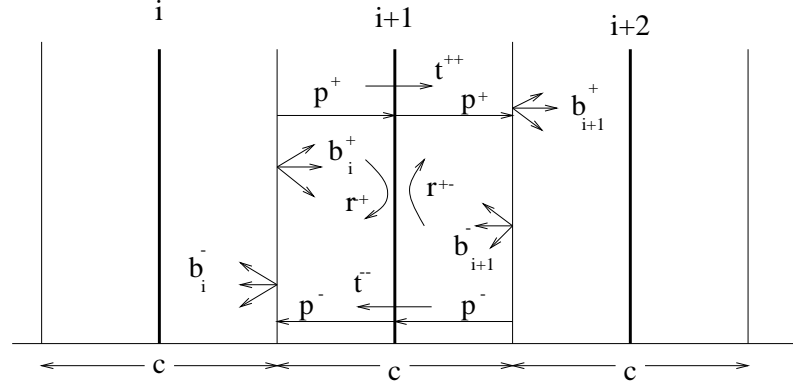
Figure 20: Bloch-wave method: Separation of the subsurface into layers

deal with the scattering between the layers of planes, the last step towards the general solution.

Bloch-Wave method As we mentioned in the introduction of this section, we use Bloch wave representation in the direction perpendicular to the surface for the part of it that has well-defined periodicity. Let us divide the region below the surface, the *subsurface*, into layers $1, 2, \ldots, i-1, i, i+1, \ldots$, as in figure 20. Then the plane wave expansion of the Bloch wave will be given by:

$$\phi_i(\vec{r}) = \sum_g \left\{ b_{ig}^+ e^{i\vec{k}_g^+ \cdot \vec{r}} + b_{ig}^- e^{-i\vec{k}_g^- \cdot \vec{r}} \right\} \tag{52}$$

where symbols are explained in the figure 20. Using the propagator $p_g^\pm = \exp(\pm i\vec{k}_g^\pm \cdot \vec{c}/2)$, we can have for the reflection and transmission coefficients:

$$R_{g'g}^{-+} = p_{g'}^- M_{g'g}^{-+} p_g^+ \tag{53}$$

$$R_{g'g}^{+-} = p_{g'}^+ M_{g'g}^{+-} p_g^- \tag{54}$$

$$T_{g'g}^{++} = p_{g'}^+ M_{g'g}^{++} p_g^+ \tag{55}$$

$$T_{g'g}^{--} = p_{g'}^- M_{g'g}^{--} p_g^-$$ (56)

Looking at the figure we infer that:

$$b_{i+1}^+ = T^{++}b_i^+ + R^{+-}b_{i+1}^-$$ (57)

$$b_i^- = T^{--}b_{i+1}^- + R^{-+}b_i^+$$ (58)

and if $\vec{c}$ is the period of the layers, then from the Bloch condition $\phi(\vec{r}+\vec{c}) = \phi(\vec{r})$ we can get:

$$b_{i+1}^+ = b_i^+ e^{i\vec{k}_B \cdot \vec{c}}$$ (59)

$$b_{i+1}^- = b_i^- e^{i\vec{k}_B \cdot \vec{c}}$$ (60)

where $\vec{k}_B$ is the Bloch wave number that will be found as solution of the system of the four equations (57, 58, 59, 60), which can be written in a readable matrix equation as:

$$\begin{pmatrix} T^{++} & R^{+-} \\ (T^{--})^{-1}R^{-+}T^{++} & -(T^{--})^{-1}R^{-+}R^{-+} + (T^{--})^{-1} \end{pmatrix} \begin{pmatrix} b_i^+ \\ b_{i+1}^- \end{pmatrix} = e^{i\vec{k}_B \cdot \vec{c}} \begin{pmatrix} b_i^+ \\ b_{i+1}^- \end{pmatrix}$$
(61)

Of all the values of $\vec{g}$ involved we will keep only one half, the ones corresponding to the diffracted beams, the other half being accosiated with the transmitted waves. The total reflected function will be a linear combination of Bloch waves in the form of

$$\sum_m a_m \phi_m$$ (62)

This combination consists of waves traveling towards the surface (index (+)) and waves moving away from the surface (index (−)). This combination of waves

has to be matched with the initial incident beam of electrons as well as with the initially reflected electrons. We will give an example of how we work by assuming a suddenly truncated surface with periodic bulk, period $\vec{c}$. The incident part of (62) will have to match the initial incident beam at the surface, that is, at $\vec{r} = 0$; in other words:

$$\sum_m a_m b_{mg}^+ e^{i\vec{k}_g \cdot (\vec{r}=0)} \;=\; e^{i\vec{k}_{\mathrm{in}} \cdot (\vec{r}=0)} \Rightarrow$$

$$\sum_m a_m b_{mg}^+ = \delta_{g0} \tag{63}$$

Similarly, the part of the combination (62) moving away from the surface should have to match with $\sum_g c_g^- \exp(i\vec{k} \cdot \vec{r})$ at the surface giving:

$$\sum_m a_m b_{mg}^- = c_g^- \tag{64}$$

(63) will determine the b_m's and (64) the c_g^-'s. Then we can use the simple relation (22) to calculate the intensities we should expect to measure.

Layer-Stacking and Layer-Doubling method According to this method, we use the results of the diffraction between layers of planes and calculate the scattered wave between a stack of layers.

We start off by calculating the amplitude of the diffracted beam from the stack of two layers, A and B, as in figure 21. Then the transmission and diffraction coefficients will be given by:

$$R^{-+} \;=\; r_A^{-+} + t_A^{--} P^- r_B^{-+} P^+ (I - r_A^{+-} P^- r_B^{-+} P^+)^{-1} t_A^{++} \tag{65}$$

$$T^{++} \;=\; t_B^{++} P^+ (I - r_A^{+-} P^- r_B^{-+} P^+)^{-1} t_A^{++} \tag{66}$$
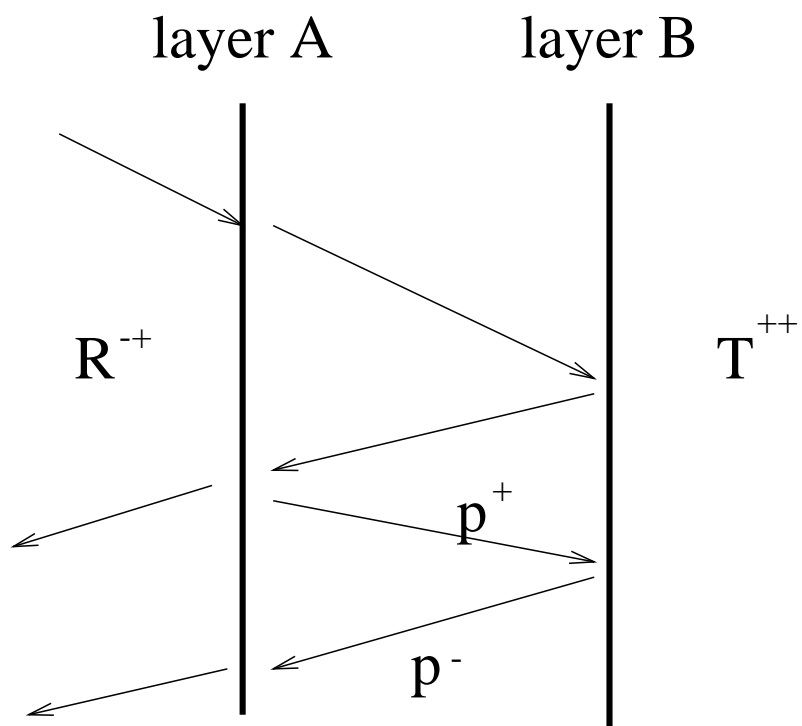
Figure 21: Layer-Stacking method
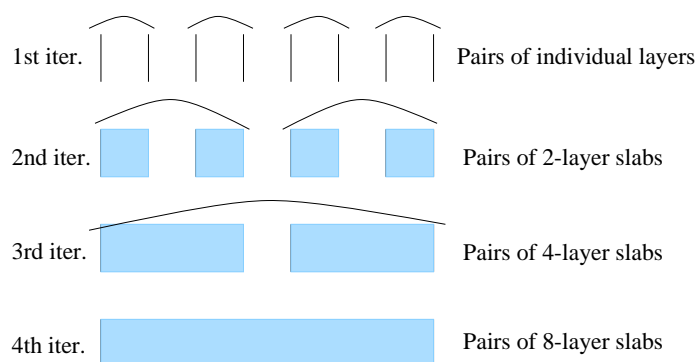
Figure 22: Layer-Doubling method
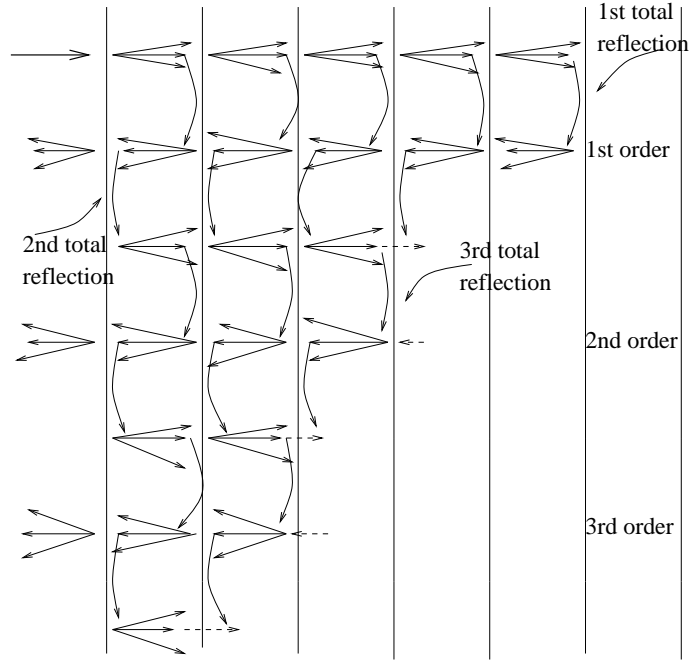
Figure 23: Renormalized-Forward-Scattering method

with $P^{\pm} = \exp(\pm i\vec{k}_g \cdot \vec{r}_{BA})$ where $\vec{r}_{BA}$ connects different points between the two layers. Next we will have to generalize this method to more than two layers. To do that we follow the so-called *Layer-Doubling* techique developed by Pendry[?]. According to it we start with the two-layer diffraction and at every iteration we double the thickness of the layers by combining two identical slabs of layers as shown in the figure 22. The usage of this method has shown that a number of about ten layer, or three iterations, suffies to make it converge.

Renormalized-Forward-Scattering (RFS) method This method which is ilustrated in figure 23, is also developed by Pendry[?] and uses the fact that the probability for forward scattering is greater than that for the backward scattering. We start by

following the incident beam in the plane wave representation as it forward-scatters to the deepest layer, this being determined by inelastic scattering effects. Then, at the deepest layer it undergoes its only reflection. The reflected beam forward-scatters from layer to layer towards the outter surface and emerges out of it giving rise to the first order of reflected beams. Next, we follow the beam emerging from the previous iteration as it collects reflected beams from emerging ones and as it reflects off the top layer all the way to the deepest layer and where undergoes its third reflection. The emerging beam, having collected reflected waves from penetrating beams consists the second order of the method. We keep doing that until we run into convergence. Formalism of the method can be found in the given bibliography.

Before we finish our brief tour to the dynamic theory, we should mention a very important factor; the computation time. All those matrix inversions consume a lot of time even when the programs are run by supercomputers. Thus, on choosing a method to work with we will have to take into consideration how time consuming this method will be. One can get an idea of the time spent by seeing that, for example, for the matrix inversion method this time is proportional to $N^3(\ell_{\max} + 1)^6$ whereas for the reverse scattering perturbation method it is proportional to $N^2(\ell_{\max} + 1)^4$. This last method has been developed by Zimmer and Holland[?] and improved by Tong and van Hove[?].

2.3.4   Influence of the temperature

Finishing this chapter we wish to dedicate a few lines to a very important factor which always shows up and which is a phenomenon present whenever we have scattering; we are talking about the effects the temperature, under which the experiment takes place, has on the diffraction spots. One major disturbance has to do with the weakening of their intensity. This is easy to be understood; as the temperature increases so does the intensity of the scatterers vibrations. So, the scattered beams from two, say, atoms will have arbitrary phases, giving neither constructive nor destructive interference but something in between.

The temperature enters into our equations for the dynamic theory through the so-called *Debye-Waller factor*, $\exp(-2M)$, which for isotropic vibrations is given by:

$$e^{-2M} = \exp\left(-\frac{3\hbar^2 |\vec{q}|^2 T}{mk_B\theta_D^2}\right) \tag{67}$$

where $\vec{q}$ is the momentum transfered in the scattering of the electron from $\vec{k}$ to $\vec{k}'$, $(\vec{q} = \vec{k}' - \vec{k})$, k_B the Boltzman constant, m the mass of the scattering atoms and θ_D the Debye temperature. All we will have to do is multiply the atomic scattering factor, $f(\theta)$, with $\exp(-M)$ to make the intensity proporional to $|f(\theta)|^2 \exp(-2M)$. The phase shifts of the scattering do get influenced by the temperature and it is proved that this dependence is given by:

$$\delta_\ell(T) = \frac{1}{2\imath} \ln\left(1 - \frac{4km\imath}{\hbar^2} t_\ell(T)\right) \tag{68}$$

The fact that the addition of the Debye-Waller factor makes the atomic scattering amplitude sharper with increasing temperature has as result the increase of the number of

phase shifts used.

Chapter 3

Electron Holography as a tool for surface exploration
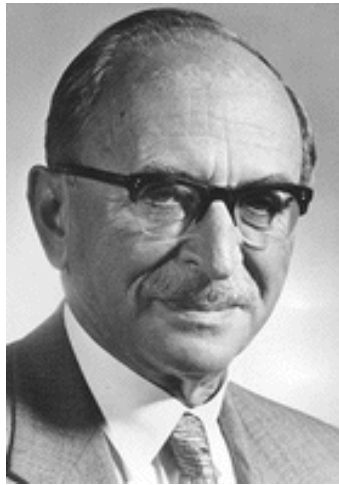
Figure 24: Dennis Gabor (1900-1979)

3.1 Introduction

In 1947, the Hungarian engineer Dennis Gabor (figure 24) was working with the Thomson-Houston Company in England trying to improve the resolution in images obtained with an electron microscope. One year later he published in *Nature* the famous paper[**?**] that gave him in 1971 the Nobel Prize on the wavefront reconstruction or *holography* as it is known today. Two more publications followed in 1949[**?**] and in 1951[**?**]. The etymology of the word has Greek origin and consists of the adjective $\acute{o}\lambda o\varsigma$ that means "whole" and the verb $\gamma\rho\acute{a}\varphi\omega$ that means "to write" or "to record", whereas *hologram* is the recording on a photographic plate of the interference pattern of a wave emitted by a coherent source and the part of it that has been scattered by an object; the former being called "the reference wave" and the latter "the object wave". By shining the hologram with the same reference wave we obtain a three-dimensional feature that appears at the original position of the object and possesses all the characteristics thereof, that is, depth and parallax, but one; it is not touchable. Although holography as is broadly known today uses visible light, nevertheless, in principle, we can repeat the method employing any wave from the electromagnetic spectrum, as well as, any particle. In this thesis we make use of the electron as a coherent wave to understand the geometrical structure of the crystal surfaces.
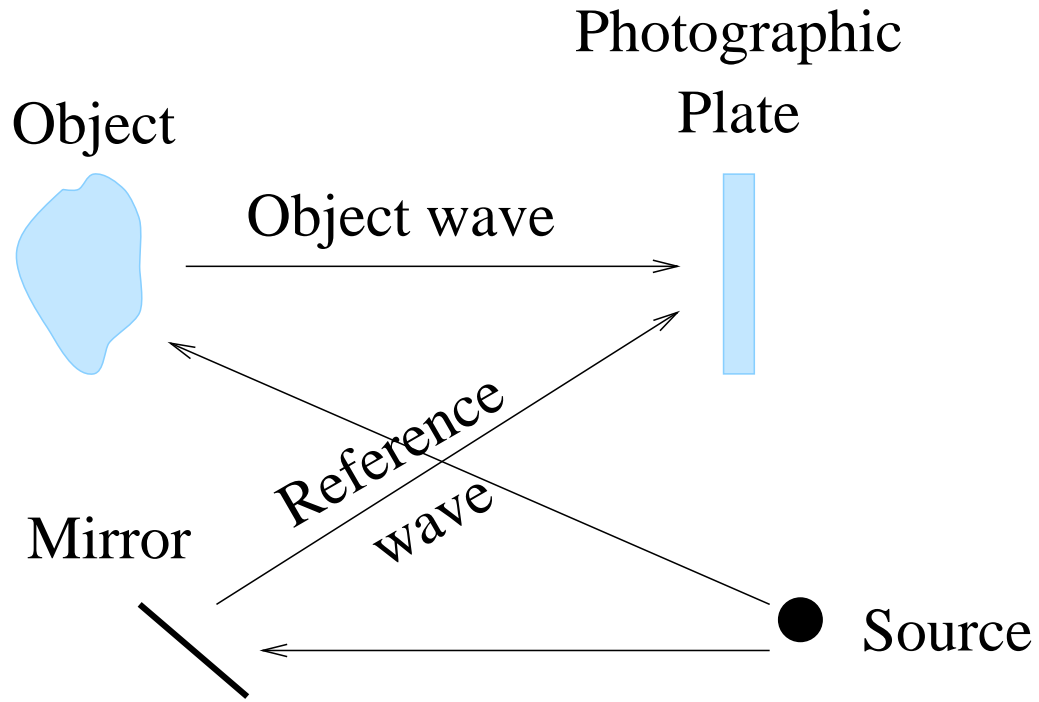
Figure 25: Reference and Object waves

3.2 A short review of holography

In this section we will attempt to discuss, in brief, the basic principles of holography, thus setting the foundation of the electron holography as a method of surface exploration.

After the first excitement, holography was almost forgotten and abandoned since people lacked the ability to produce coherent (monocromatic) light, the most important prerequisite for the success of the method. With the invention of the *LASER* in 1961 this obstacle was eliminated and the usage skyrocketed with the today's known results where everybody thinks of holography as a stereoscopic photography. In conventional photography we obtain the recording of the intensity of the light reflected by an object and only that. On the other hand, what differentiates a hologram is that it, along

with the intensity of the light, includes the phase difference between the reference and the object waves, the feature that contains all the three-dimensional information of the object. Let us assume the $\vec{R}$ and $\vec{O}$ are the time independent complex amplitudes of the electric field vectors for the reference and the object waves respectively, defined in figure 25. If $\vec{r}, \vec{o}, \phi_r$ and ϕ_o are the real amplitudes and the phases then the two waves can be written as:

$$\vec{R} = \vec{r}e^{\imath\phi_r} \tag{69}$$

$$\vec{O} = \vec{o}e^{\imath\phi_o} \tag{70}$$

Their interference on the phographic plate will produce the standing wave $\vec{R} + \vec{O}$ with intensity:

$$
\begin{aligned}
I &= |\vec{R} + \vec{O}|^2 = (\vec{R} + \vec{O})(\vec{R}^* + \vec{O}^*) \\
&= (\vec{r}e^{\imath\phi_r} + \vec{o}e^{\imath\phi_o})(\vec{r}e^{-\imath\phi_r} + \vec{o}e^{-\imath\phi_o}) \\
&= r^2 + o^2 + \vec{r}\cdot\vec{o}e^{\imath(\phi_r - \phi_o)} + \vec{o}\cdot\vec{r}e^{-\imath(\phi_r - \phi_o)} \\
&= I_r + I_o + 2\vec{r}\cdot\vec{o}\cos(\phi_r - \phi_o) \tag{71}
\end{aligned}
$$

From the last equation we clearly see what we have said before, that is, along with the intensities from both waves, I_r and I_o, we obtain their phase difference as well. Of course, for mutually perpendicular polarized waves we obtain no hologram since in that case the third term of (71) is nullified. The interference theory proves that the intensity I will take maximum (constructive interference) and when we have $\phi_r - \phi_o = 2n\pi$, where $n = 0, 1, 2, \ldots$ and the distance d between these maxima will be given by the Bragg's
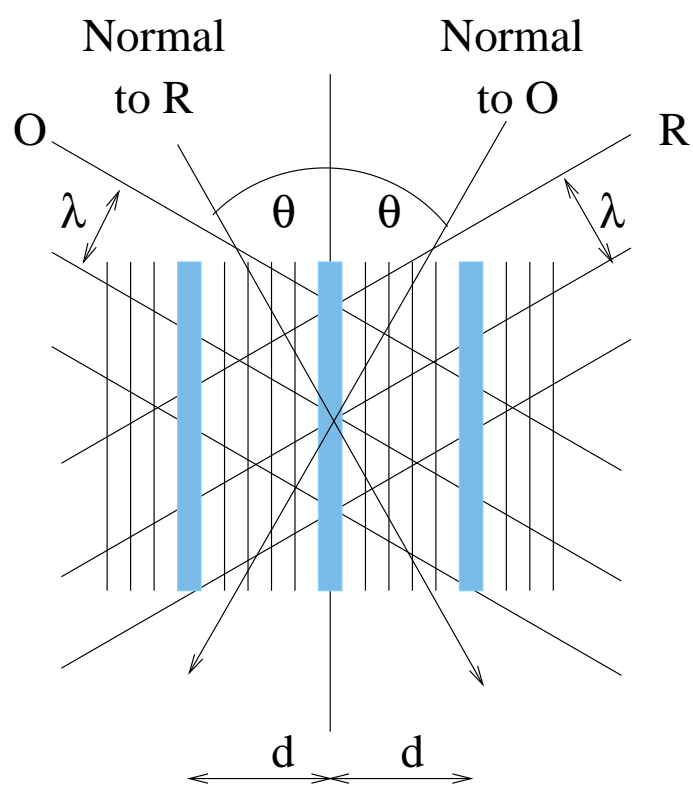
Figure 26: Interference and Reconstruction
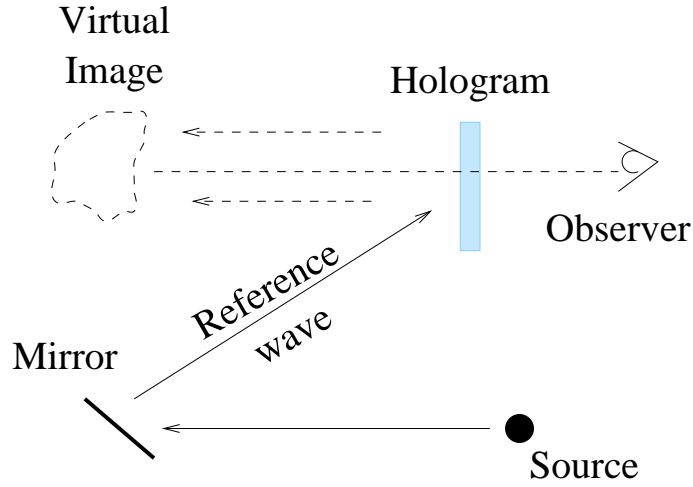
Figure 27: Reconstructing a virtual image

relation $2d \sin \theta = \lambda$, where θ is the angle between the normal to the plane wave and the generated maximum intensity planes (figure 26).

Reconstructing the original object is equivalent to illuminating the thus created hologram with the same reference wave, $\vec{R}$. The maximum intensity planes will have converted the photographic plate into a grating with constant d. The reference wave will be diffracted by this artificial grating according to the Bragg's law of diffraction, that is, $2d \sin \theta = \lambda$, where θ is the angle between the wavefront normal and the intensity plane (figure 26). In other words the wave that will come out of the hologram will have the same direction as the object wave $\vec{O}$, the wave that contains the information about the object.

Let us see now the formation of the hologram and the reconstruction process from a different perspective. Let us rewrite the basic holographic equation in the following
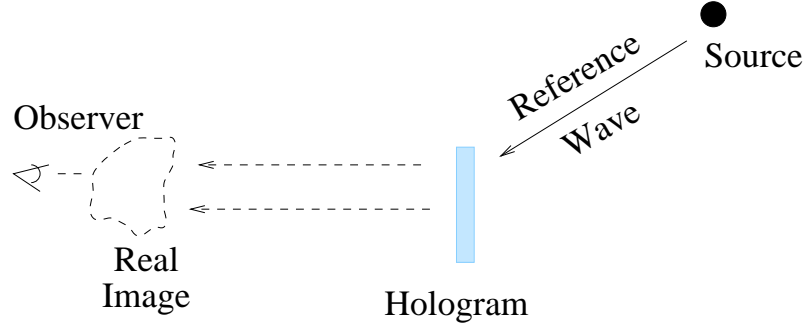
Figure 28: Reconstructing a real image

form:

$$
\begin{aligned}
I &= |\vec{R} + \vec{O}|^2 = (\vec{R} + \vec{O})(\vec{R}^* + \vec{O}^*) \\
&= \vec{R} \cdot \vec{R}^* + \vec{O} \cdot \vec{O}^* + \vec{R} \cdot \vec{O}^* + \vec{O} \cdot \vec{R}^* \\
&= I_r + I_o + \vec{R} \cdot \vec{O}^* + \vec{O} \cdot \vec{R}^* \tag{72}
\end{aligned}
$$

which is equivalent to (71). For the reconstruction we will have to shine the hologram with the original reference wave $\vec{R}$ or $\vec{R}^*$, the second being the so-called *conjugate* reference wave which differs from the original in the fact that has opposite direction, that is, $\vec{R}^* = \vec{r} \exp(-\imath \phi_r)$. Figures 27 and 28 show the kind of reconstructed image we obtain according to what reference wave we use. Illuminating the hologram with the original wave $\vec{R}$, that is, shining from the front of the plate, is equivalent to multiplying I with $\vec{R}$ which results to:

$$
\begin{aligned}
\vec{R} I &= \vec{R}(I_r + I_o + \vec{R} \cdot \vec{O}^* + \vec{O} \cdot \vec{R}^*) \\
&= \vec{R}(I_r + I_o) + \vec{R}(\vec{R} \cdot \vec{O}^*) + \vec{R}(\vec{O} \cdot \vec{R}^*) \\
&= \vec{R}(I_r + I_o) + (\vec{R})^2 \vec{O}^* + I_r \vec{O} \tag{73}
\end{aligned}
$$

If I_r and I_o are constants then the first term of (73) represents the original reference wave, the third term gives the original object wave whereas the second term represents the conjugate of the object wave which converges at the position of the object; this is what an observer sitting behind the hologram will see, *i.e.*, a virtual image. If we illuminate the hologram with the conjugate reference wave, $\vec{R}^*$, that is, shining from the back of the plate, the wave emerging from it will consist of:

$$\begin{aligned}
\vec{R}^* I &= \vec{R}^*(I_r + I_o + \vec{R} \cdot \vec{O}^* + \vec{O} \cdot \vec{R}^*) \\
&= \vec{R}^*(I_r + I_o) + I_r \vec{O}^* + (\vec{R}^*)^2 \vec{O}
\end{aligned} \tag{74}$$

the conjugate reference and object waves as well as the object wave. In this case an observer sitting in front of the plate will see a real image. In the case of electron holography we make use of this reconstruction procedure. What is characteristic in both cases is the fact that the emerging wave contains both the object wave and its complex conjugate. This latter is called *the twin image* because it is reconstructed at a position which, with respect to a coordinate system, is opposite to that of the real image.

In the treatment above we have touched on the main principles of optical holography and have seen, in brief, how one uses it in order to reconstruct in three-dimensional space an object with all its characteristics. In the next section we will see how people have used the above concepts to investigate the crystal surface.

3.3 Application of Gabor's ideas to surface crystallography

3.3.1 Introduction

As we mentioned in the previous section, one, theoretically, can apply the ideas of holography using electromagnetic waves from the entire spectrum, as well as using the waves associated with the particles according to de Broglie principle of duality. Thus, the usage of electron waves as probes among the atoms of the crystal surfaces comes naturally since they (the electrons), in the LEED energy range, have mean free path of the order of the few atom layers consisting a typical surface (look also at figure 2).

One can think of an electron wave as being split into two parts; one part traveling towards a remote detector while the second getting scattered by an atom (or a cluster of atoms) and then going towards the same detector. The two waves interfere as soon as they reach their target. This procedure is similar to what we described in the previous section between the reference and the object light wave. In the new case the electrons that go directly to the detector consist the reference wave whereas those that are scattered first and then travel to the detector consist the object wave. The detector is actually a photographic plate on which the interference of the two waves will create the corresponding *electron hologram*. If one illuminates this pattern with the complex conjugate (or time reverse) reference electron wave, that will diffract to a new wave part of which will converge at the point where the scattering atom was.

Thus far we have not said anything new as far as the procedure is concerned. One

basic difference from the light holography is that in the former case the source of the electrons are some atoms of the surface. Depending on the methods we employ to generate the reference and the object waves, we distinguish:

Photoelectrons In this case the electrons are ejected from the atoms that absorb photons.

Auger electrons The Auger electrons are excited from an energy transition that takes place in atomic cores.

Kikuchi electrons Inelastically scattered electrons on their way out of the crystal can be elastically scattered and produce the so-called Kikuchi pattern.

DLEED electrons Diffuse LEED is the case of electrons being shot from an electron gun (see figure 4) at the crystal surface which contains atoms disorderedly adsorbed thus creating the so-called *lattice-gas* picture. These atoms behave as electron beam splitters thus producing reference and object waves which interfere upon a fluorescent screen giving rise to a diffuse pattern after which the method takes its name.

Xiang Chen[**?**] in his doctorate thesis analyzed the photoelectron holography. We, on the other hand, will attempt in this thesis, to see how one can use DLEED electrons and Gabor's ideas in order to enhance the big success that LEED has been having in the surface investigations.

3.3.2 DLEED holography

A diffuse LEED experiment is not at all different from that of LEED we examined in the first chapter. As always, before we start with the experiment we pay special attention to the preparation of the sample. As we mentioned in the introduction, on the clean surface of the sample we wish to have atoms (usually of a different kind than those of the surface) disorderedly adsorbed. The preparation of the sample as well as a description of the entire experiment is elaborately described in a paper by H. Wedler *et at.*[**?**]. In that experiment a clean nickel (Ni) surface cut in an orientation (100) was covered with potassium (K) up to a coverage of $\Theta = 0.25\,ML$. Usually, in order to obtain a diffuse diffraction pattern we need to ascertain that the coverage will not surpass $\Theta = 0.25\,L$. An external generator of electrons, that is, the electron gun, shoots electrons upon the sample. Figure 29 shows their fate as soon as they reach their target. Some of them (actually the majority) fall in regions of the surface empty of adsorbed atoms. There they are scattered by the atoms of the clean surface (the substrate atoms) and detected on the fluorescent screen where their trace is recorded according to what we described in the first chapter (beams labeled "1" in figure 29). The pattern produced thus is the LEED diffraction pattern with the Bragg spots indicating the sizes of the Brillouin zones of the reciprocal lattice of the substrate. A small part of the incident electrons is scattered by the adsorbate atoms. Here we discern two major categories of scattering. In the first category belong all those paths that have as the last encounter an adsorbate atom before they start their trip to the detector (beams labeled "2" in figure 29). In the second category belong all paths that have as their last encounter a substrate atom
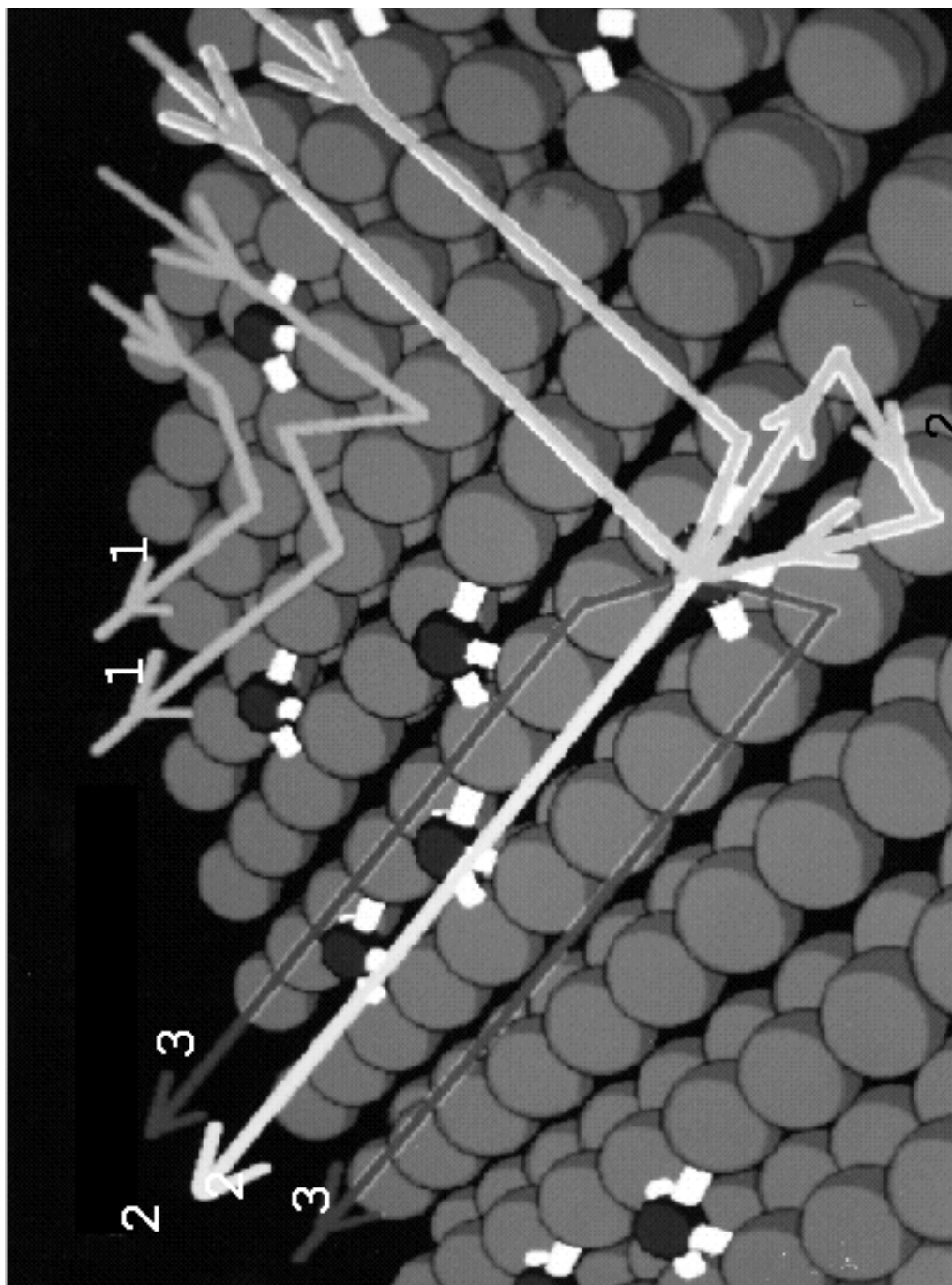
Figure 29: Diagram illustrating the scattering paths on a crystal surface containing disordered adsorbate atoms giving rise to (a) substrate Bragg spots (beams labeled "1") and (b) elastic diffuse intensities (beams labeled "2" and "3")

and at least once have encountered an adsorbate atom (beams labeled "3" in figure 29). A consequence of the short range order is that every neighborhood of an adsorbate is identical to any other neighborhood and so is the scattering proccess within it. Thus, an infinite clean surface with only one ad-atom to disturb its periodicity gives the same diffraction pattern (apart from a scaling factor) as the actual surface and this kind of ideal surface we study here. In the case of DLEED the source for the electrons is not the electron gun (this just directs them upon the surface) but, as far as the holography concepts are concerned, the adsorbed atom that acts as a beam splitter. The paths that belong to the first category (beam labeled "2") give rise to the reference wave whereas those of the second category (beam labeled "3") produce the object wave. These two waves interfere on the fluorescent screen and, due to the lack of long-range order among the adsorbates the result is the diffuse pattern between the Bragg spots which makes the DLEED hologram. The Bragg spots do not concern us in DLEED because they carry partial information about the adsorbate atoms and, in any case, information that is hard to be extracted. This is the reason that after we perform the experiment we subtract them from the total diffuse pattern (look at figure 46). Only the interference between beams that have "seen" ad-atoms and substrate atoms contain information about the phase change that the reference wave acquires upon encountering the substrate layer. Under these conditions holographic diffuse LEED is a method for the determination of the the local geometry in the vicinity of an adsorbate. Below we discuss the theoretical approach of holographic DLEED based on the general equation of holography given in the first section.

3.3.3   Theory of DLEED holography

We start out by considering the amplitude of the waves that reach for the first time an adsorbate at position $\vec{r}_a$, following Saldin and Chen[?]. These waves will include the electron waves that are incident on the adsorbate coming from the electron gun and the Bragg waves reflected from the surface. Thus, the total amplitude of the wave that reaches the adsorbate will be:

$$\exp(\imath \vec{k}_o^+ \cdot (\vec{r}_a - \vec{r}_o)) + \sum_g R_g(\vec{k}_\parallel^{\mathrm{inc}}) \exp(\imath \vec{k}_g^- \cdot (\vec{r}_a - \vec{r}_o)) \tag{75}$$

where the wave vectors $\vec{k}_g^\pm = (\vec{k}_\parallel^{\mathrm{inc}} + \vec{g}, k_{g\perp}^\pm)$, $\vec{g}$ is a reciprocal lattice vector, $\vec{k}_\parallel^{\mathrm{inc}}$ is the component of the wave vector parallel to the surface and $k_{g\perp}^\pm = \pm[2(E-V_o) - |\vec{k}_\parallel^{\mathrm{inc}} + \vec{g}|^2]^{1/2}$ with E being the total energy of the electrons and V_o the inner potential which we defined in the first chapter and $\vec{r}_o$ is the conventional origin for LEED calculations relative to which R_g is defined. The superscripts $(\pm)$ indicate directions from the vacuum towards $(+)$ and away $(-)$ from the surface. This wave will be scattered off the adsorbate atom and at position $\vec{r}$ with respect to it the total amplitude will be:

$$A(\hat{r}) = \exp(\imath \vec{k}_o^+ \cdot (\vec{r}_a - \vec{r}_o)) f_{\mathrm{a}}(\hat{k}_o^+ \cdot \hat{r}) + \sum_g R_g(\vec{k}_\parallel^{\mathrm{inc}}) \exp(\imath \vec{k}_g^- \cdot (\vec{r}_a - \vec{r}_o)) f_{\mathrm{a}}(\hat{k}_g^- \cdot \hat{r}) \tag{76}$$

where:

$$f(\hat{k}_1 \cdot \hat{k}_2) = \frac{1}{k_1} \sum_\ell (2\ell + 1) \sin \delta_\ell(k_1) \exp(\imath \delta_\ell(k_1)) P_\ell(\hat{k}_1 \cdot \hat{k}_2) \tag{77}$$

is the atomic scattering factor of an atom when a wave with direction $\vec{k}_1$ is scattered to a direction $\vec{k}_2$. δ_ℓ is the phase shift with angular momentum quantum number ℓ and $P_\ell(\vec{k}_1 \cdot \vec{k}_2 / k_1 k_2)$ are the Legendre polynomials. The amplitude $A(\hat{r})$ belongs to the wave

labeled "2" in figure 29 and is the reference wave which has the form:

$$R(\vec{k}) = A(\hat{k})\frac{\exp(\imath kr)}{r} \tag{78}$$

Actually on determining the reference wave we have made the assumption that all the wave paths between the first and last encounter with the adsorbed atom are negligible since they contain backscatterings from its neighborhood that weaken the resulting wave[?]. As we have said previously, part of this wave travels directly to the detector and part of it is scattered by the substrate atoms of its vicinity, thus generating the object wave which will be of the form:

$$O(\vec{k}) = \sum_j A(\hat{r})\frac{\exp(\imath kr_j)}{r_j}f_{\rm s}(\hat{r}_j \cdot \hat{k})\frac{\exp(\imath k|\vec{r} - \vec{r}_j|)}{|\vec{r} - \vec{r}_j|} \tag{79}$$

at the same position $\vec{r}$ relative to the ad-atom. In the above formula $f_{\rm s}$ is the atomic scattering factor of the substrate atom. Since $r_j \ll r$ we can have:

$$
\begin{aligned}
|\vec{r} - \vec{r}_j| &= (r^2 + r_j^2 - 2\vec{r} \cdot \vec{r}_j)^{1/2} \\
&\simeq r(1 - 2\frac{\vec{r} \cdot \vec{r}_j}{r^2})^{1/2} \\
&\simeq r - \frac{\vec{r} \cdot \vec{r}_j}{r} \\
&= r - \hat{r} \cdot \vec{r}_j
\end{aligned}
\tag{80}
$$

and so $k(|\vec{r} - \vec{r}_j| - r) \simeq -k\hat{r} \cdot \vec{r}_j = -\vec{k} \cdot \vec{r}_j$, since $\vec{k}$ has the direction of $\hat{r}$. Taking that into consideration (79) becomes:

$$O(\vec{k}) = \left(\sum_j A(\hat{r})\frac{f_{\rm s}(\hat{r}_j \cdot \hat{k})}{r_j}\exp(\imath(kr_j - \vec{k} \cdot \vec{r}_j))\right)\frac{\exp(\imath kr)}{r} \tag{81}$$

These two waves will interfere on the fluorescent screen and the intensity of the

resultant wave will be (if we account for only the amplitudes of (78) and (81)):

$$
\begin{aligned}
H(\vec{k}) &= |R(\vec{k}) + O(\vec{k})|^2 \\
&= |R(\vec{k})|^2 + R(\vec{k})^* O(\vec{k}) + R(\vec{k}) O(\vec{k})^* + |O(\vec{k})|^2 \\
&= |A(\hat{k})|^2 \\
&+ A(\hat{k}) \sum_j A(\hat{r}_j)^* \frac{f_s(\hat{r}_j \cdot \hat{k})^*}{r_j} \exp(-\imath(kr_j - \vec{k} \cdot \vec{r}_j)) \\
&+ A(\hat{k})^* \sum_j A(\hat{r}_j) \frac{f_s(\hat{r}_j \cdot \hat{k})}{r_j} \exp(\imath(kr_j - \vec{k} \cdot \vec{r}_j)) \\
&+ |O(\vec{k})|^2
\end{aligned}
\tag{82}
$$

The reference wave that travels towards the substrate atoms has already been weakened having been split into as many waves as the number j of the surface atoms. It might be argued that by being scattered by each one of them it will be further enfeebled in a way that the object wave that travels to the detector will be negligible compared to the reference one. Thus, the last term of (82) may be dropped without loss of important information.

Our main goal here is to reconstruct the geometrical positions, $(\vec{r}_j)$, of the substrate atoms with respect to the adsorbed one. A look at (82) will reveal that only the second and the third terms contain the positions of the substrate atoms explicitly. We are trying to "invent" a mathematical formula such that at any point $\vec{r} \neq \vec{r}_j$ of the real space it will be negligible and only at $\vec{r} = \vec{r}_j$ will have significant values. The diffraction pattern is a two-dimensional array that mirrors the reciprocal lattice of the sample. So, this formula must contain an integral that will sweep the pattern, in other words, an integral with respect to $\vec{k}$ vector. If the integration results in a δ-function of the form $\delta(\vec{r} - \vec{r}_j)$ we

will be convinced that indeed we get large values at the positions of the sub-atoms. Let us try to put the above thinking into work. Looking at the two cross terms of (82) we understand that only if the coefficient of the exponential somehow dissappears will we end up having the exponential alone under the integral. In other words, if we multiply the second term by:

$$\left[A(\hat{k})^* A(\hat{r}) \frac{f_\mathrm{s}(\hat{r} \cdot \hat{k})^*}{r}\right]^{-1} \exp(\imath(kr - \vec{k} \cdot \vec{r}))$$
(83)

we will obtain for one substrate atom at $\vec{r} = \vec{r}_j$:

$$\left(\frac{A(\hat{k})}{A(\hat{k})^\star}\right) \left(\frac{r}{A(\hat{r}) f_\mathrm{s}(\hat{r} \cdot \hat{k})}\right) \left(A(\hat{r}_j) \frac{f_\mathrm{s}(\hat{k} \cdot \hat{r}_j)}{r_j}\right) \exp(\imath k(r - r_j)) \exp(-\imath \vec{k} \cdot (\vec{r} - \vec{r}_j))$$
(84)

If we integrate (84) over all $\vec{k}$ space we will see that at positions $\vec{r} = \vec{r}_j$ and $r = r_j$ the terms in the second and third parentheses cancel each other out and since the term $A(\hat{k})/A(\hat{k})^*$ is independent of $\vec{r}$ we get two δ-functions, $\delta(\vec{r} - \vec{r}_j)$ and $\delta(r - r_j)$, for the position and the magnitude of $\vec{r}_j$. In the discussion above we have tacitly omitted the fact that the suggested integration is over the three-dimensional $\vec{k}$ space whereas any particular pattern is two-dimensional. In order to show that there is no discrepancy present we may rewrite $\exp(\imath(kr - \vec{k} \cdot \vec{r})$ as follows:

$$\exp(\imath(kr - \vec{k}_\| \cdot \vec{r}_\| - k_\perp z)) = \exp(\imath(kr - k_\perp z) \exp(-\imath\vec{k}_\| \cdot \vec{r}_\|)$$
(85)

where $\vec{k}_\|$ is the wave vector parallel to the pattern, $\vec{r}_\|$ represents the two-dimensional real space lattice, $k = (2(E - V_o))^{1/2}$ and $k_\perp = (k^2 - |\vec{k}_\| + \vec{g}|^2)^{1/2}$, the component of $\vec{k}$ normal to the pattern. Calling kernel $K(\vec{k}, \vec{r})$, the term in front of the exponential in (83), we can write:

$$K(\vec{k}, \vec{r}) = \left[A(\hat{k})^* A(\hat{r}) \frac{f_s(\hat{r} \cdot \hat{k})^*}{r}\right]^{-1}$$
(86)

Thus the suggested algorithm will have the form:

$$B(\vec{r}) = \int \int \int H(\vec{k}) K(\vec{k}, \vec{r}) \exp(\imath(kr - k_\perp z)) \exp(-\imath \vec{k}_\parallel \cdot \vec{r}_\parallel) dk_\perp d\vec{k}_\parallel \qquad (87)$$

and one can see that (87) is a double integral over k_x and k_y and a single integral over the energy through $k_\perp$. The above procedure is similar to that suggested in optical holography where we had to illuminate the hologram with the time reverse reference wave in order to obtain the position of the original object. In this case $B(\vec{r})$ will be the wave emerging from the hologram and that will converge at the positions of the substrate atoms. The plot of $|B(\vec{r})|^2$, that is, of its intensity, against $\vec{r}$ will give, theoretically, maximum values at the positions of the atoms, thus reconstructing their real-space distribution.

So far in our discussion, we have not taken into consideration any long-range order factor among the substrate atoms we spoke about in the introduction. Let us try to see how this affects the intensities of the scattered waves. In general, the relationship between the amplitude A_o for the scattering from a single adsorbate, and that A from an entire surface layer in LEED is:

$$A(\vec{k}) = A_o(\vec{k}) \sum_{j=1}^{N} e^{-\imath(\vec{k} - \vec{k}') \cdot \vec{r}_j} \qquad (88)$$

where in the above expression $\vec{k}'$ is the wavevector of the electron beam incident on the surface, $\vec{k}$ that of a detected electron, and $\vec{r}_j$ the position vector of the jth adsorbate atom. The detected intensity will be:

$$H(\vec{k}) \;\; = \;\; |A(\vec{k})|^2$$

$$= |A_o(\vec{k})|^2 \sum_{j=1}^{N} e^{\imath(\vec{k}-\vec{k}')\cdot\vec{r}_j} \sum_{n=1}^{N} e^{-\imath(\vec{k}-\vec{k}')\cdot\vec{r}_n}$$

$$= H_o(\vec{k}) \left[N + \sum_{n\neq j}^{N} e^{\imath\vec{q}\cdot(\vec{r}_j-\vec{r}_n)} \right] \tag{89}$$

where $\vec{q} = \vec{k} - \vec{k}'$, the momentum transfer, $H_o(\vec{k})$ is the intensity from only one adsorbate atom and $\vec{r}_j, \vec{r}_n$ are the position vectors of the adsorbate atoms j and n and are parallel to the surface. Thus, $\vec{q}\cdot(\vec{r}_j - \vec{r}_n)$ can be written as $\vec{q}_\parallel \cdot (\vec{r}_j - \vec{r}_n)$. We call $S(\vec{q}_\parallel)$, a structure factor, where:

$$S(\vec{q}_\parallel) = \sum_{n,j}^{N} e^{\imath\vec{q}_\parallel\cdot(\vec{r}_j-\vec{r}_n)} \tag{90}$$

$$= N + \sum_{n\neq j}^{N} e^{\imath\vec{q}_\parallel\cdot(\vec{r}_j-\vec{r}_n)} \tag{91}$$

which depends only on $\vec{q}_\parallel$ or $\vec{k}_\parallel$ and thus (89) can be written as:

$$H(\vec{k}) = H_o(\vec{k})S(\vec{q}_\parallel) \tag{92}$$

$S(\vec{q}_\parallel)$ depends only on the order or disorder of the distribution of the ad-atoms on the surface. We also define:

$$H_{\rm av}(\vec{k}) = \frac{\int H(\vec{k})dk_\perp}{\int dk_\perp}$$

$$= \frac{\int H_o(\vec{k})S(\vec{q}_\parallel)dk_\perp}{\int dk_\perp}$$

$$= \frac{\int H_o(\vec{k})dk_\perp}{\int dk_\perp}S(\vec{q}_\parallel) \tag{93}$$

where $S(\vec{q}_\parallel)$, since it depends only on the parallel to the surface component of $\vec{k}$, can get out of the integral. The idea behind this definition is to account for all the reference waves that have the same $\vec{k}_\parallel$ component but not the same $k_\perp$ one, and to get an average

of this intensity. Besides, with this definition we isolate the structure factor. Eventually accouting for (92) and (93) we introduce the χ-function as follows:

$$
\begin{aligned}
\chi(\vec{k}) &= \frac{H(\vec{k}) - H_{\text{av}}(\vec{k})}{H_{\text{av}}(\vec{k})} \\
&= \frac{H_o(\vec{k}) - \left[\int H_o(\vec{k})dk_\perp / \int dk_\perp\right]}{\int H_o(\vec{k})dk_\perp / \int dk_\perp}
\end{aligned}
\tag{94}
$$

which is obviously independent from S. The sum in (91) can be zero if there is fully disordered adsorption, since in that case $\vec{r}_j - \vec{r}_n$ will have all the possible values, and thus S will be equal to the number of the adsorbates, N. On the other hand if the adsorption is fully ordered then from (90) we see that S is equal to N^2 since in that case all $\vec{q}_\parallel$'s will be reciprocal lattice vectors. In diffuse LEED this quantity is unknown since we have neither full order nor full disorder. Thus, in the way we have defined the χ-function we eliminate this unknown factor that is present in the experiment. This is one of the reasons we introduced χ. Another is that in this way we enhance the contrast of $H(\vec{k}_\parallel)$ with respect to the $H(\vec{k})$.

From (82) we see that only the first term, $|A(\hat{k})|^2$, does not depend on $k_\perp$. Then, if we approximately set $H_{\text{av}}(\vec{k}_\parallel)$ equal to this term and substitute (82) into (94) we will have:

$$
\begin{aligned}
\chi(k_\perp, \vec{k}_\parallel) &= \frac{|A(\hat{k})|^2 + \left[A(\hat{k})^* \sum_j A(\hat{r}_j)\left(f_{\text{s}}(\hat{r}_j \cdot \hat{k})/r_j\right)\exp(\imath(kr_j - \vec{k}\cdot\vec{r}_j)) + c.c.\right] - |A(\hat{k})|^2}{|A(\hat{k})|^2} \\
&= \frac{A(\hat{k})^*}{A(\hat{k})A(\hat{k})^*}\sum_j A(\hat{r}_j)\frac{f_{\text{s}}(\hat{r}_j \cdot \hat{k})}{r_j}\exp(\imath(kr_j - \vec{k}\cdot\vec{r}_j)) + c.c. \\
&= \sum_j \left[\frac{A(\hat{r}_j)}{A(\hat{k})}\frac{f_{\text{s}}(\hat{r}_j \cdot \hat{k})}{r_j}\exp(\imath(kr_j - \vec{k}\cdot\vec{r}_j)) + c.c.\right]
\end{aligned}
\tag{95}
$$

In (95) $c.c.$ means the complex conjugate of the expression in front of it.
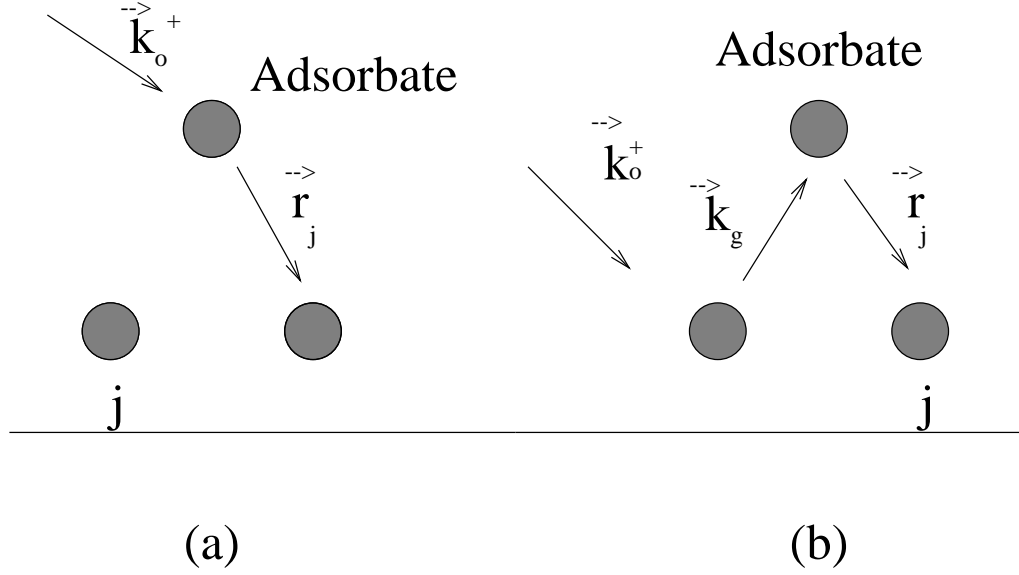
Figure 30: $f_a^+(\hat{k}_o^+ \cdot \hat{r}_j)$ (a) and $f_a^-(\hat{k}_g^- \cdot \hat{r}_j)$ (b) for (97)

Following the same thinking we did when we previously discussed the construction of the algorithm we end up obtaining a new kernel function with form:

$$K(k_\perp, \vec{k}_\parallel; \vec{r}) = \left[\frac{A(\hat{r})}{A(\hat{k})} \frac{f_s^-(\hat{r} \cdot \hat{k})}{r} \right]^{-1} \tag{96}$$

Using (76), $A(\hat{r})$ and $A(\hat{k})$ will be:

$$A(\hat{r}) = \exp(\imath \vec{k}_o^+ \cdot \vec{r}_a) f_a^+(\hat{k}_o^+ \cdot \hat{r}) + \sum_g R_g(\vec{k}_\parallel^{inc}) \exp(\imath \vec{k}_g^- \cdot \vec{r}_a) f_a^-(\hat{k}_g^- \cdot \hat{r}) \tag{97}$$

$$A(\hat{k}) = \exp(\imath \vec{k}_o^+ \cdot \vec{r}_a) f_a^-(\hat{k}_o^+ \cdot \hat{k}) + \sum_g R_g(\vec{k}_\parallel^{inc}) \exp(\imath \vec{k}_g^- \cdot \vec{r}_a) f_a^+(\hat{k}_g^- \cdot \hat{k}) \tag{98}$$

In (96), (97), (98), we have used the atomic scattering factor notation for the substrate and adsorbed atoms introduced by Wei and Tong[?] where the (+) sign superscript indicates forward scattering ($\theta < 90$) and the ($-$) sign indicates backward scattering ($\theta > 90$). Figures 30, 31 and 32 help us understand that better.

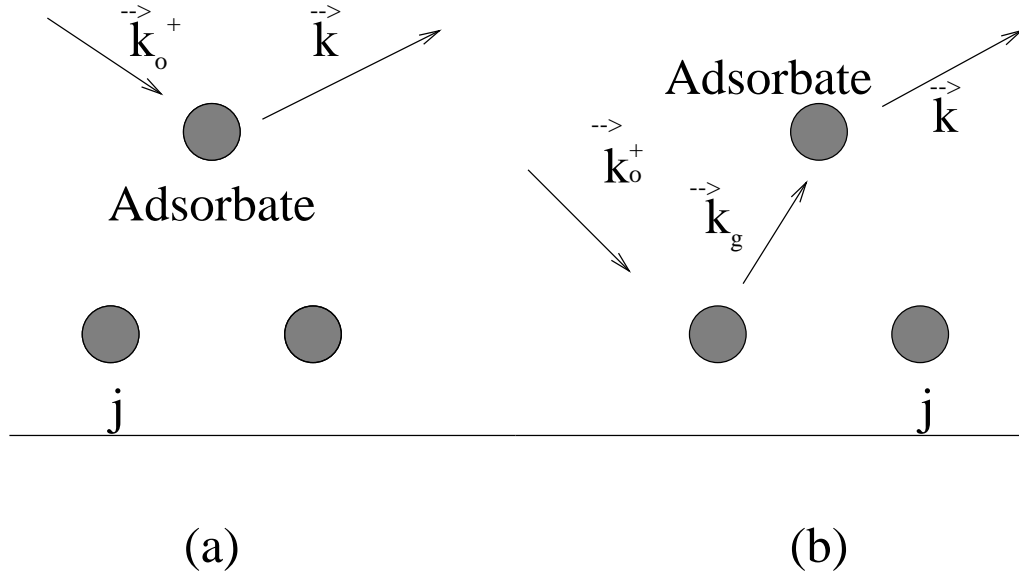Figure 31: $f_a^-(\hat{k}_o^+ \cdot \hat{k})$ (a) and $f_a^+(\hat{k}_g^- \cdot \hat{k})$ (b) for (98)
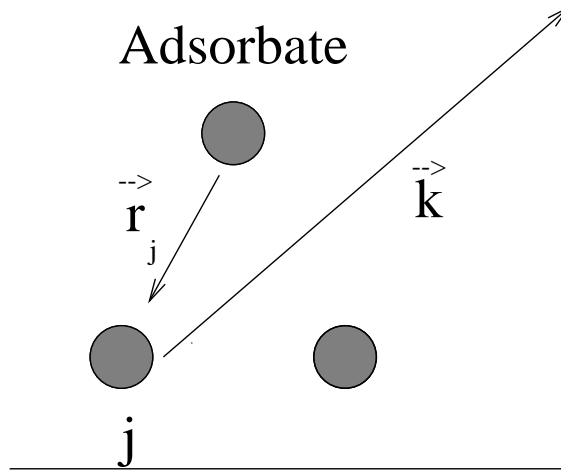

Figure 32: $f_s^-(\hat{r}_j \cdot \hat{k})$ for (96)

Substituting (97) and (98) into (96) and factorizing out the coefficient $\exp(\imath \vec{k}_o^+ \cdot \vec{r}_a)$ from the numerator and denominator of the fraction $A(\hat{r})/A(\hat{k})$, we obain:

$$K(k_\perp, \vec{k}_\parallel; \vec{r}) = \left[\left(f_a^+(\hat{k}_o^+ \cdot r) + C \right) \frac{f_s^-(\hat{k} \cdot r)}{Dr} \right]^{-1} \tag{99}$$

where

$$C = \sum_g R_g(\vec{k}_\parallel^{inc}) \exp(\imath(\vec{k}_g^- - \vec{k}_o^+) \cdot \vec{r}_a) f_a^-(\hat{k}_g^- \cdot \hat{r}) \tag{100}$$

$$D = f_a^-(\hat{k}_o^+ \cdot \hat{k}) + \sum_g R_g(\vec{k}_\parallel^{inc}) \exp(\imath(\vec{k}_g^- - \vec{k}_o^+) \cdot \vec{r}_a) f_a^+(\hat{k}_g^- \cdot \hat{k}) \tag{101}$$

In the above expressions for C and D we see that the position of the adsorbed atom appears as a phase factor. Since we do not know $\vec{r}_a$ in advance we use the spirit of the maximum entropy[?] and approximately take for C and D:

$$C \simeq \left[\left| \sum_g R_g(\vec{k}_\parallel^{inc}) f_a^-(\hat{k}_g^- \cdot \hat{r}) \right|^2 \right]^{1/2} \tag{102}$$

$$D \simeq f_a^-(\hat{k}_o^+ \cdot \hat{k}) + \left[\left| \sum_g R_g(\vec{k}_\parallel^{inc}) f_a^+(\hat{k}_g^- \cdot \hat{k}) \right|^2 \right]^{1/2} \tag{103}$$

It is known that the atomic scattering factor in the energy range that LEED and DLEED experiments are performed varies greatly with the scattering angle from forward to back scattering. This can be seen in figure 33 where we have plotted the magnitude $|f|$ against the scattering angle for the oxygen at an energy of $233\,eV$. From the figure we see that for $\theta < 90$ there is a fast variation of $|f|$ whereas for $\theta > 90$ it remains almost constant. Due to this property of f we can take f^- in equations (99), (102) and (103) constant. Considering what we just said, kernel (99) takes the form:

$$K(k_\perp, \vec{k}_\parallel; \vec{r}) = \left[\frac{(f_a^+(\hat{k}_o^+ \cdot r) + C)}{Dr} \right]^{-1} \tag{104}$$
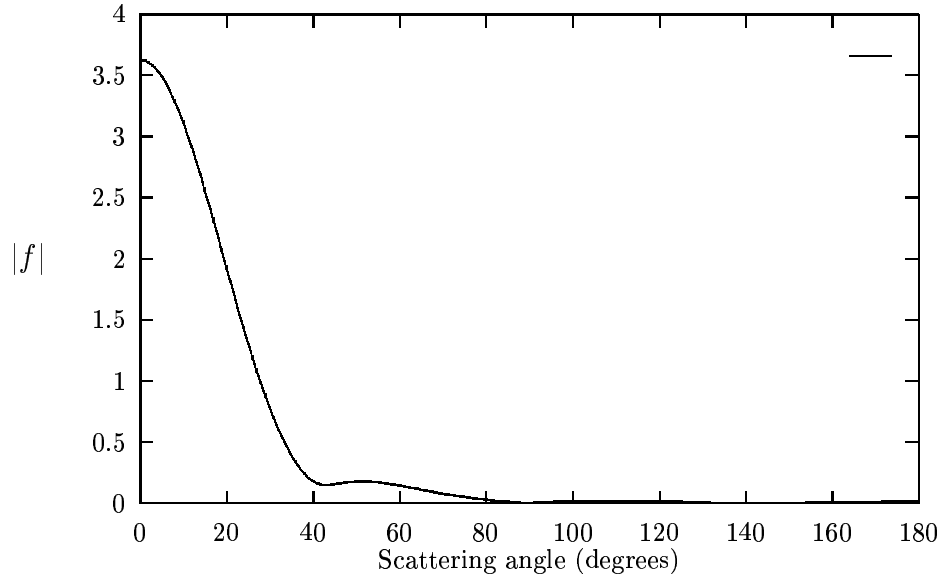
Figure 33: Variation of the magnitude of the atomic scattering factor of oxygen with the scattering angle at $233\,eV$

where the constant for the backscattering factor has been absorbed into D.

The sum in (103) represents the forward scattering of all waves that have been scattered off the substrate atoms (figure 31b) and each term of it takes maximum value when $f_{\mathrm{a}}^{+}(\hat{k}_g^{-}\cdot\hat{k})$ is peaked at $\hat{k}_g^{-}\parallel\hat{k}$. Since the sum sweeps the diffraction pattern in its entirety through the vectors $\vec{k}_g$ and since the first term is a constant due to our argument in the previous paragraph, it will not be a bad approximation if we set the factor D equal to a constant. Thus the final form of (104) and (87) to within a constant will be:

$$K(k_{\perp},\vec{k}_{\parallel};\vec{r}) = \left[\frac{(f_{\mathrm{a}}^{+}(\hat{k}_o^{+}\cdot r)+C)}{r}\right]^{-1} \tag{105}$$

$$B(\vec{r}) = \int\int\int \chi(k_{\perp},\vec{k}_{\parallel})K(\vec{k},\vec{r})\exp(\imath(kr-k_{\perp}z)\exp(-\imath\vec{k}_{\parallel}\cdot\vec{r}_{\parallel})dk_{\perp}d\vec{k}_{\parallel} \tag{106}$$

Before we finish this chapter we would like to demonstrate the advantages one has, employing the algorithm (106) in doing holographic DLEED. In particular (106) deals successfully with three major problems, $i.e.$, the anisotropy of the reference and object

waves, the twin image and effects of the multiple scattering.

The anisotropy of the reference and the object waves As we know the incident and scattered electrons in the LEED experiments have energies of a few hundreds of electron volts. We mentioned before that in these energies the atomic scattering factors are highly forward peaked (figure 33). The reference and object waves can be written as sums of spherical harmonics, $\sum_{lm} A_{lm} h_l^{(1)} Y_{lm}$, where $h_l^{(1)}$ are the Hankel functions of the first kind (corresponding to outgoing waves). It has been found that an atom is best reconstructed from an intensity that comes from spherical waves with $l = m = 0$, that is, from isotropic waves. Thus the forward peaked scattering factor is an obstacle to the clear reconstruction of the atom. By inserting the kernel $K(k_\perp, \vec{k}_\parallel; \vec{r})$, (105), as we discussed when we introduced its concept, the anisotropies dissapear since what we get under the reconstruction algorithm integral is a δ-function that peaks at both the positions of the atom and its twin image.

The twin image As we mentioned in the previous section, the twin image that always appears at the reconstruction and is associated in holographic LEED with the reconstruction of another atom at position $\vec{r} = -\vec{r}_j$ along with the position of the real atom at $\vec{r} = \vec{r}_j$. This is a serious drawback since there is no way to distinguish between the two images! This obstacle can be eliminated by the use of a multi-energy reconstruction algorithm. Here is what we mean. If $B_k(\vec{r})$ is the wave emerging from the hologram for one energy k then (106) without the kernel will

give:

$$
\begin{aligned}
B_k(\vec{r}) &= \int \chi(\vec{k}) e^{-i\vec{k}\cdot\vec{r}} d\vec{k} \\
&= \sum_j \left[\frac{A(\vec{r}_j)^*}{A(\hat{k})^*} \frac{e^{-ikr_j}}{r_j} f_s^*(\hat{k}\cdot\hat{r}_j) \int e^{-i\vec{k}\cdot(\vec{r}+\vec{r}_j)} d\vec{k} \right. \\
&\quad + \left. \frac{A(\vec{r}_j)}{A(\hat{k})} \frac{e^{ikr_j}}{r_j} f_s(\hat{k}\cdot\hat{r}_j) \int e^{-i\vec{k}\cdot(\vec{r}-\vec{r}_j)} d\vec{k} \right] \\
&= \sum_j \left[\frac{A(\vec{r}_j)^*}{A(\hat{k})^*} \frac{e^{-ikr_j}}{r_j} f_s^*(\hat{k}\cdot\hat{r}_j) \delta(\vec{r}+\vec{r}_j) \right. \\
&\quad + \left. \frac{A(\vec{r}_j)}{A(\hat{k})} \frac{e^{ikr_j}}{r_j} f_s(\hat{k}\cdot\hat{r}_j) \delta(\vec{r}-\vec{r}_j) \right]
\end{aligned}
\tag{107}
$$

The δ functions make sure that both real and twin images are reconstructed at $\vec{r} = \vec{r}_j$ and $\vec{r} = -\vec{r}_j$ but we still do not know which is which. Yet if we take the sum of (107) over more than one energy we will obtain:

$$
\begin{aligned}
B(\vec{r}) &= \sum_k B_k(\vec{r}) e^{-ikr} \\
&\approx \int B_k(\vec{r}) e^{-ikr} dk \\
&= \left[\sum_j [\frac{A(\vec{r}_j)^*}{A(\hat{k})^*} \frac{f_s(\hat{k}\cdot\hat{r}_j)}{r_j} \delta(\vec{r}+\vec{r}_j) \int e^{-ik(r+r_j)} dk \right. \\
&\quad + \left. \frac{A(\vec{r}_j)}{A(\hat{k})} \frac{f_s(\hat{k}\cdot\hat{r}_j)}{r_j} \delta(\vec{r}-\vec{r}_j) \int e^{ik(r-r_j)} dk \right] \\
&= \sum_j \left[\frac{A(\vec{r}_j)^*}{A(\hat{k})^*} \frac{f_s^*}{r_j} \delta(\vec{r}+\vec{r}_j) \delta(r+r_j) \right. \\
&\quad + \left. \frac{A(\vec{r}_j)}{A(\vec{r})} \frac{f_s(\hat{k}\cdot\hat{r}_j)}{r_j} \delta(\vec{r}-\vec{r}_j) \delta(r-r_j) \right]
\end{aligned}
\tag{108}
$$

Now the second δ function suppresses the twin image since we cannot have $r = -r_j$ (i.e., negative value of r).

Effects of multiple scattering. It is now known that multiple scattering is not an obstacle to the reconstruction of good images of the atoms around the reference wave sources

since the multi-energy reconstruction algorithm (106) is sensitive only to the single-scattering parts of the multiple-scattering series used to express the diffracted intensities. We will demonstrate that through a simple calculation. We are going to account for the object wave from single, double and triple scattering, and attempt to see whether the last two affect the reconstruction process. To this goal figure 34 will be a visual guide. Equation (79) without the sum gives the form of the object wave when only single scattering from substrate atom j has been taken into consideration (figure 34a), that is:

$$O_j^{(\mathrm{s})} = A(\hat{r}_j)\frac{\exp(\imath k r_j)}{r_j}f_{\mathrm{s}}(\hat{r}_j \cdot \hat{k})\exp(-\imath \vec{k} \cdot \vec{r}_j) \tag{109}$$

In the case of the double scattering the reference wave is scattered first from atom l and then from atom j (figure 34b):

$$
\begin{aligned}
O_{lj}^{(\mathrm{d})} &= A(\hat{r}_l)\frac{\exp(\imath k r_l)}{r_l}f_{\mathrm{s}}(\hat{r}_l \cdot \hat{\rho}_{lj})\frac{\exp(\imath k \rho_{lj})}{\rho_{lj}} \\
&\times f_{\mathrm{s}}(\hat{\rho}_{lj} \cdot \hat{k})\exp(-\imath \vec{k} \cdot \vec{r}_j)
\end{aligned}
\tag{110}
$$

The triple scattering term will contain scattering off atom m, then off atom l and finally off j (figure 34c):

$$
\begin{aligned}
O_{mlj}^{(\mathrm{t})} &= A(\hat{r}_m)\frac{\exp(\imath k r_m)}{r_m}f_{\mathrm{s}}(\hat{r}_m \cdot \hat{\rho}_{ml})\frac{\exp(\imath k \rho_{ml})}{\rho_{ml}} \\
&\times f_{\mathrm{s}}(\hat{\rho}_{ml} \cdot \hat{\rho}_{lj})\frac{\exp(\imath k \rho_{lj})}{\rho_{lj}} \\
&\times f_{\mathrm{s}}(\hat{\rho}_{lj} \cdot \hat{k})\exp(-\imath \vec{k} \cdot \vec{r}_j)
\end{aligned}
\tag{111}
$$

Then the object wave will be given by the summation of all three terms:

$$O_j = O_j^{(\mathrm{s})} + O_{lj}^{(\mathrm{d})} + O_{mlj}^{(\mathrm{t})} \tag{112}$$
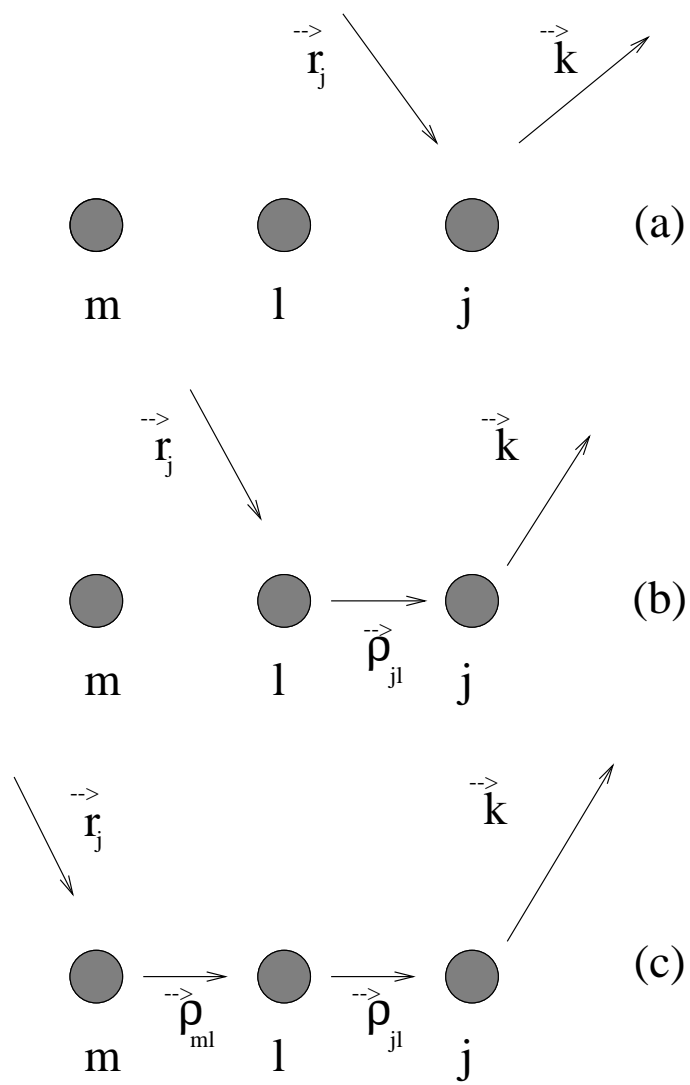
Figure 34: Multiple scattering

and the χ-function will have the form:

$$
\begin{aligned}
\chi(\vec{k}) &= \frac{\sum_j (R^* O_j + R O_j^*)}{RR^*} = \sum_j \left(\frac{O_j}{R} + \frac{O_j^*}{R^*} \right) \\
&= \sum_j \left(\frac{O_j^{(s)}}{R} + \frac{O_j^{(s)*}}{R^*} \right) + \sum_{lj} \left(\frac{O_{mj}^{(d)}}{R} + \frac{O_{mj}^{(d)*}}{R^*} \right) + \sum_{mlj} \left(\frac{O_{mlj}^{(t)}}{R} + \frac{O_{mlj}^{(t)*}}{R^*} \right) \\
&= \sum_j \left[\frac{A(\hat{r}_j) \, (\exp(\imath k r_j)/r_j) \, f_{\mathrm{s}}(\hat{r}_j \cdot \hat{k}) \exp(-\imath \vec{k} \cdot \vec{r}_j)}{A(\hat{k})} \right. \\
&\quad + \left. \frac{A(\hat{r}_j)^* \, (\exp(-\imath k r_j)/r_j) \, f_{\mathrm{s}}(\hat{r}_j \cdot \hat{k})^* \exp(\imath \vec{k} \cdot \vec{r}_j)}{A(\hat{k})} \right] \\
&\quad + \sum_{lj} \left[\frac{A(\hat{r}_l) \, (\exp(\imath k r_l)/r_l) \, f_{\mathrm{s}}(\hat{r}_l \cdot \hat{\rho}_{lj}) \, (\exp(\imath k \rho_{lj})/\rho_{lj}) \, f_{\mathrm{s}}(\hat{\rho}_{lj} \cdot \hat{k}) \exp(-\imath \vec{k} \cdot \vec{r}_j)}{A(\hat{k})} \right. \\
&\quad + \left. \frac{A(\hat{r}_l)^* \, (\exp(-\imath k r_l)/r_l) \, f_{\mathrm{s}}(\hat{r}_l \cdot \hat{\rho}_{lj})^* \, (\exp(-\imath k \rho_{lj})/\rho_{lj}) \, f_{\mathrm{s}}(\hat{\rho}_{lj} \cdot \hat{k})^* \exp(\imath \vec{k} \cdot \vec{r}_j)}{A(\hat{k})^*} \right] \\
&\quad + \sum_{mlj} \left[\left(A(\hat{r}_m) \, (\exp(\imath k r_m)/r_m) \, f_{\mathrm{s}}(\hat{r}_m \cdot \hat{\rho}_{ml}) \, (\exp(\imath k \rho_{ml})/\rho_{ml}) \, /A(\hat{k}) \right) \right. \\
&\quad \times \; f_{\mathrm{s}}(\hat{\rho}_{ml} \cdot \hat{\rho}_{lj}) \, (\exp(\imath k \rho_{lj})/\rho_{lj}) \, f_{\mathrm{s}}(\hat{\rho}_{lj} \cdot \hat{k}) \exp(-\imath \vec{k} \cdot \vec{r}_j) \\
&\quad + \; \left(A(\hat{r}_m)^* \, (\exp(-\imath k r_m)/r_m) \, f_{\mathrm{s}}(\hat{r}_m \cdot \hat{\rho}_{ml})^* \, (\exp(-\imath k \rho_{ml})/\rho_{ml}) \, /A(\hat{k}^*) \right) \\
&\quad \times \; \left. f_{\mathrm{s}}(\hat{\rho}_{ml} \cdot \hat{\rho}_{lj})^* \, (\exp(-\imath k \rho_{lj})/\rho_{lj}) \, f_{\mathrm{s}}(\hat{\rho}_{lj} \cdot \hat{k})^* \exp(-\imath \vec{k} \cdot \vec{r}_j) \right] \tag{113}
\end{aligned}
$$

Substituting (113) into (105) we will obtain:

$$
\begin{aligned}
A(\vec{r}) &= \sum_j \left[\frac{A(\hat{r}_j) f_{\mathrm{s}}(\hat{k} \cdot \hat{r}_j)}{A(\hat{r}) r_j} \int e^{-\imath \vec{k} \cdot (\vec{r} + \vec{r}_j)} d\hat{k} \int e^{\imath k(r + r_j)} dk \right. \\
&\quad + \left. \frac{A(\hat{r}_j)^* f_{\mathrm{s}}(\hat{k} \cdot \hat{r}_j)^*}{A(\hat{r})^* r_j} \int e^{-\imath \vec{k} \cdot (\vec{r} - \vec{r}_j)} d\hat{k} \int e^{\imath k(r - r_j)} dk \right] \\
&\quad + \sum_{lj} \left[\frac{A(\hat{r}_l) f_{\mathrm{s}}(\hat{\rho}_{lj} \cdot \hat{r}_l) f_{\mathrm{s}}(\hat{\rho}_{lj} \cdot \hat{k})}{A(\hat{r}) r_l \rho_{lj}} \int e^{-\imath \vec{k} \cdot (\vec{r} + \vec{r}_j)} d\hat{k} \int e^{\imath k(r + r_l + \rho_{lj})} dk \right. \\
&\quad + \left. \frac{A(\hat{r}_l)^* f_{\mathrm{s}}(\hat{\rho}_{lj} \cdot \hat{r}_l)^* f_{\mathrm{s}}(\hat{\rho}_{lj} \cdot \hat{k})^*}{A(\hat{r})^* r_l \rho_{lj}} \int e^{-\imath \vec{k} \cdot (\vec{r} - \vec{r}_j)} d\hat{k} \int e^{\imath k(r - r_l - \rho_{lj})} dk \right] \\
&\quad + \sum_{mlj} \left[\frac{A(\hat{r}_m) f_{\mathrm{s}}(\hat{\rho}_{ml} \cdot \hat{r}_m) f_{\mathrm{s}}(\hat{\rho}_{ml} \cdot \hat{\rho}_{mj}) f_{\mathrm{s}}(\hat{\rho}_{mj} \cdot \hat{k})}{A(\hat{r}) r_m \rho_{ml} \rho_{mj}} \right. \\
&\quad \times \int e^{-\imath \vec{k} \cdot (\vec{r} + \vec{r}_j)} d\hat{k} \int e^{\imath k(r + r_m + \rho_{ml} + \rho_{mj})} dk
\end{aligned}
$$

$$+ \quad \frac{A(\hat{r}_m)^* f_\mathrm{s}(\hat{\rho}_{ml} \cdot \hat{r}_m)^* f_\mathrm{s}(\hat{\rho}_{ml} \cdot \hat{\rho}_{mj})^* f_\mathrm{s}(\hat{\rho}_{mj} \cdot \hat{k})^*}{A(\hat{r})^* r_m \rho_{ml} \rho_{mj}}$$

$$\times \quad \int e^{-\imath \vec{k} \cdot (\vec{r} - \vec{r}_j)} d\hat{k} \int e^{\imath k (r - r_m - \rho_{ml} - \rho_{mj})} dk \Bigg] \tag{114}$$

Each of the terms above in (114) has two integrals. Only the second of these terms gives δ-function from the angular and the energy integrals that peak at the same position. This serves to filter out the twin image and the effect of multiple scattering in the resulting image.

This result renders the consideration of multiple scattering in the DLEED holographic analysis unimportant.

At this point we have completed our brief survey of the theory of holographic diffuse LEED. In the next chapter we will discuss the way we tried to expand it in order that we study real systems.

Chapter 4

Holographic DLEED

4.1   Introduction

In the previous chapter we introduced the ideas of Dennis Gabor on holography and explained how one can combine them with the diffuse LEED method. We also presented the step-by-step development of a mathematical algorithm that is theoretically capable of taking as input the intensities of a DLEED experiment and outputting in real space the geometrical recontruction of the sample surface that produced these intensities.

In this chapter we will see how succesful our algorithm is by looking at image reconstructions of two systems: O/Ni(001) and K/Ni(001). We will also attempt to explore its flexibility by considering more realistic structures. But first let us get the insight of it thereby completing the discussion started in the previous chapter.

4.2 The CORRECT algorithm

Equation (106) is the analytical form of our algorithm which for convenience we reproduce here.

$$B(\vec{r}) = \int \int \int \chi(k_\perp, \vec{k}_\parallel) K(\vec{k}, \vec{r}) \exp(-\imath(kr + k_\perp z)) \exp(-\imath \vec{k}_\parallel \cdot \vec{r}_\parallel) dk_\perp d\vec{k}_\parallel \qquad (106)$$

where,

$$K(k_\perp, \vec{k}_\parallel; \vec{r}) = \left[\frac{(f_{\mathrm{a}}^+(\hat{k}_o^+ \cdot r) + C)}{r} \right]^{-1} \qquad (105)$$

and

$$\chi(\vec{k}) = \frac{H(\vec{k}) - H_{\mathrm{av}}(\vec{k})}{H_{\mathrm{av}}(\vec{k})} \qquad (94)$$

By looking at (106) we can make a few observations:

1. It contains a three dimensional integral with respect to the Cartesian coordinates of the reciprocal space vector $\vec{k} = (k_x, k_y, k_z)$. Comparing with a typical Fourier-transform integral:

$$f(a) = (\frac{1}{2\pi})^{1/2} \int_{-x}^{x} F(x) e^{\imath a x} dx \qquad (115)$$

we will see that (106) is a Fourier-like (since the kernel K depends on both $\vec{k}$ and $\vec{r}$) integral that transforms from the reciprocal to the three dimensional real space.

2. The kernel function $K(\vec{k}, \vec{r})$, defined in (105), represents an approximation to the amplitude of the reference wave at position $\vec{r}$. The numerator contains the two most important parts of this wave, namely the wave scattered by the adsorbed atom, represented by the atomic scattering factor f_{a}, and the wave that is first
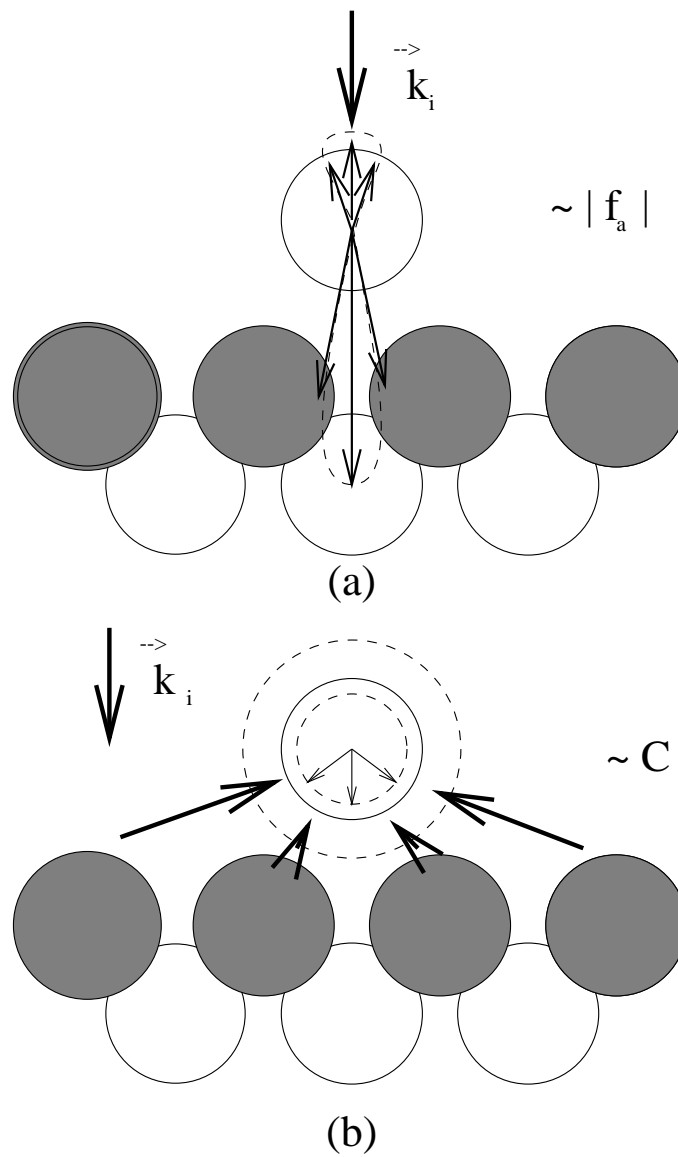
$$\sim |f_a|$$

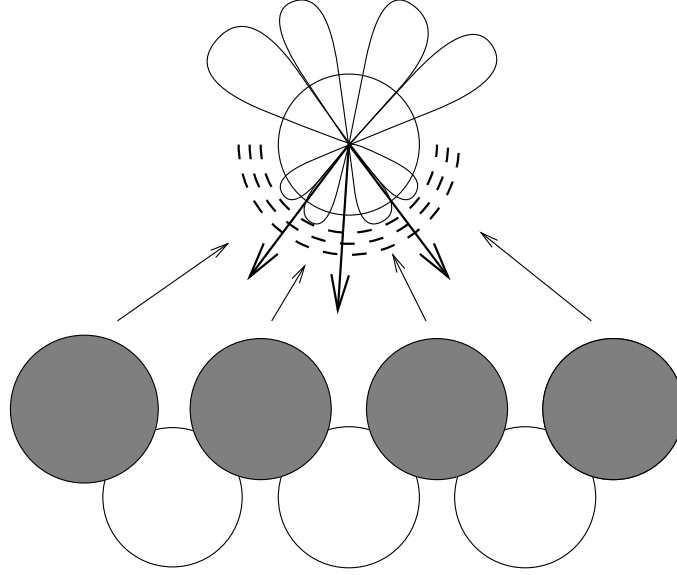(a)

$$\sim C$$

(b)

Figure 35: The Kernel function

Figure 36: The constant C in kernel function

scattered off the substrate and then travels toward the adsorbate, represented by the constant C thus compensating for its anisotropy. A better visualization of these two terms can be seen in figure 35 (a) and (b) respectively. Figure (36) helps us understand the reason for choosing a constant to represent that part of the reference wave scattered by the substrate layer. In the above we have taken into consideration figure 33, *i.e.*, that the atomic scattering factor has stronger magnitude in the forward than the backscattering direction, and that the backscattered wave has a more isotropic angular distribution. Of course the denominator in (105) is the familiar $1/r$ factor of every spherical wave.

3. The χ-function, (94), has been extensively discussed in section 2.3 but here we would like to show one more of its traits. Looking at figure 37 we see that the
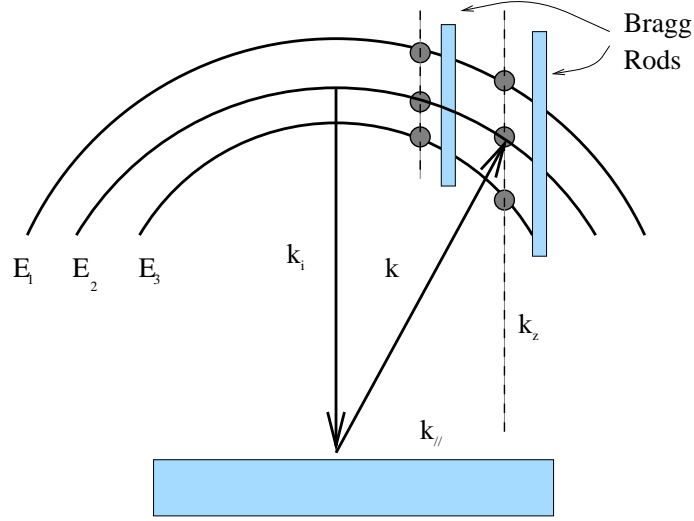
Figure 37: Use of χ-function

integration over the third coordinate, k_z, could be thought of as being over the energy k since $k_z = (k^2 - k_{\|}^2)^{1/2} = (2mE - k_x^2 - k_y^2)^{1/2}$. The Bragg-spots for different incident energies are found in rods normal to the surface. The way we have defined the χ-function enables us to avoid running into these rods and thus considering Bragg-spots intensities as well (that, as we know, carry only partial information of the position of the adsorbate relative to the substrate).

4. Multiple scattering is a process that is always present. Although in the previous chapter we proved that it does not play any important role in our reconstruction algorithm (since the usage of more than one energies negates its effects) neverthe-less its omnipresence is proved very usefull in making the object waves that reach the fluoresent screen more isotropic[?]. Figure 38 illustrates that idea.
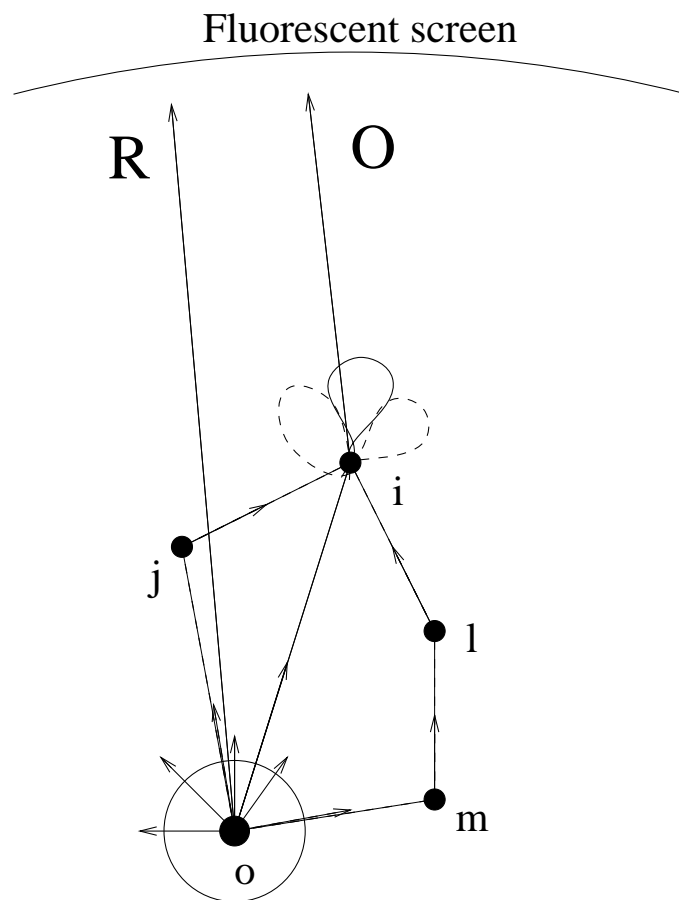
Figure 38: Schematic diagram illustrating the role of multiple scattering into making the object waves more isotropic

Accounting for all the above we suggested the name CORRECT (or **C**ompensated **O**bject- and **R**eference-wave **R**econstruction by an **E**nergy dependent **C**artesian **T**ransform) for our algorithm, thus expressing our belief in its capability to *correctly* (pun intended) perform the holographic reconstruction[**?**].

4.3 Testing the algorithm

After this analytical presentation of the CORRECT algorithm we will now try to see how successful (or unsuccessful) this has been. We will attempt to holographically reconstruct two systems: O/Ni(001) and K/Ni(001). Both of these have been thoroughly investigated and analyzed with the help of simple LEED and thus they can play the role of a guide that will show us how trustworthy our method is towards the investigation of unknown surface structures.

In each structure, atoms (oxygen or potassium) have been adsorbed on hollow sites of the nickel substrate that has been cut parallel to the (001) plane. This can been seen in figure 39 where the sphere labeled "A" is the adsorbate, spheres labeled "B", "C", "D" and "E" represent the first layer of the substrate Ni, whereas the sphere labeled "F" belongs to the second layer of substrate atoms. Figure 40 shows a schematic diagram of the three possible adsorption sites (top, bridge and hollow) of an atom on a fcc (001) surface and a better view of figure 39. We set up a coordinate system at the origin of which is located the adsorbed atom. Then we determine the positions of the substrate atoms with respect to it. Table 4.3 shows the coordinates of A, B, C, D, E and F atoms (figure 39) for both structures which have been determined by conventional
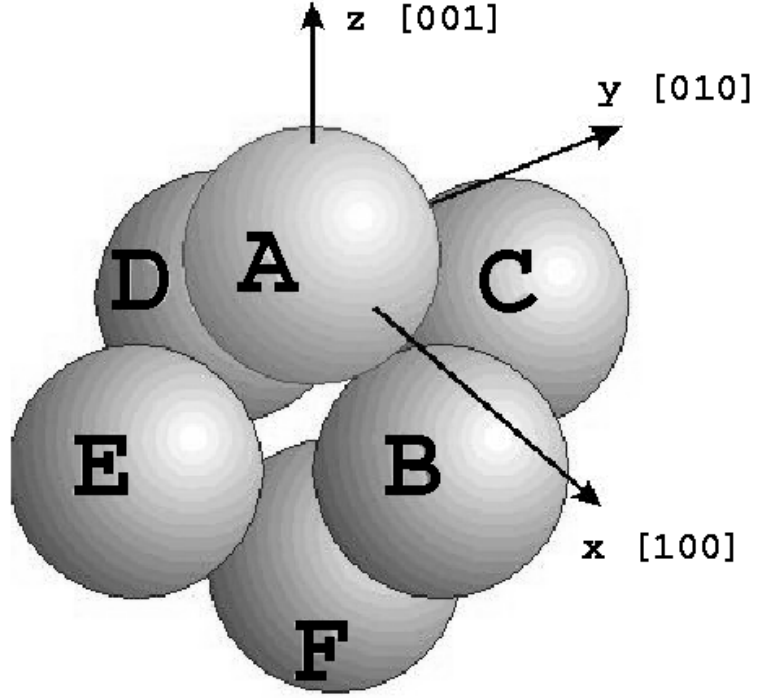
Figure 39: Hollow site adsorption along the (001) orientation

	O/Ni(001)			K/Ni(001)		
	$x(\text{Å})$	$y(\text{Å})$	$z(\text{Å})$	$x(\text{Å})$	$y(\text{Å})$	$z(\text{Å})$
A	0.00	0.00	0.00	0.00	0.00	0.00
B	1.25	1.25	-0.9	1.25	1.25	-2.7
C	1.25	-1.25	-0.9	1.25	-1.25	-2.7
D	-1.25	-1.25	-0.9	-1.25	-1.25	-2.7
E	-1.25	1.25	-0.9	-1.25	1.25	-2.7
F	0.00	0.00	-2.7	0.00	0.00	-4.4

Table 1: Positions of atoms A, B, C, D, E and F for the hollow site adsorption of figure 39 for O/Ni(001) and K/Ni(001)
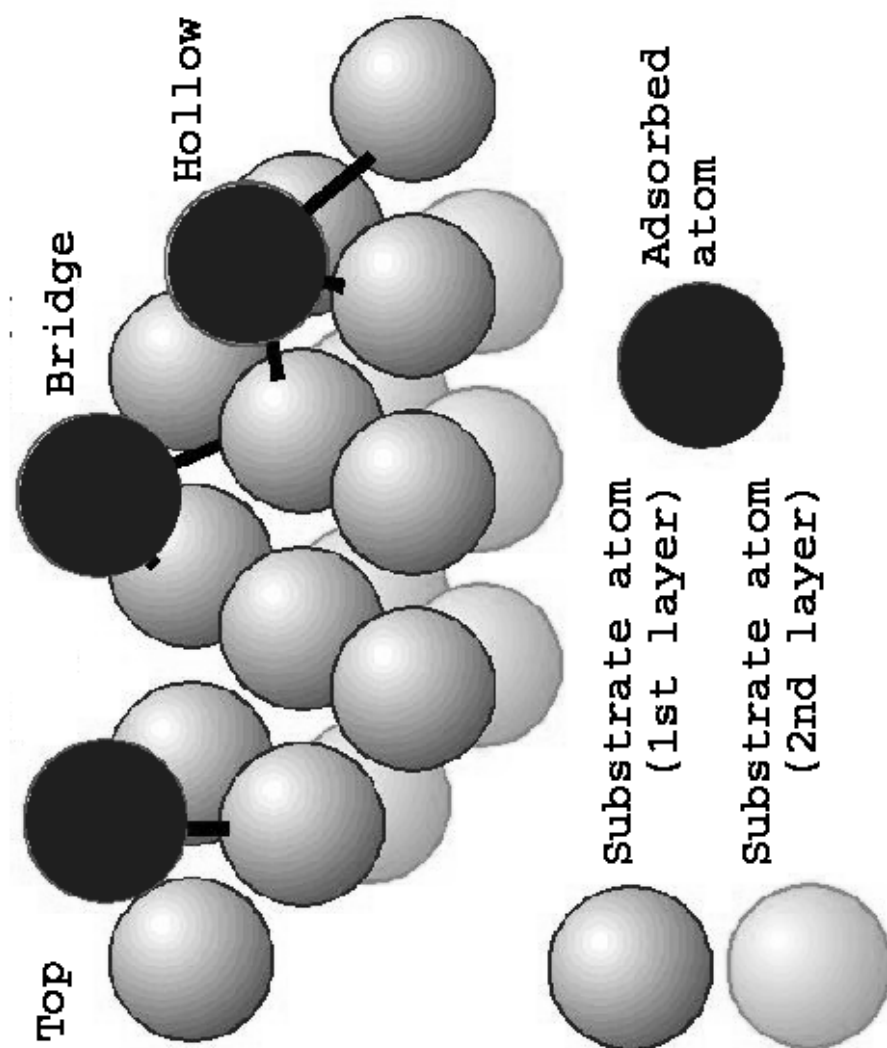
Figure 40: Top, bridge and hollow site adsorption

LEED calculations[?, ?].

When one wants to see how successful a theory is the first thing he usually does is to compare the results it produces with those produced by the experiment. Our method is based on the trial-and-error technique, that is, our algorithm inputs a diffraction pattern (actually more than one) and outputs, in real space, the structure that is responsible for this. We compare the reconstructed image to the accepted one and then re-do the calculations having slightly changed the parameters the algorithm depends upon. (An example of such a parameter is the C constant in the definition of the kernel K, (105). Choosing a very large C for the reconstruction is equivalent to not correcting for the anisotropic reference wave. The corresponding images will consequently contain only the atoms in the area just below the adsorbate atom (searchlight effect). When reducing the absolute value of C, the images exhibit also atoms in other regions of the local geometry. This is because a smaller C gives more weight to the anisotropic direct illumination and hence corrects more strongly for the reference wave. Finally, for too low a value of C, only atoms outside the forward-lobe directions will be visible, for now the reference wave anisotropy is overcompensated.) We keep on doing that until we obtain the optimum reconstructed image. Of course someone might argue that re-investigating a known structure is redundant. The answer to such an argument is that testing the method with known structures helps us improve the algorithm. When we are confident that it works with a number of different structures (in this thesis we prove that it gives fine results with two of them) then we can put it to the test with unknown ones. The advantage of our method is that it is faster compared to the traditional LEED and that it

can give three-dimensional results the way humans perceive "three dimensions". Going back to our initial argument we should add that one has to find a practical way to have experimental results to compare with without actually doing the experiment; in other words, he has to simulate the experiment. This is exactly what we have been doing in our case. In 1986 Saldin and Pendry wrote a program[**?**] that simulates a DLEED experiment. All that the program needs as input are the positions of the atoms of the cluster and the phase shifts for the different kinds of atoms at different energies and angular momenta. It outputs a two-dimensional array (usually 81×81 or 8×8 pixels per surface Brillouin zone) of intensities in the reciprocal space. Figure 41 shows three thus calculated diffraction patterns for the case of O/Ni(001) and for three different incident energies, 9, 10 and 11 $Hartrees$ (245, 272 and 299 eV) respectively. These patterns are the inputs of a ForTran program containing the algorithm, originally written by Dr. Xiang Chen and modified by the author and Dr. Dilano Saldin. What it follows are two sets of reconstructed images in three dimensions and in real space. Each set contains the same structure seen from different angles in order to give the viewer the perception of the third dimension. The adsorbed atom (O in figure 42 or K in figure 43) is not shown but is supposed to be at the origin of the coordinate system. The distance scales are specified by the ticks of the axes, at 1-Å intervals (1-Å corresponds to 5 pixels). The intensities of the reconstructed images are represented by small spheres whose radii are proportional to the intensity at that voxel (or volume picture element). Depending on the energy range, we employed 30 patterns for energy range 113-235 eV or 37 patterns for 70-435 eV. The phrase "Reconstruction using the χ-function" seen in the captions

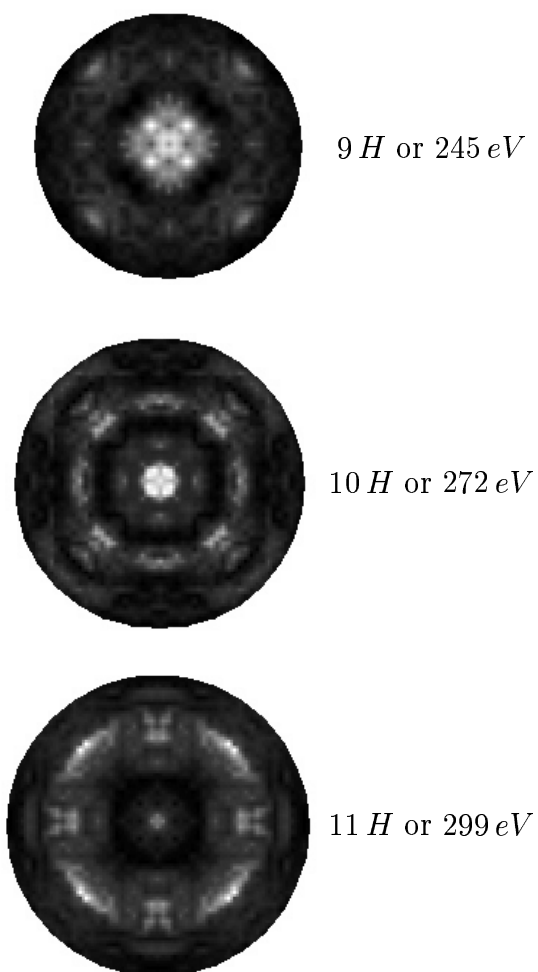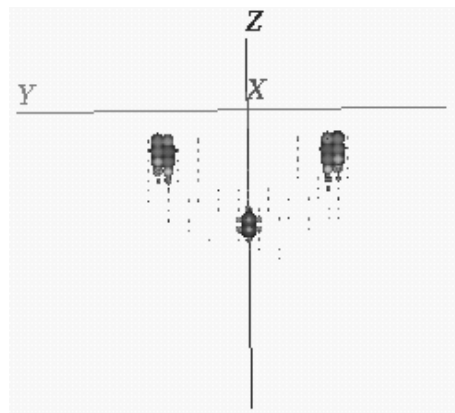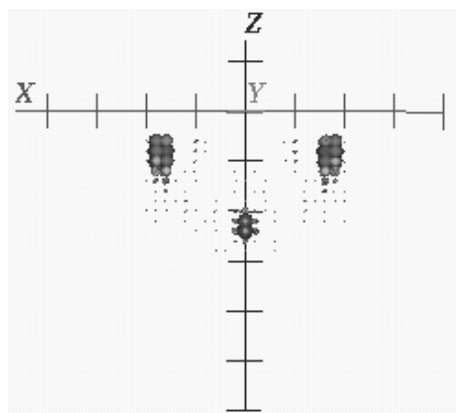9 H or 245 eV

10 H or 272 eV

11 H or 299 eV

Figure 41: Theoretically calculated diffraction patterns for O atoms adsorbed as a disordered lattice gas on a Ni(001) surface. The three patterns correspond to energies of 9, 10 and 11 $Hartrees$
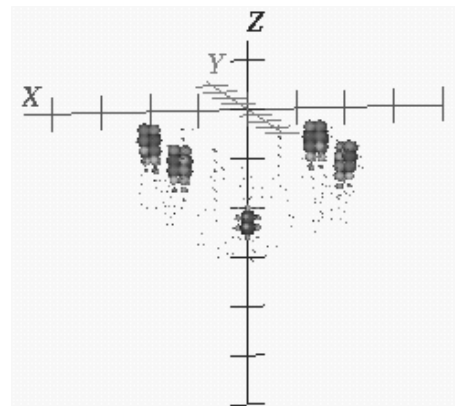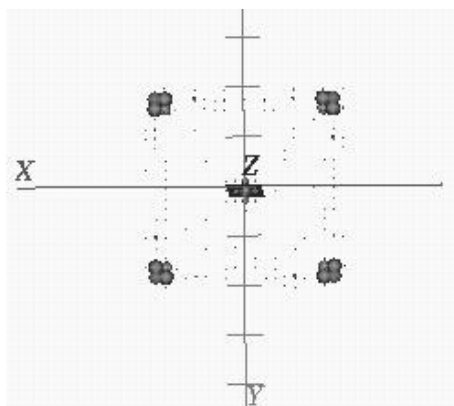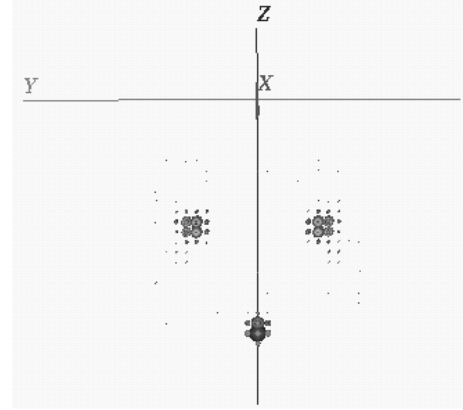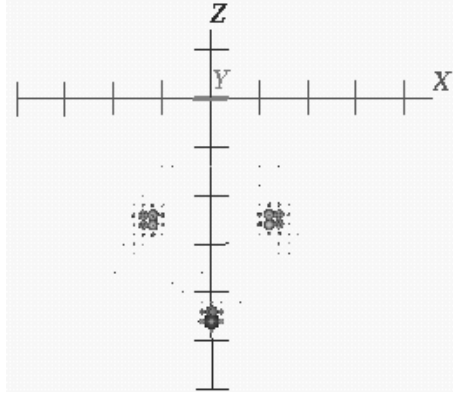
O/Ni(001)

Figure 42: Reconstruction of O/Ni(001) structure from theoretically calculated DLEED diffraction patterns. Energy range: 113-235 eV, $C = 1.0\,a.u.$ and usage of χ-function was made.
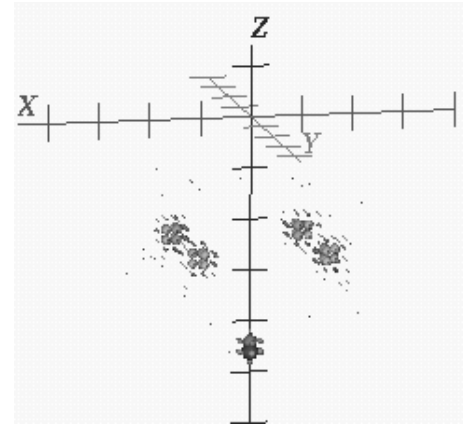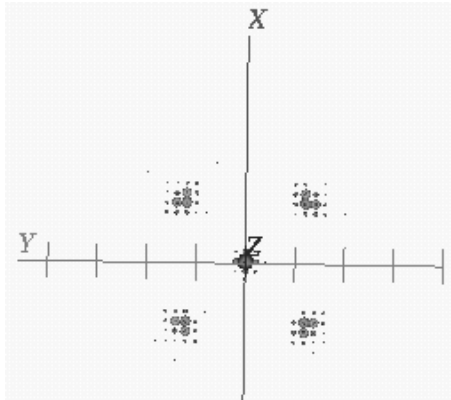
K/Ni(001)

Figure 43: Reconstruction of K/Ni(001) structure from theoretically calculated DLEED diffraction patterns with energy range: 70-435 eV, $C = 1.5\,a.u.$ and usage of χ-function.
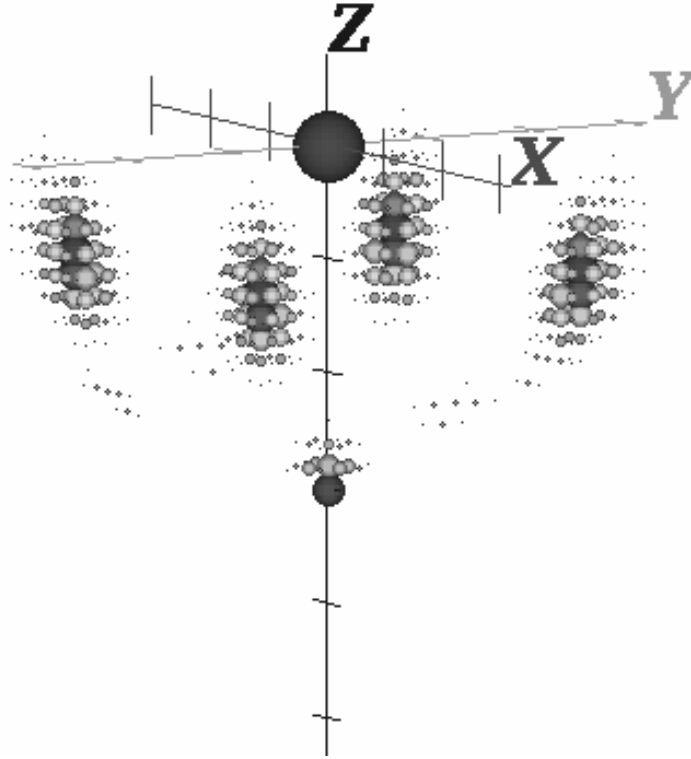
Figure 44: Reconstruction of O/Ni(001) structure from experimental DLEED diffraction patterns

of them and the following figures refers to the known χ-function we spoke about in the beginning of the chapter when we presented the CORRECT algorithm. The meaning of that phrase will become obvious in chapter 5. In each figure the reader will find the value of the constant C of (105) used for the particular reconstruction[?, ?]. Figures 44 and 45 show the corresponding results we obtained by doing reconstruction of the two structures using the same algorithm but experimental diffraction patterns.

Figure 45: Reconstruction of K/Ni(001) structure from experimental DLEED diffraction patterns

4.4   Further investigation

The diffraction patterns we take from a DLEED experiment do not look quite like those in figure 41. First of all, they are not completely symmetrical. Besides the dark shadow of the electron gun projected onto the pattern, what dominates them are the bright spots left by the electrons scattered by the substrate atoms, the Bragg spots. As we have explained earlier these spots carry only partial information as far as the position of the adsorbates is concerned, which rather distorts the reconstructed images. Thus they have to be removed from the patterns. The reason we keep repeating that the Bragg spots carry only partial information about the position of the adsorbates is that their presence cover a significant portion of diffuse intensity, the very one that actually holds the above mentioned information. The procedure of Bragg spot removal and symmetrization of the experimental diffraction patterns is depicted in figure 46. As one can see, the process of the Bragg spot removal consists in cutting out a considerably large area around each spot. By doing this we remove some diffuse data as well that possess exactly the information we are seeking out. Our goal is to find out how much damage we do to the pattern, or in other words, how many diffuse spots we are allowed to remove and still obtain a good, acceptable reconstructed image from the rest of the pattern. One more issue that one has to account for is the number of data he has to use in his investigation. The logic behind that is for one to use as little data as possible, and thus, reduce the amount of time needed for their collection and study. Towards those two goals we conducted some theoretical investigations making use of our algorithm and reconstruction program.
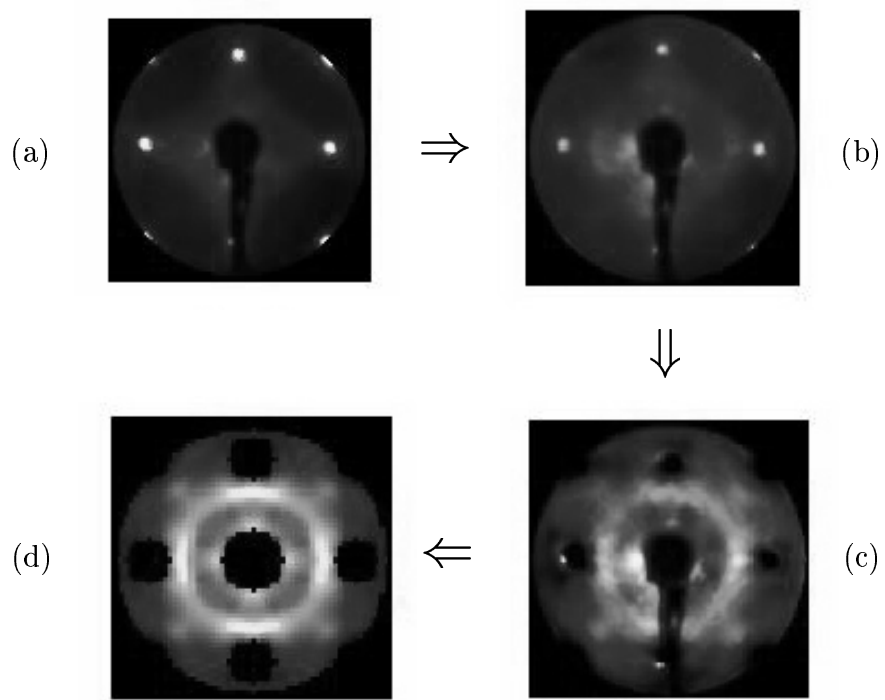
Figure 46: Bragg spots removal and symmetrization of an experimental diffraction pattern. $a \to b$: Subtraction of LEED pattern **before** adsorption. $b \to c$: Removal of the substrate Bragg spots. $c \to d$: Four-fold symmetrization of the diffraction pattern.

Looking first at the second case, that is, the issue of the amount of data, we understand from figure 46 that we will have to decide on the number of pixels of diffuse data between the bright Bragg spots we wish to include. We started by collecting a diffuse LEED array sampled on an 8 × 8 grid of points per surface Brillouin zone. We have already seen the results of such a reconstruction in the previous figures 42 and 43 for the two structures respectively. We were satisfied with such an output and we decided to collect now diffuse data within a 4 × 4 array per surface Brillouin zone. These new results can be seen in figure 47 and 48. It is obvious from the figures that one can observe no deterioration in the reconstruction of the images for both structures. Thus, from this point forward and for the investigation of the removal of the Bragg spots, we decided to use only 4 × 4 data sampling for one more reason; our reconstruction program needs only a few seconds of real computer time to run (at least for the CPU R10000 processor of Silicon Graphics Indigo^2 (IRIX 6.2)), which made our job a lot easier. We started by removing only the area that the Bragg spots would occupy on the experimental diffraction patterns (we should understand that the calculated diffraction patterns do not contain Bragg spots) as can be seen in figure 49. Then we proceeded in cutting out a circle the center of which was the Bragg spot and its radius equal to $1/8\,g$, where g is the reciprocal lattice vector, figure 50. Next we removed a circular area with radius $1/4\,g$. After each such removal we followed the reconstruction procedure from the remained patterns. The outcome for both O/Ni(001) and K/Ni(001) structures are seen in figures 51, 52 and 53, respecively. From these figures we can conclude that one can safely remove a circular area of radius $0.125\,g$ for the O/Ni(001) surface and only
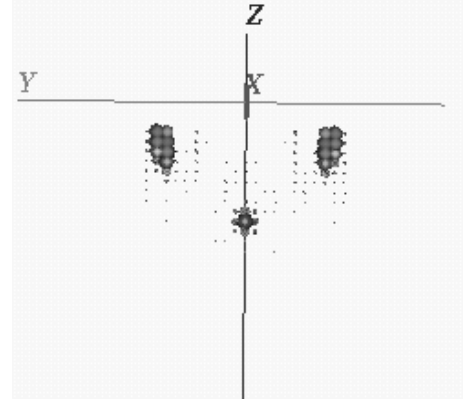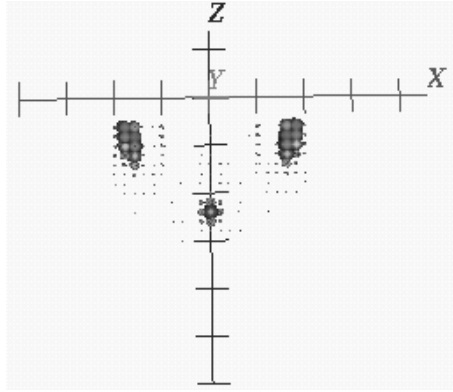
O/Ni(001)

Figure 47: Reconstruction of O/Ni(001) structure from theoretically calculated DLEED diffraction patterns with 4×4 data sampling. Energy range: 113-235 eV, $C = 1.0\,a.u.$ and usage of χ-function was made.

K/Ni(001)

Figure 48: Reconstruction of K/Ni(001) structure from theoretically calculated DLEED diffraction patterns with 4×4 data sampling and removal of the Bragg spots. Energy range: 70-435 eV, $C = 2.5\,a.u.$ and usage of χ-function was made.
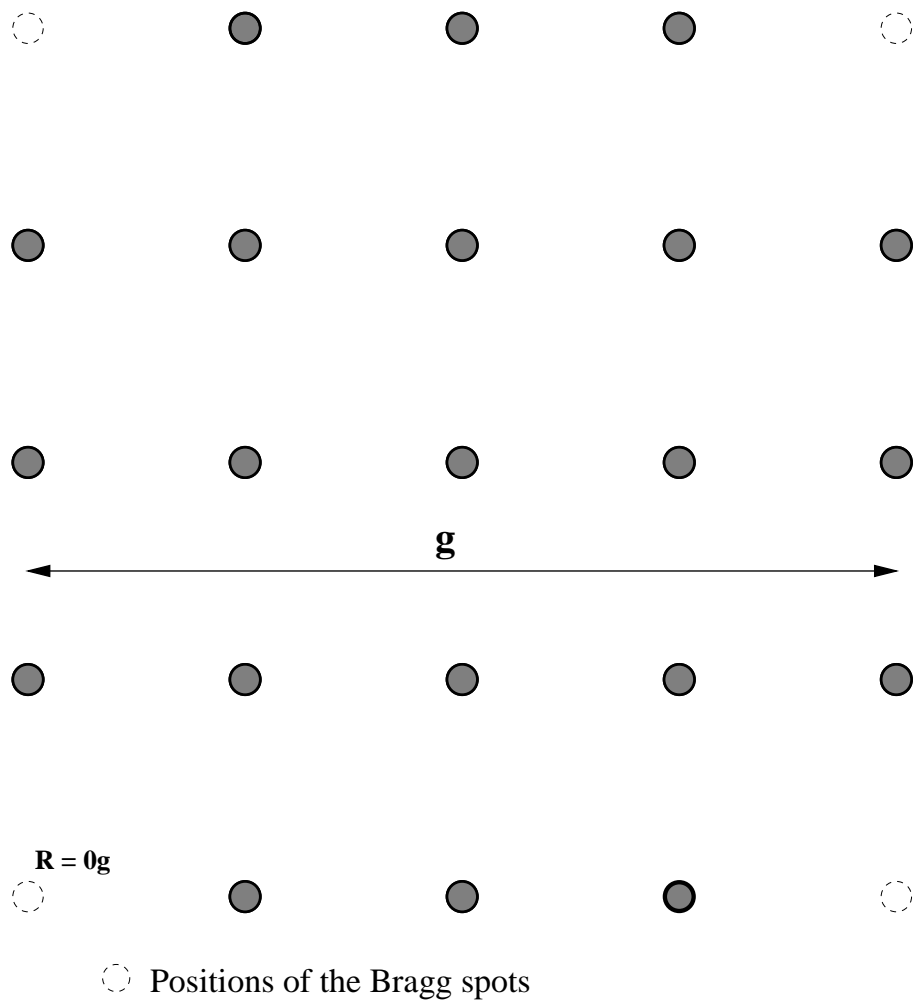
Figure 49: 4×4 data sampling per surface Brillouin zone; removal of circle radius $R = 0\,g$ around Bragg spots
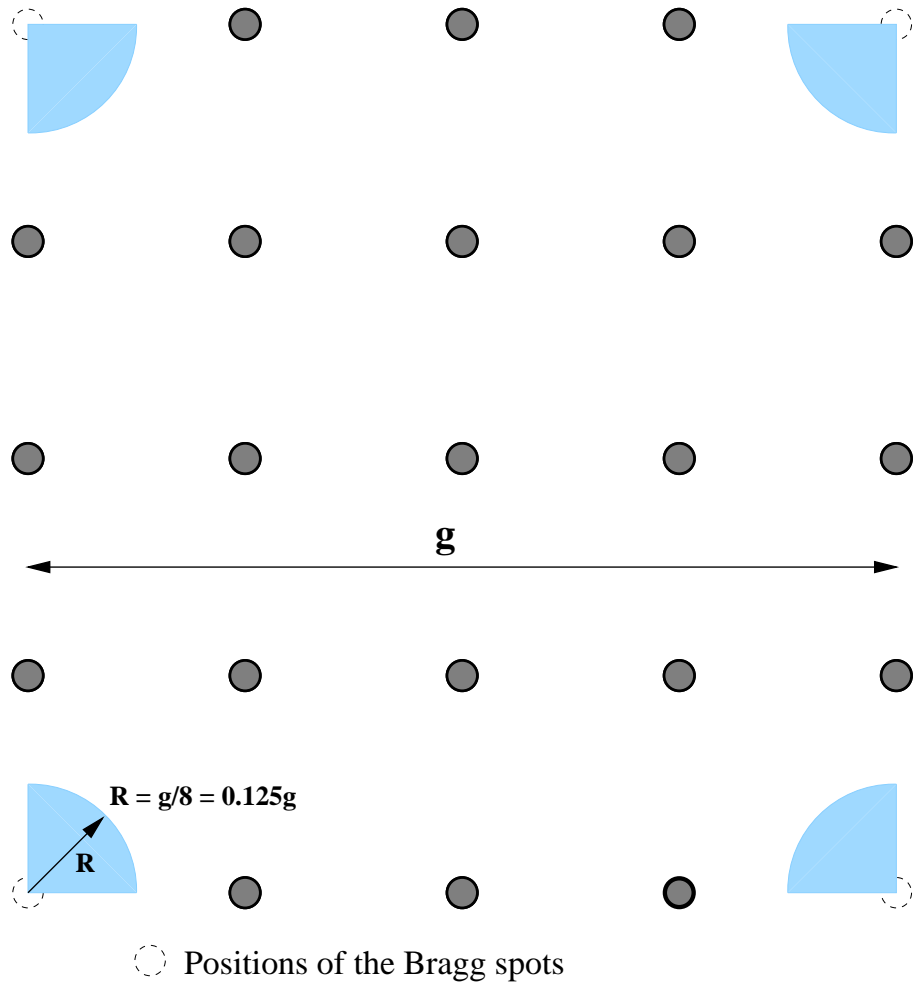
Figure 50: 4×4 data sampling per surface Brillouin zone; removal of circle radius $R = 0.125\,g$ around Bragg spots
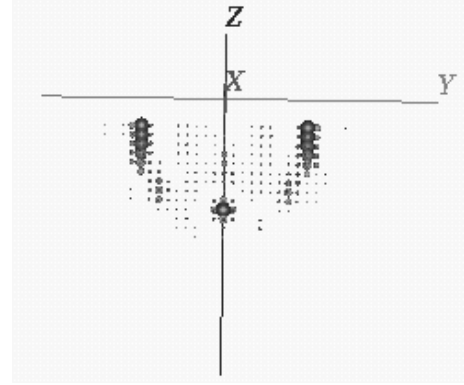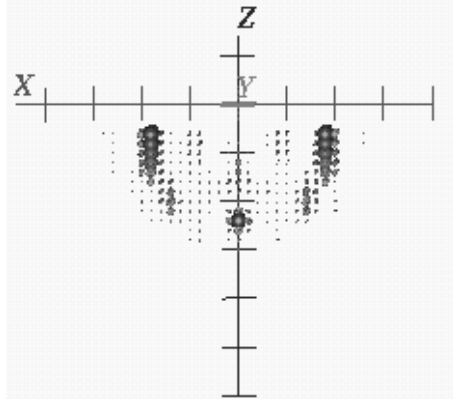
O/Ni(001)
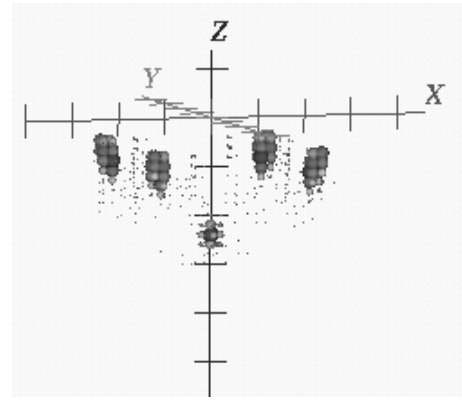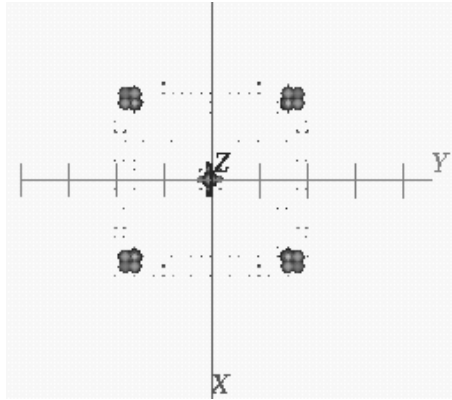
Figure 51: Reconstruction of O/Ni(001) structure from theoretically calculated DLEED diffraction patterns with 4×4 data sampling and removal of the Bragg spots. Energy range: 113-235 eV, $C = 2.5\,a.u.$ and usage of χ-function was made.
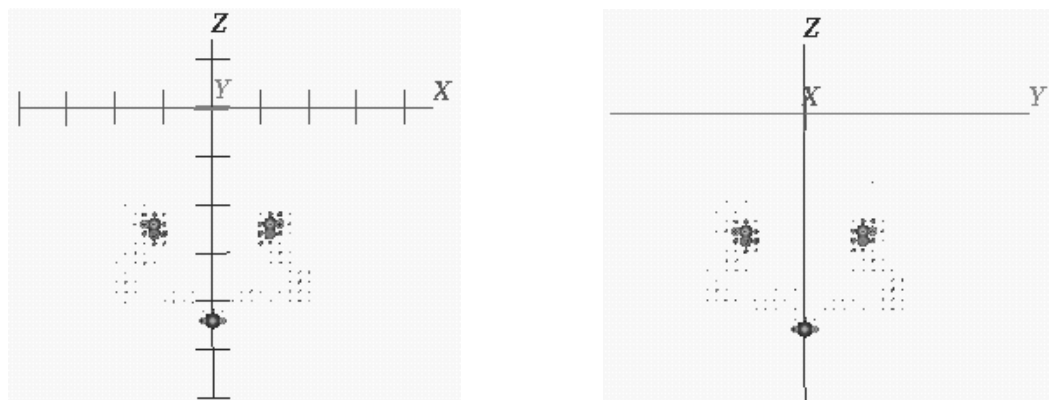
O/Ni(001)

Figure 52: Reconstruction of O/Ni(001) structure from theoretically calculated DLEED diffraction patterns with 4×4 data sampling and removal of a circular area radius $0.125\,g$ around the Bragg spots. Energy range: $113\text{-}235\,eV$, $C = 2.5\,eV$ and usage of the χ-function.
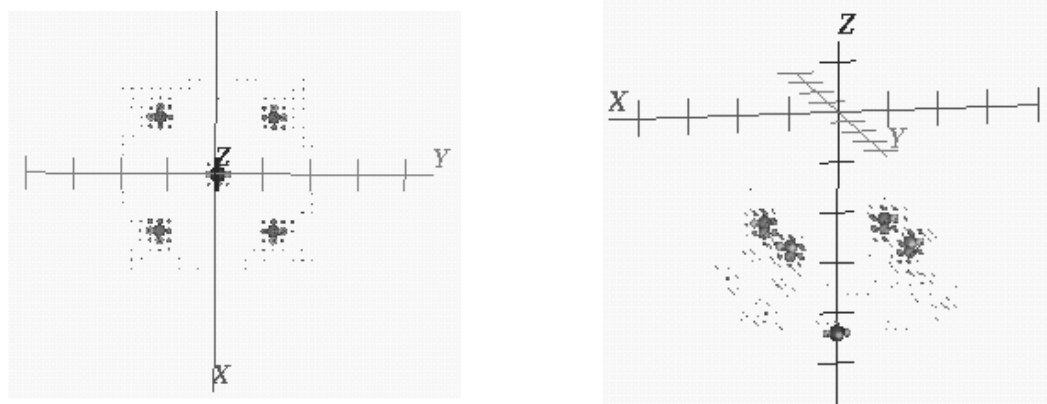
K/Ni(001)

Figure 53: Reconstruction of K/Ni(001) structure from theoretically calculated DLEED diffraction patterns with 4×4 data sampling and removal of the Bragg spots. Energy range: 70-435 eV, $C = 2.5\,a.u.$ and usage of χ-function was made.

the Bragg spot for the K/Ni(001) one.

So far we have studied and successfully reconstructed two structures utilizing diffraction patterns obtained by performing diffuse LEED experiments. By now, the reader will have already realized that we have not said anything about investigating surfaces containing ordered adsorbates. In attempting to employ as little data as possible we, previously, moved from the 8×8 sampling of diffraction intensity per surface Brillouin zone to the 4×4. Unfortunately, a $p(4 \times 4)$ overlayer of O/Ni(001) or K/Ni(001) is not an often encountered phenomenon in nature. On the other hand, $p(2 \times 2)$ layers are very common structures. The upper panel of figure 54 shows the real space mesh of such a layer on a (1×1) clean surface (top site adsorption), whereas the lower panel shows the reciprocal space mesh. The above discussion sets out our next goal; that is, to successfully perform a reconstruction of the above same two systems which will now have coverage $p(2 \times 2)$. Actually, when in the beginning we spoke about the two structures as having been investigated by traditional LEED methods that was the sort of coverage we had in mind. We employed for one more time our reconstruction algorithm on a 2×2 grid of data points per substrate surface Brillouin zone. Figures 55 and 56 present the results we came up with. They are pretty discouraging. Although we still get blobs at almost the right atomic positions what is most disappointing is the heavily artifacted images. Were we studing a completely unknown surface we would not be able to tell which of those blobs are the atoms and which the artifacts.

We will have to look upon our algorithm one more time and determine the cause of this anomaly. In chapter 5 we present our argumentation towards solving this problem.
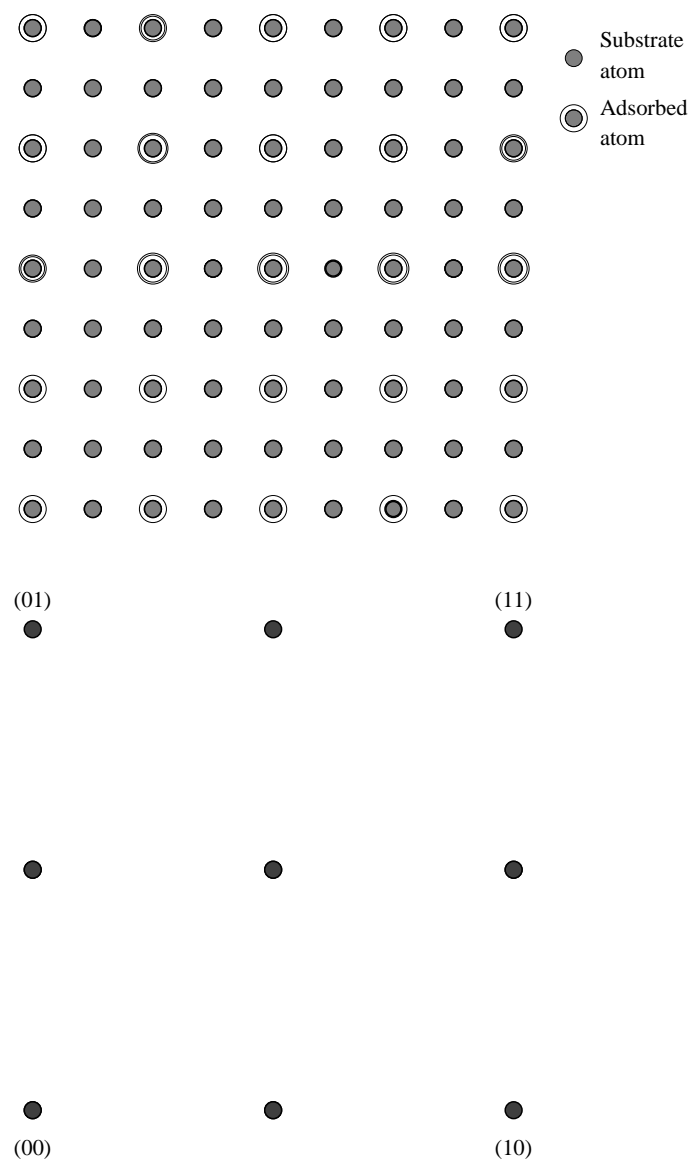
Figure 54: A $p(2 \times 2)$ surface mesh (upper panel) with the corresponding reciprocal space LEED pattern (lower panel)
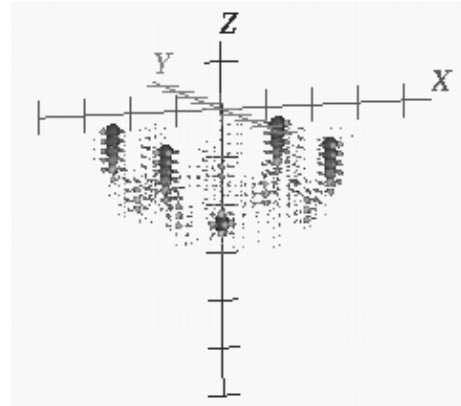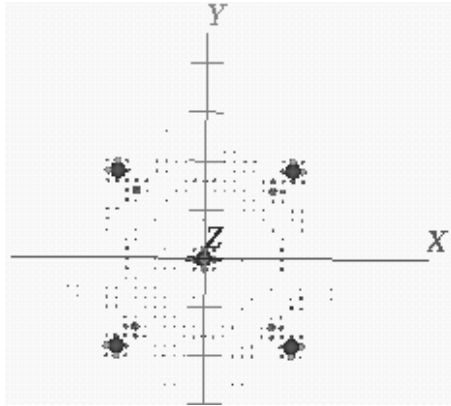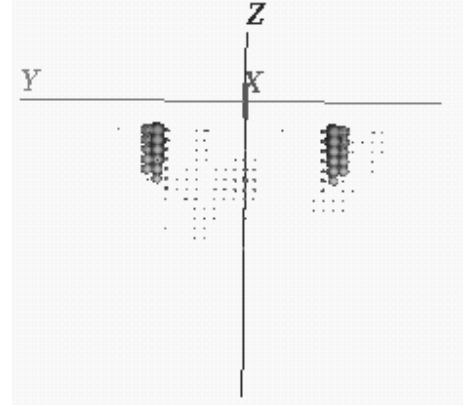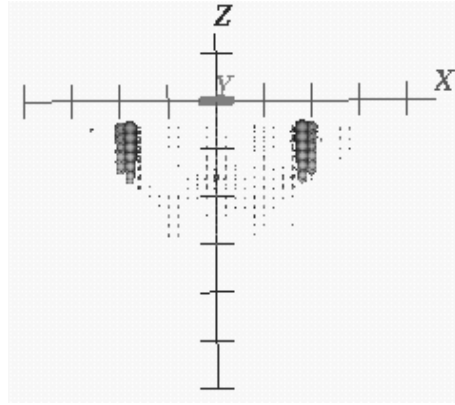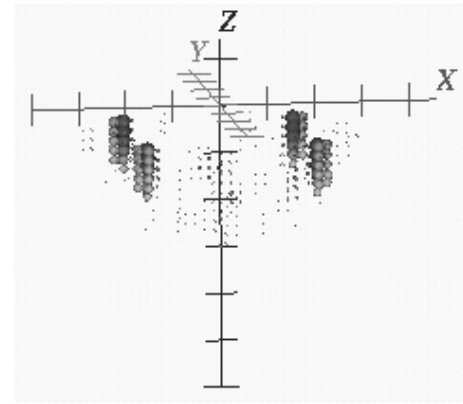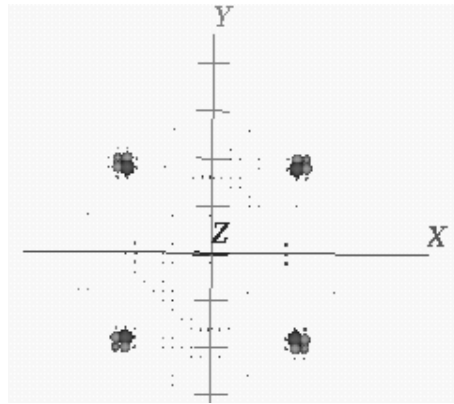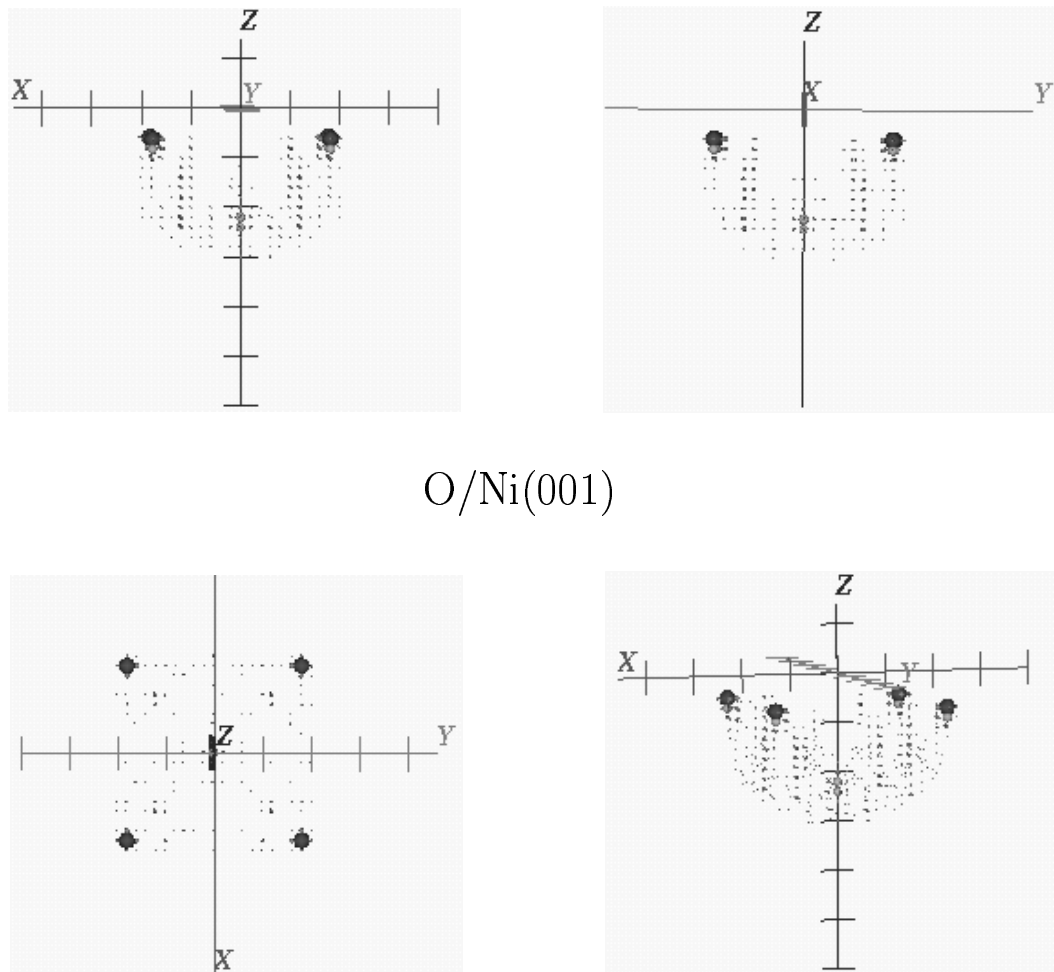
O/Ni(001)

Figure 55: Reconstruction of O/Ni(001) structure from theoretically calculated DLEED diffraction patterns with 2×2 data sampling with energy range 113-235 eV, $C = 2.5\,a.u.$ and usage of the χ-function.
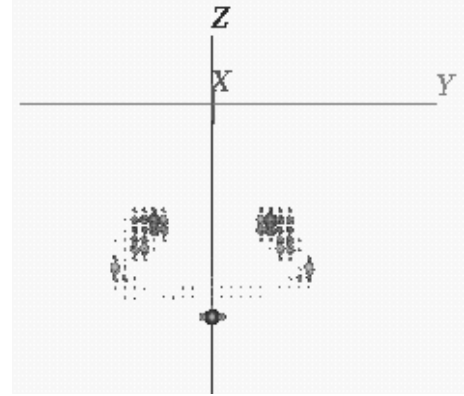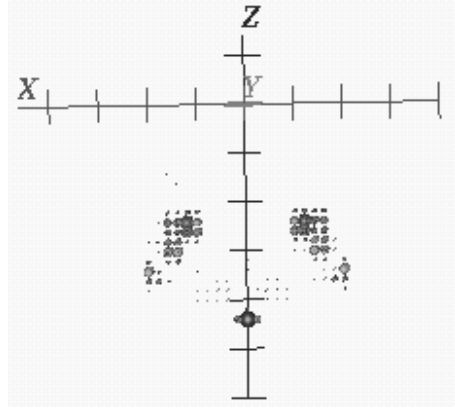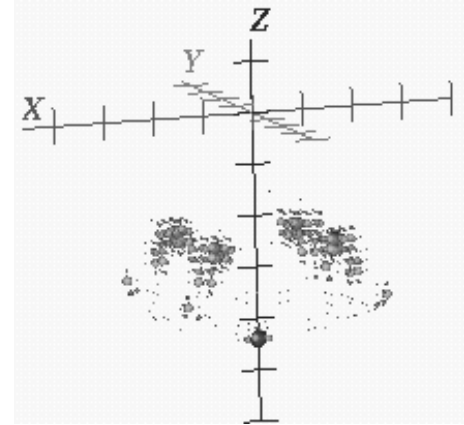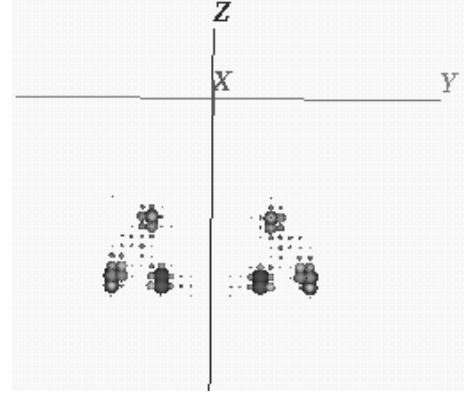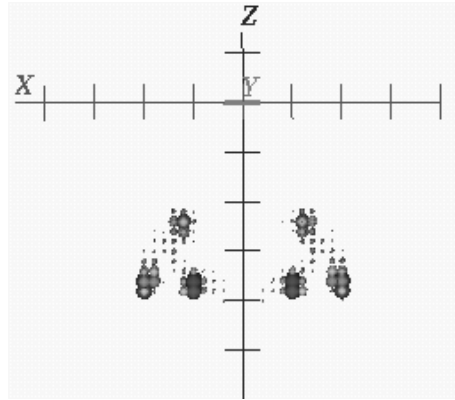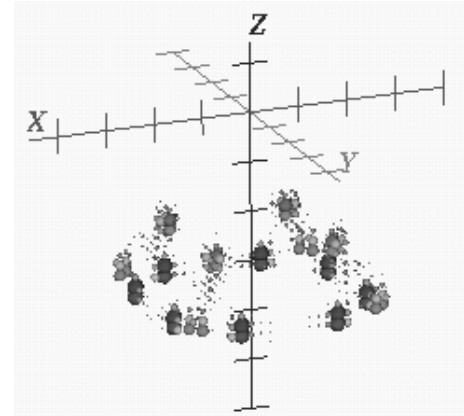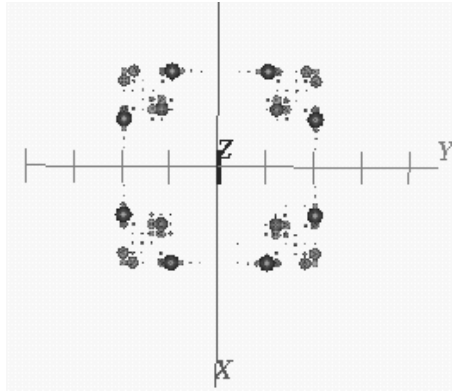
K/Ni(001)
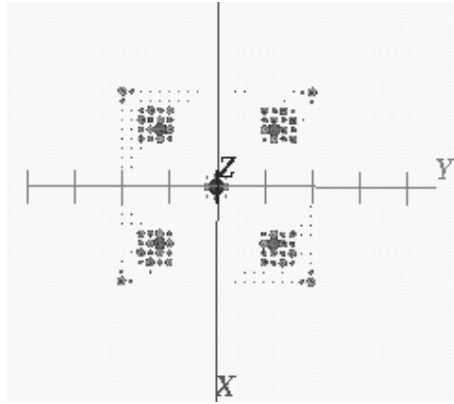
Figure 56: Reconstruction of K/Ni(001) structure from theoretically calculated DLEED diffraction patterns with 2×2 data sampling and energy range: 70-435 eV. Value of $C = 1.5\,a.u..$ χ-function usage was made.

In the meantime we needed a model simulation program that would guide us towards the right direction of our research. In the chapter that follows we present just that.

Chapter 5

The model DLEED program

5.1 Presentation of the program

In 1986 Saldin and Pendry wrote a sophisticated ForTran program[?] to calculate the
diffuse intensity distribution produced by low-energy electrons scattered from adsorbates
randomly adsorbed on locally identical sites on a clean surface. This program needs as
input data concerning the local geometry of the adsorption, phase shifts of both the
adsorbate and the substrate atoms, as well as, the energy of the incident electrons.
Since we need intensity patterns for more than one energy the user has to edit the input
file and run the program again and repeat this procedure for all the needed energies. The
run-time depends on the particular computer used but is approximately 10 minutes for
the low energies and about 60-70 minutes for the high ones for the CPU R10000 processor
Unix system of the Silicon Graphics Indigo^2 (IRIX 6.2). This, of course can be done
within the course of a day, but in the case that the user wants to change another feature

he will have to go through this again for another day! In calculating the intensities the DLEED program takes account of all the possible scatterings of the electrons, which is what a reliable simulation of an experiment is supposed to do. On the other hand the researcher who liked to do a faster exploration of the simulated experiment would use a program, maybe a bit less reliable than the DLEED one, yet flexible and supple.

That was the main reason we decided to write a simple model program that does almost what the Saldin and Pendry's does with some simplifications. One of them is that ours takes into consideration only the most important scattering paths of the electrons. In order to decide what part is more and what is less important we took, in our opinion, the most logical step, that is, we considered paths that contain up to two back scatterings per electron, assuming the more complicated ones weak enough to be left out. Thus we ended up using the following four terms:

1. The reference wave term. This contains the scattering of the incident electron off the adsorbed atoms.

2. The object wave term. This contains the scattering of the electron that, having been scattered off the adsorbate, is scattered by the substrate atom.

3. The reference-primed term. In this case the electron first is scattered by the substrate and then by the adsorbate.

4. The object-primed term. Here we consider the path followed by the electron that first gets scattered by the substrate, then by the adsorbate and finally by the substrate again.

The first two are the basic terms used to do holography; we always need a reference and an object wave. With the last two terms we take one short step towards the multiple scattering. This is a way to actually explore the degree of influence multiple scattering has. In all four cases, the electron, after finishing its scattering, travels towards the detector. All four paths are clearly shown in figure 57.

The reader can find the code of our program in appendix B but here we will attempt a short presentation of it analyzing its basic subroutines. The language used is ForTran 77 and basicaly is portable but it should be taken into consideration that some ForTran compilers are more selective than others. The program has been tested on three Unix machines, so far (IRIX 6.2, OSF1 and SunOS 4.2.1), and it has been noticed that the IRIX and SunOS compilers prefer that the subroutine arguments be declared both inside the subroutines and in the main program, whereas the OSF1 had no complaint.

subroutine ATOSFAC This subroutine is the basis of the program. It calculates the atomic scattering factor for the given energy based on the "spherical wave" form of this quantity[?], that is:

$$f_k(\theta) = \frac{1}{k} \sum_\ell (2\ell + 1) e^{i\delta_\ell} \sin \delta_\ell(k) P_\ell(\cos \theta) c_\ell(kr) \tag{116}$$

where, $c_\ell(kr)$ is the polynomial coefficient of the Hankel function of the first kind, $h_\ell^{(1)}$. It can be determined from the recurrence formula:

$$c_{\ell+1}(kr) = c_{\ell-1}(kr) + \frac{2\ell + 1}{kr} i \tag{117}$$

and $P_\ell(\cos \theta)$ are the Legendre polynomials with recurrence formula:

$$P_{\ell+1} = \frac{(2\ell + 1) P_\ell P_1 - \ell P_{\ell-1}}{\ell + 1} \tag{118}$$
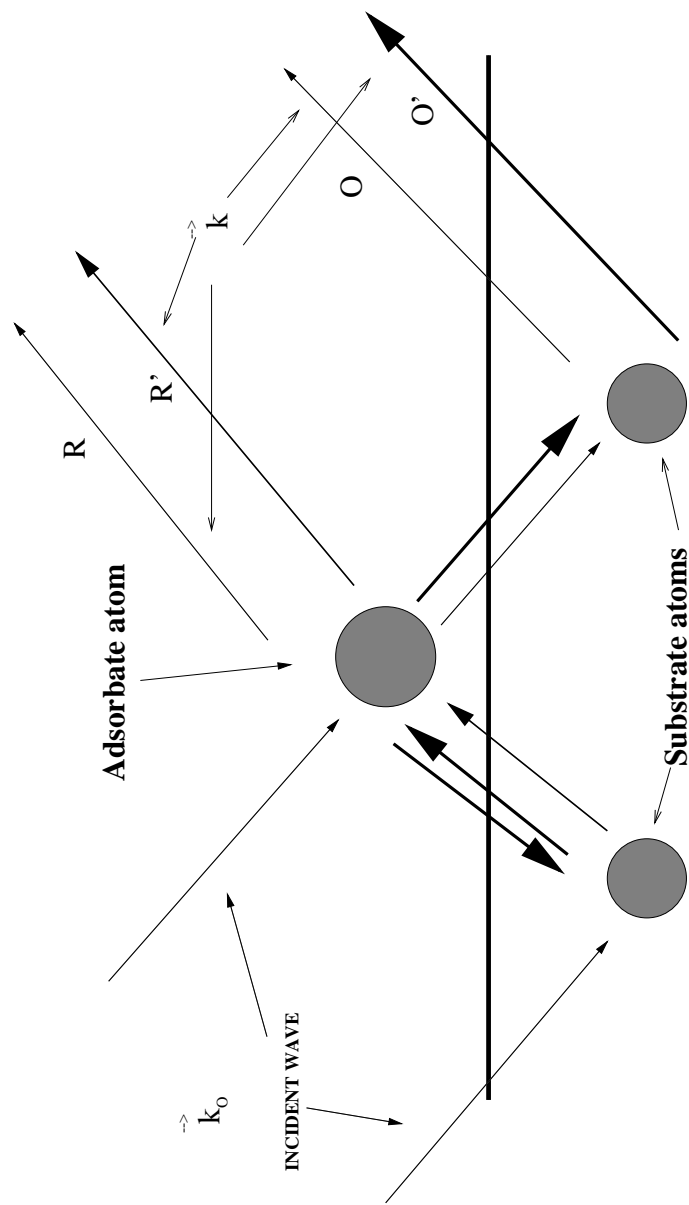
Figure 57: The simple model program
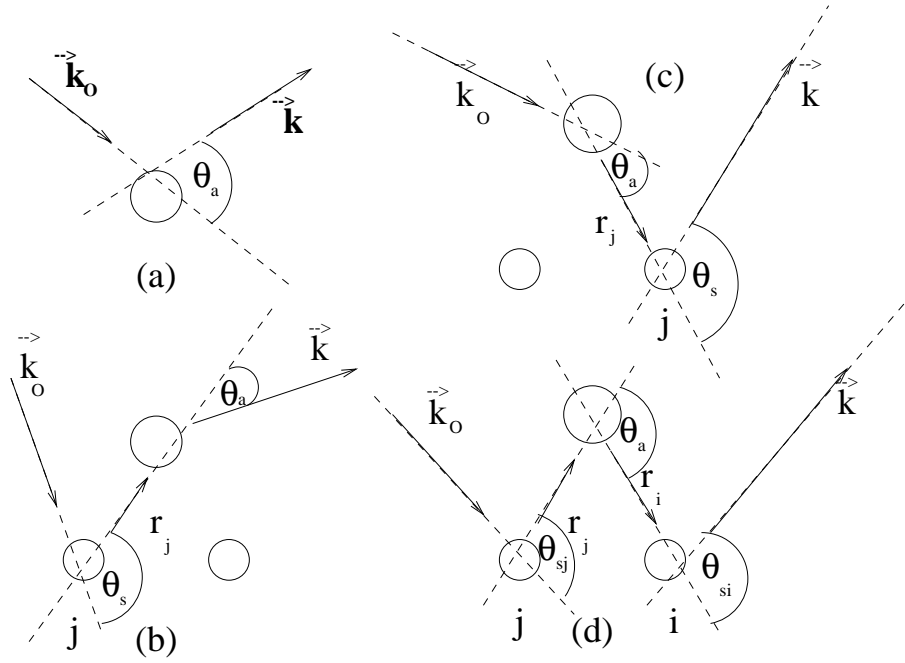
Figure 58: The four subroutines: (a) REFERENCE, (b) REFERENCE_PRIMEj, (c) OBJECTj, (d) OBJECT_PRIMEj

subroutine REFERENCE For simplicity we assume that the incident electron wave has unit amplitude. Then the scattering of the adsorbated atom will produce a wave amplitude equal to the scattering factor of the adsorbate, $f_{ad}(\theta_a)$ (figure 58(a)). If $\vec{k}_o$ and $\vec{k}$ are the wave vectors of the incident and the scattered waves respectively then the angle between them will be given by:

$$\cos\theta_a = \frac{k_{xo}k_x + k_{yo}k_y + k_{zo}k_z}{k^2} \tag{119}$$

Calling subroutine $atosfac$ we calculate f_{ad} that is returned to the main program. To indicate that the detector is comparatively in a much larger distance than the atomic distances we give an arbitrary large number for argument r (10000.0, say).

subroutine REFERENCE_PRIMEj According to figure 58(b), we have defined as second kind of reference wave the one that comes about from the scattering of the incident off a substrate atom, (j), and then off the adsorbate. The scattering off the substrate atom will change the direction of the incident wave vector by an angle:

$$\cos\theta_s = \frac{x_j k_{xo} + y_j k_{yo} + z_j k_{zo}}{k r_j} \tag{120}$$

giving rise to a wave with amplitude $f_{sb}(\theta_s)$ calculated from $atosfac$, where r_j is the distance between the the adsorbate and j-substrate atom. This wave, at the position of the adsorbate will have the form:

$$f_{sb}\frac{\exp(\imath k r_j)}{r_j} \tag{121}$$

(121) will reach the detector in the form:

$$f_{\text{ad}} \left[f_{\text{sb}} \frac{\exp(\imath k r_j)}{r_j} \right] e^{-\imath \vec{k} \cdot \vec{r}_j} \tag{122}$$

where $\exp(-\imath \vec{k} \cdot \vec{r}_j)$ is the phase difference between the original incident and the thus scattered wave.

subroutine OBJECTj Figure 58(c) shows the scattering procedure; the incident wave is scattered off the adsorbate and then off the substrate atom j. Calling *atosfac* twice will calculate the scattering factors of the ad- and the sub-atoms for angles of deflections:

$$\cos \theta_{\text{a}} = \frac{x_j k_{xo} + y_j k_{yo} + z_j k_{zo}}{k r_j} \tag{123}$$

$$\cos \theta_{\text{s}} = \frac{x_j k_x + y_j k_y + z_j k_z}{k r_j} \tag{124}$$

The wave that travels to the detector has the form:

$$f_{\text{ad}} \left[f_{\text{sb}} \frac{\exp(\imath k r_j)}{r_j} \right] e^{\imath \vec{k} \cdot \vec{r}_j} \tag{125}$$

with $\exp(\imath \vec{k} \cdot \vec{r}_j)$ being the phase difference between the incident and the scattered wave that reach the detector.

subroutine OBJECT_PRIMEj In this case (see figure 58(d)), first we have scattering off the substrate atom j. The scattered wave travels towards the adsorbate where it is scattered as:

$$f_{\text{sj}} \frac{\exp(\imath k r_j)}{k r_j} e^{-\imath \vec{k}_o \cdot \vec{r}_j} \tag{126}$$

and travels towards the substrate atom i where it takes the form:

$$f_{\text{a}} \left[f_{sj} \frac{\exp(\imath k r_j)}{k r_j} e^{-\imath \vec{k}_o \cdot \vec{r}_j} \right] \frac{\exp(\imath k r_i)}{r_i} \tag{127}$$

Finally this wave will be scattered one more time by the i atom and it will reach the detector with form:

$$f_{\text{si}} \left(f_{\text{a}} \left[f_{\text{sj}} \frac{\exp(\imath k r_j)}{k r_j} e^{-\imath \vec{k}_o \cdot \vec{r}_j} \right] \frac{\exp(\imath k r_i)}{r_i} \right) e^{-\imath \vec{k} \cdot \vec{r}_i} \tag{128}$$

Again, $\exp(-\imath \vec{k}_o \cdot \vec{r}_j)$ and $\exp(-\imath \vec{k} \cdot \vec{r}_i)$ are the phase shifts between the incident and the total scattered wave.

5.2 Testing the model program

Now it is about time to test our program. Before we even start our exploration towards solving the anomalous results we observed in the previous chapter we would like to see whether or not we can reproduce the images reconstructed from DLEED simulations by the Saldin–Pendry program. In the following pages the reader will find a set of figures showing reconstructed images of O/Ni(001) and K/Ni(001) using the theoretical diffracrtion patterns calculated with our simple program. Of course for the reconstruction we employed the Chen–Saldin–Vamvakas program. A comparison with the similar images of the previous pages (figures 42, 47, 43 and 48) renders our model program trustworthy to continue with our research. (The differences in the C value between these figures and those taken from the Saldin–Pendry program are due to the simplicity of the model program).

Before we finish with this chapter we should test our simplified model with the 2×2 sampling. We saw in chapter 3 that our algorithm, at its current form, fails to reconstruct reliable images from this kind of data distribution. The model calculation should predict
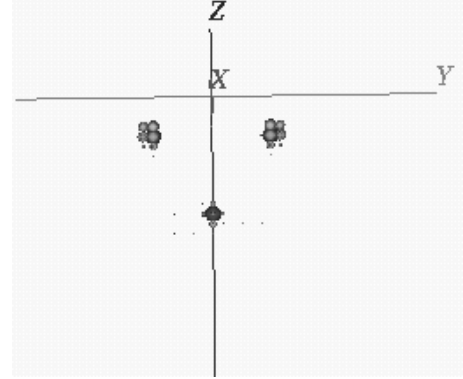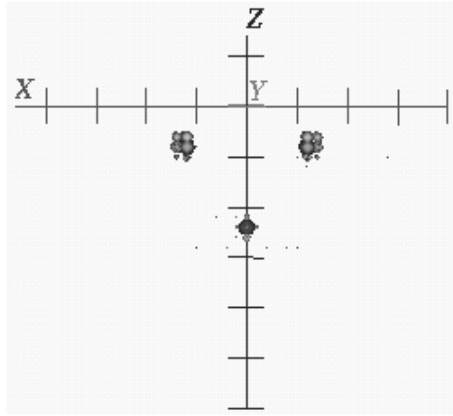
O/Ni(001)
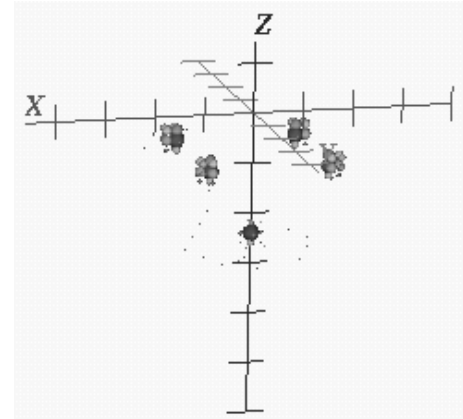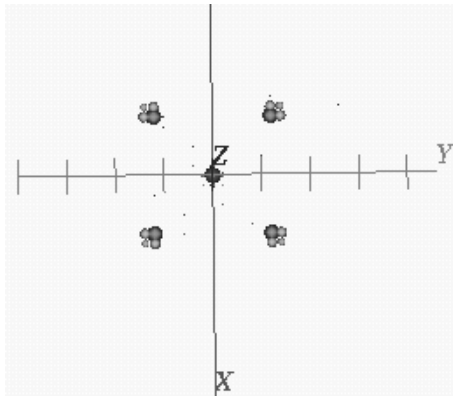
Figure 59: Reconstruction of O/Ni(001) structure from theoretically calculated diffraction patterns using the model program and 8×8 data sampling with energy range 113-235 eV, usage of χ-function and $C = 0.4\,a.u.$
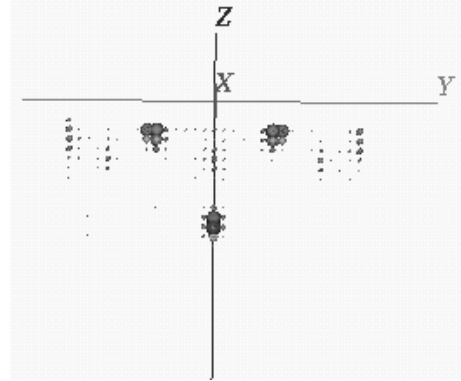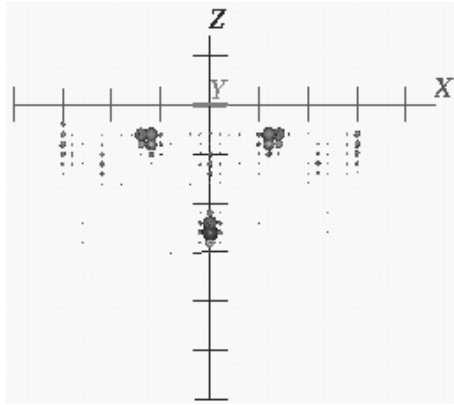
O/Ni(001)
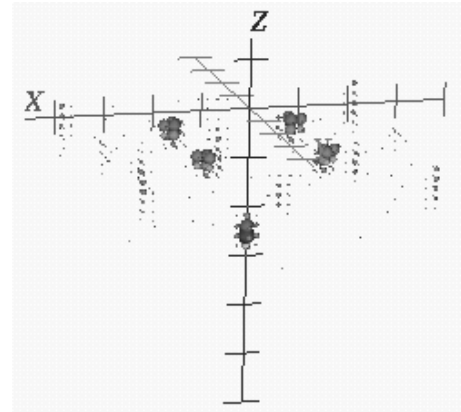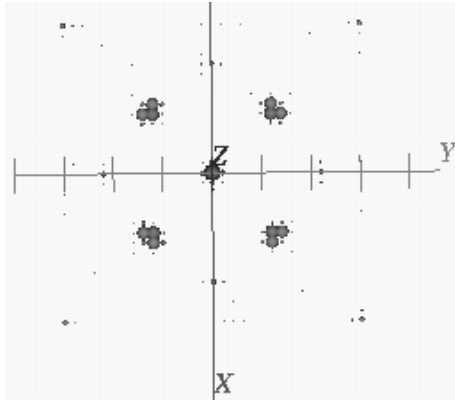
Figure 60: Reconstruction of O/Ni(001) structure from theoretically calculated diffraction patterns using the model program and 4 × 4 data sampling with energy range 113-235 eV, usage of χ-function and $C = 0.4\,a.u.$
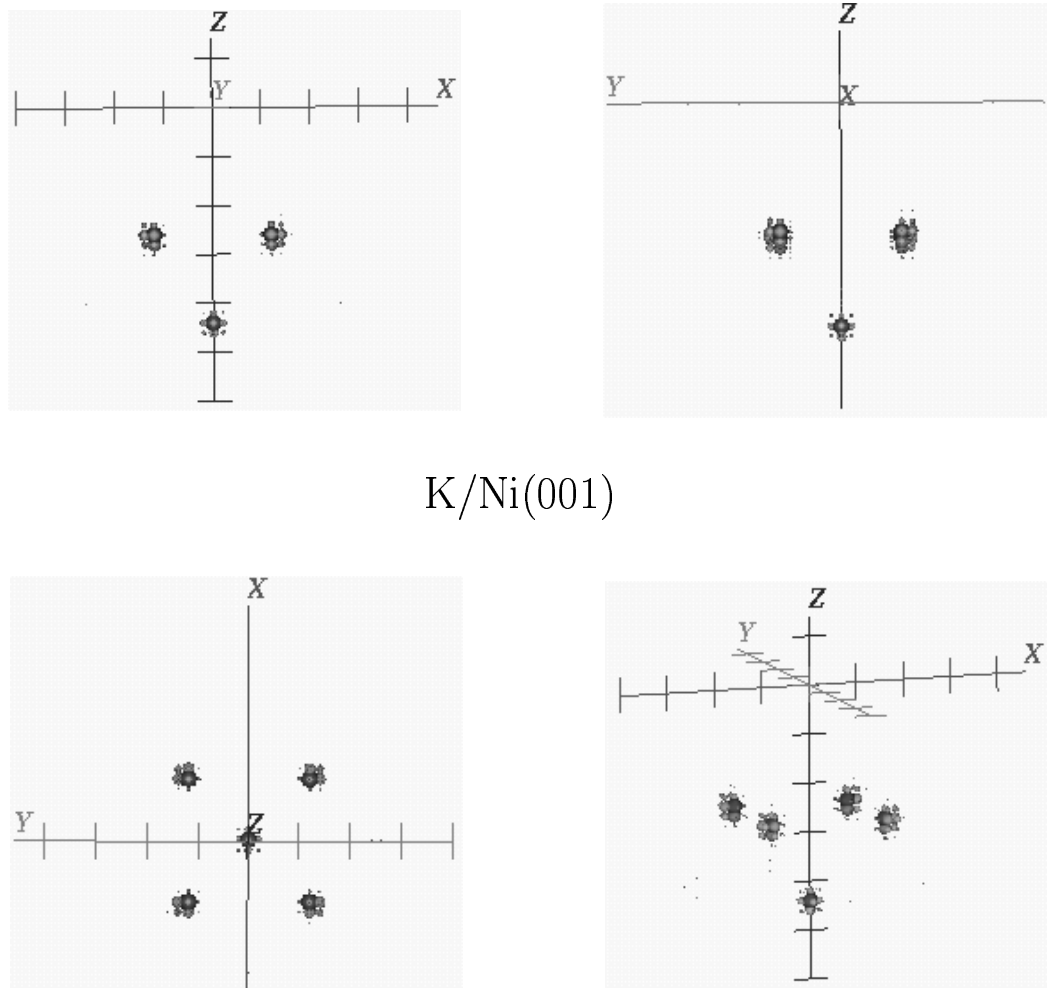
K/Ni(001)

Figure 61: Reconstruction of K/Ni(001) structure from theoretically calculated diffraction patterns using the model program and 8×8 data sampling with energy range 70-235 eV, usage of χ-function and $C = 3.5\,a.u.$
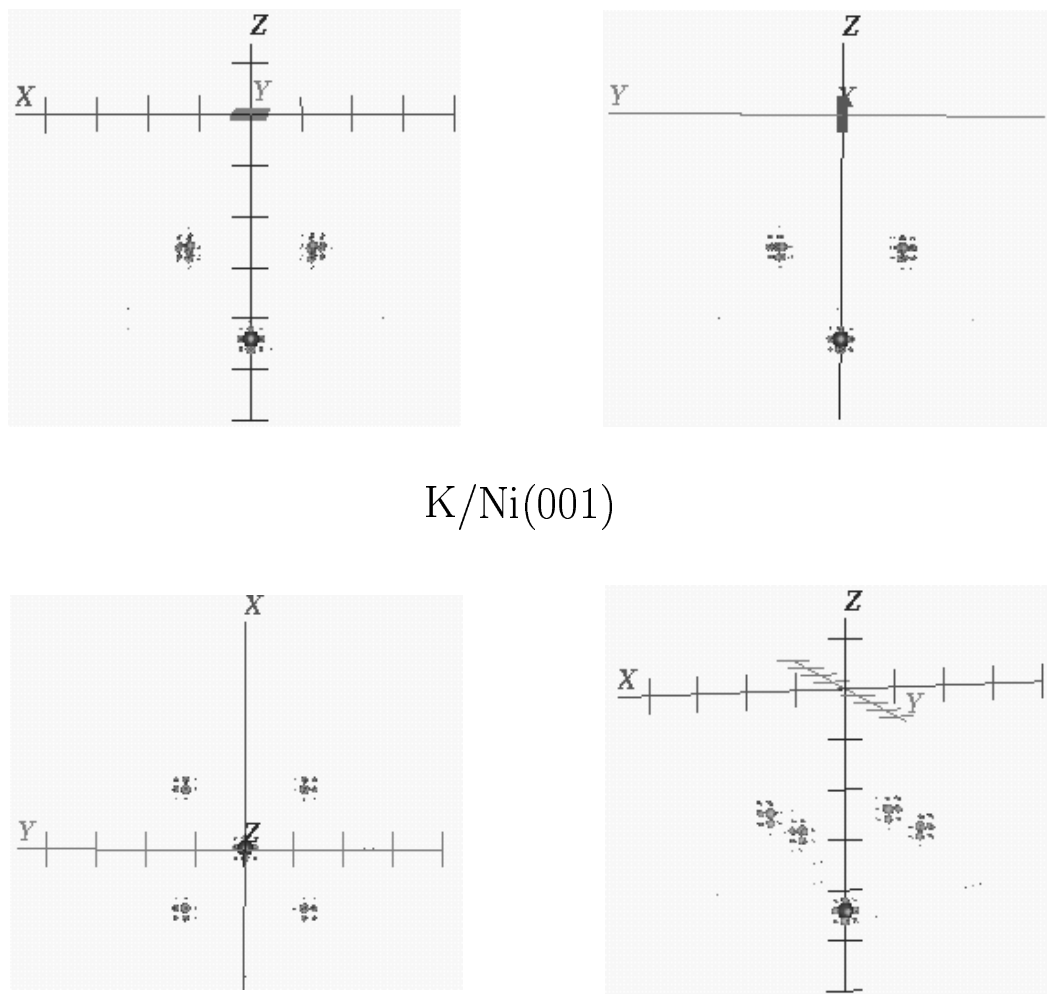
K/Ni(001)

Figure 62: Reconstruction of K/Ni(001) structure from theoretically calculated diffraction patterns using the model program and 4×4 data sampling with energy range 70-235 eV, usage of χ-function and $C = 3.5\,a.u.$
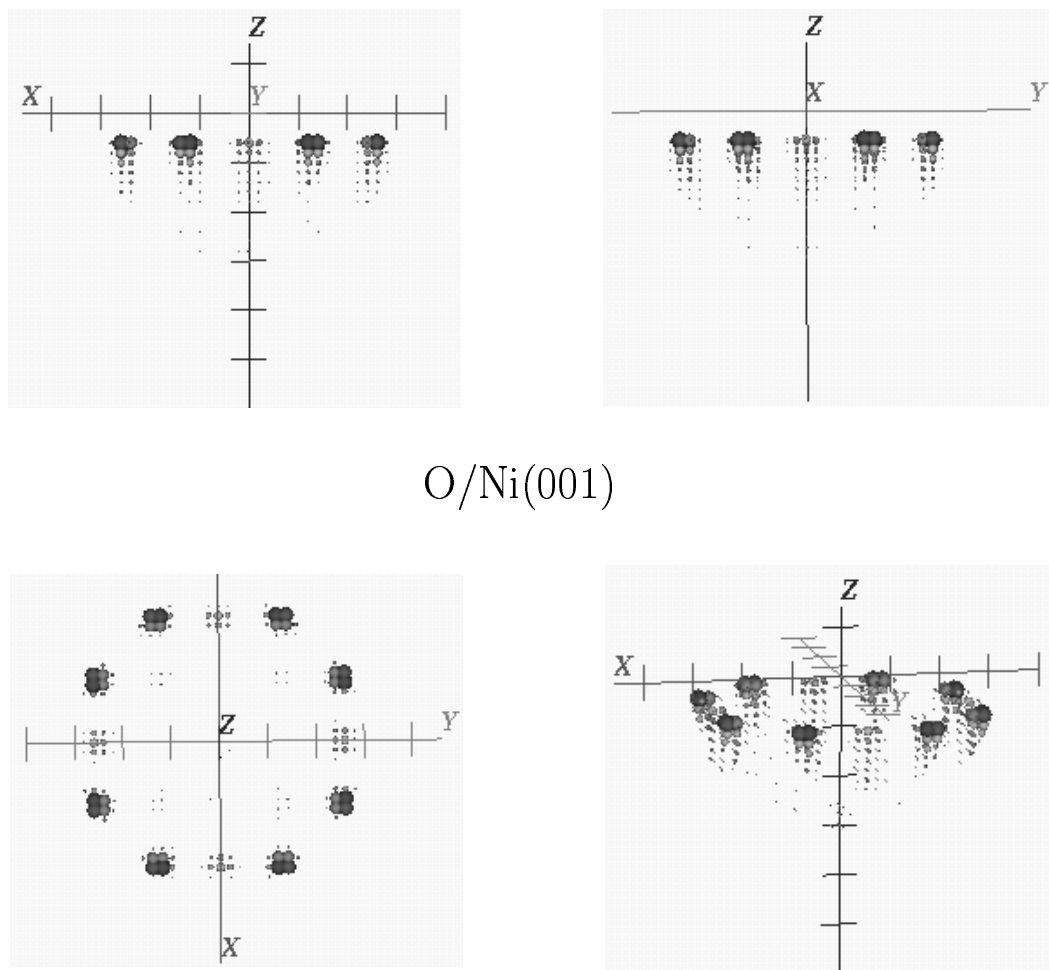
O/Ni(001)

Figure 63: Reconstruction of O/Ni(001) structure from theoretically calculated diffraction patterns using the model program and 2 × 2 data sampling with energy range 113-235 eV, usage of χ-function and $C = 0.4\,a.u.$
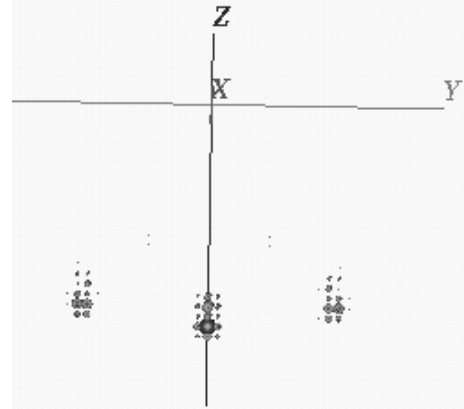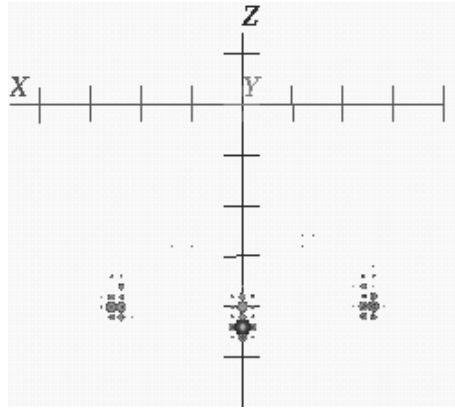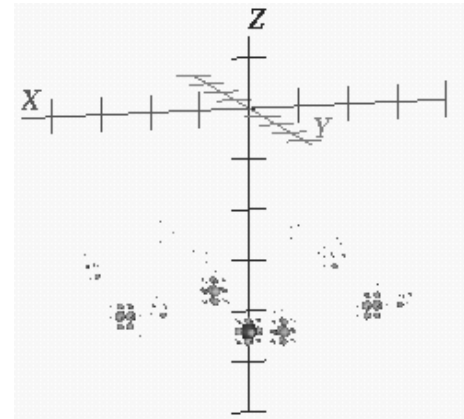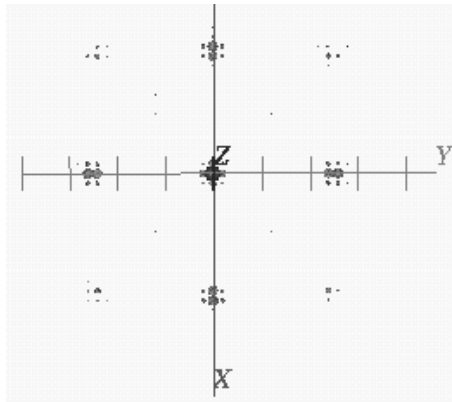
K/Ni(001)

Figure 64: Reconstruction of K/Ni(001) structure from theoretically calculated diffraction patterns using the model program and 2×2 data sampling with energy range 70-235 eV, usage of χ-function and $C = 1.5\,a.u.$

something similar. Figures 63 and 64 show heavily artifacted reconstructed images which

shows the validity of our model program.

Chapter 6

Holographic reconstruction from superstructure Bragg spots

6.1   Introduction

In the last chapter of this thesis we show the reader that electron holography can even be applied to conventional LEED to reconstruct three-dimensional images of atomic adsorption sites even when they form ordered overlayers with surface unit cells as small as $p(2 \times 2)$.

We will start with a section dedicated to the research we have done during our effort to improve our reconstructed algorithm. We will discuss the reason the algorithm we have seen so far fails to provide us with reasonable images of the local adsorption sites of $p(2 \times 2)$ adsorbed overlayers and report on how we approached and solved the problem. We will also discuss the handling of other factors that may allow the reconstruction of

less distorted images.

Finally, we will show the reader reconstructed 3-dimensional images of the two systems we have been considering in the previous chapters using a version of the CORRECT algorithm.

6.2   The story of an algorithm

The holographic reconstruction algorithm, the one we have been employing thus far and whose final form we are discussing in this chapter, had its origins in the work of John Barton[?, ?] ten years ago. As we saw in the previous chapters, Dennis Gabor was the inventor of holography. In its optical form this is nowadays much applied in the stereoscopic photography. Yet, it was A. Szöke[?] and chiefly J. Barton[?] who first tried to apply Gabor's method with photoelectrons and introduced the idea of photoelectron holography. In that case a photoelectron diffraction pattern may be regarded as arising from the interference between the wavefunction of an electron emerging directly from a photoemitter and those arising from subsequent scattering by other atoms close to the photoemitter. Then, if the former wavefunction is identified with the reference wave and the latter with the object waves, a diffraction pattern created this way may be regarded as a hologram. Szöke suggested that a computer algorithm can be employed to recover the positions of the near-neighbor scattering atoms relative to the photoemitter. Barton employed the Helmholtz-Kirchoff[?] integral theorem to suggest the following algorithm:

$$U(\vec{r}) = \frac{1}{2\pi R^2} \int \int \chi(\hat{k}) \exp\left[\imath k z (1 - \hat{k}_x^2 - \hat{k}_y^2)^{1/2} \right] \exp\left[\imath k (x\hat{k}_x + y\hat{k}_y) \right] d\hat{k}_x d\hat{k}_y \qquad (129)$$

where $\chi(\hat{k})$ represents the intensities of the diffraction pattern, $\hat{k}_x$ and $\hat{k}_y$ are the Cartesian components of a unit reciprocal space vector and $U(\vec{r})$ gives the amplitudes as a function of the real vector $\vec{r}$. According to Barton, photoelectron diffraction produces a two-dimensional pattern as a function of reciprocal space vectors $\hat{k}_x$ and $\hat{k}_y$. His algorithm is nothing more than a double fast Fourier transform between the two-dimensional reciprocal space to the two-dimensional real space with unit vectors $\hat{x}$ and $\hat{y}$. In order that we have the notion of the third dimension the z-component appears in (129) as the parameter z. Giving different values to z we get x-y slices of the three-dimensional real reconstructed image.

The source of electrons in the Szöke-Barton algorithm was the atoms themselves. Saldin and de Andrés[?] suggested another application of electron holography. They considered low energy electrons, electrons whose the source is external of the scattering surface, and suggested that a LEED pattern could be holographically interpreted. As we have explained in detail in chapter 2, these patterns result from the diffraction of an electron that has been scattered by an adsorbed atom (the reference wave) and those that first scattered off the adsorbate and then by the substrate ones. The initial focus was lattice-gas adsorption, that is, the one that is similar to the early stages of the adsorption of gas atoms on a clean surface. Each adsorbate "sees" the same local environment of substrate atoms but interacts very weakly with its neighbor adsorbates. This allows us to tackle the problem as if we had only one atom adsorbed on the entire clean surface. This lone atom acts as a beam splitter that is responsible for the reference and the object waves that interfere. Due to the lack of long-range order amongst the adsorbate atoms,

these two waves do not necessarily interfere destructively between the Bragg spots of the typical LEED diffraction pattern, but give rise to diffuse intensity that is spread amongst the bright Bragg spots. The pattern received after the subtraction of the Bragg spots is called the DLEED diffraction pattern. Making again use of the Helmholtz-Kirchoff theorem, they suggested a similar to (129) algorithm for the LEED electrons:

$$U(\vec{r}) = \int \int I(k, \hat{k}) \exp\left[-\imath k z (i - \hat{k}_x^2 - \hat{k}_y^2)^{1/2}\right] \exp(-\imath k (x\hat{k}_x + y\hat{k}_y)) d\hat{k}_x d\hat{k}_y \qquad (130)$$

Like (129), (130) gives the real space amplitudes on the x-y plane at distance z from the origin of the coordinate system where the adsorbates is located.

In 1992 Wei and Tong[?] suggested an energy-dependent form of the algorithm in analogy with earlier work in photoelectron holography[?, ?, ?, ?]:

$$U(\vec{r}) = \sum_{\hat{k}} \int_{k_{\min}}^{k_{\max}} \chi(k, k_i) e^{-\imath(kr - \vec{k}\cdot\vec{r})} dk \qquad (131)$$

where $\vec{k}_i$ is the wavevector of the incident electron and $k_{\min}$ and $k_{\max}$ are the minimum and maximum values of k of the detected electron. χ in this case is not simply the diffraction intensities in the reciprocal space but a function given by:

$$\chi(k, k_i) = \frac{H(k_i, \vec{k}) - H'(k_i, \vec{k})}{H'(k_i, \vec{k})} \qquad (132)$$

where $H'(k_i, \vec{k})$ is a smooth background function fitted separately to each of the lines in k-space radiating from the origin. The new feature in (131) is the usage of the χ-function defined in (132) instead of the intensities themselves. Using this algorithm, Wei and Tong were able to reconstruct well atoms that were close to the directions of forward scattering of incident electrons from adsorbate atoms on the surface, (the so-called *searchlight effect*), but not those in other directions. Consequently, in order to

reconstruct an image of full three dimensional structure of atoms around the adsorbate it was necessary, in general, to collect diffraction patterns for a range of directions of the incident electrons, $\hat{k}_i$ and a range of electron energies.

Finally, Saldin *et al.*[?], suggested the *compensated object- and reference-wave reconstruction by an energy-dependent Cartesian transform* (CORRECT) algorithm:

$$B(\vec{r}) = \sum_{k_\parallel} \left[\sum_{k_\perp} K(\vec{k}, \vec{r}) \chi(\vec{k}) e^{-(\imath k r - k_\perp z)} \right] e^{\imath \vec{k}_\parallel \cdot \vec{r}_\parallel} \tag{133}$$

which produces reliable three-dimensional images. The three most salient points to note about this algorithm are that (1) it operates not directly on the measured intensities H, but on a contrast-enhancing and normalizing function:

$$\chi(\vec{k}) = \frac{H(\vec{k}) - H_{\mathrm{av}}(\vec{k}_\parallel)}{H_{\mathrm{av}}(\vec{k}_\parallel)} \tag{134}$$

where $H_{\mathrm{av}}(\vec{k}_\parallel)$ is the average value of H for a given $\vec{k}_\parallel$, (2) the data are provided on a Cartesian grid in reciprocal space, and (3) a kernel K:

$$K(\vec{k}, \vec{r}) = \left[\frac{|f_{\mathrm{a}}| + C}{r} \right]^{-1} \tag{135}$$

compensates for the amplitude of the reference wave at the position of a scatterer. The reason this algorithm works even in the presence of partial ordering of an adsorbate is that χ has been constructed such that it contains information on the short-range order around the adsorbate *via* H, but that the long-range order term S is cancelled out in the process of evaluating the quotient in (134).

6.3 DLEED to LEED transition

After this short review of the different forms algorithm (133) has assumed over the years and the different approaches researchers have taken, we need to point out the main differences between DLEED and LEED intensities in order that we take the reader through a smooth transition from the former to the latter.

A question that has to be answered is, since we have proven and shown in the previous chapters that DLEED intensities can provide enough input for our algorithm to do a successful reconstruction, why bother with LEED? Why do we have to modify it in order that it works for LEED intensities too? The answer can be imagined effortlessly if we remember that the vast majority of structures under investigation or already investigated manifest long-range order in the plane parallel to the surface. As we have pointed out earlier in this thesis and will again in the next section, diffuse LEED intensities are the result of low energy electron scattering from disorderedly adsorbed atoms. We will see later that long-range order amongst the adsorbates results in destructive interference between the waves originating from different adsorbate-surface clusters extinguishing thus all diffraction intensities but those concentrating in the newly formed sharp superstructure spots. The reader can compare figure 41 that shows samples from DLEED diffraction patterns and figure 65 showing a LEED one. In the latter case all the diffuse intensity of the former has been concentrated on the newly born superstructure Bragg spots. It has been proven[?, ?] that if the basic presupposition in both DLEED and LEED scattering applies, that is, if the scattering between different adsorbates can be neglected (and it has been shown[?] that this holds even for dense superstructures
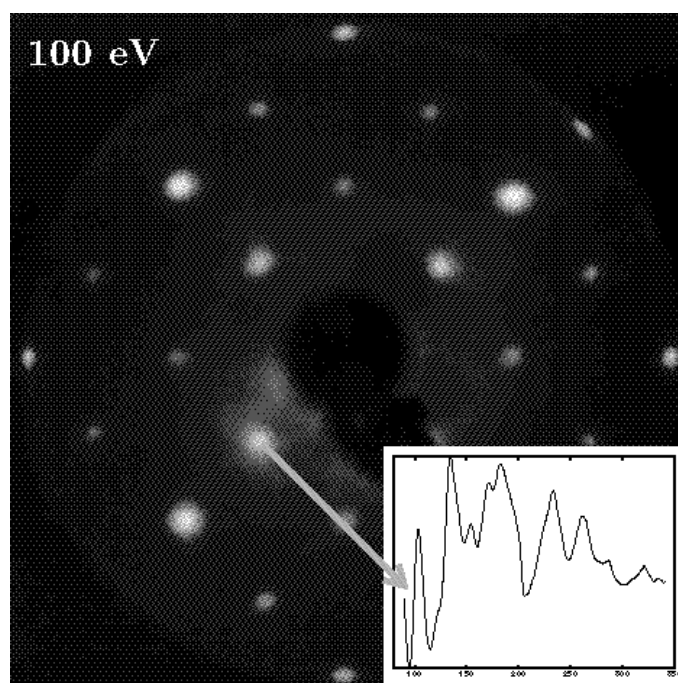
Figure 65: Experimental LEED pattern from a O/Ni(001)-p(2×2) surface for an electron energy of 100 eV. The inset shows the I-V curve of the (1/2 0) beam.

provided we have normal incidence of the electrons), then the newly born bright spots of LEED patterns contain the same crystallographic information on the local enviroment of the adsorbate as the corresponding diffuse intensity of DLEED pattern, or to put it in different words, the diffuse intensity from an adsorbate and its local surroundings corresponding to a particular value of $\vec{k}_{\parallel}$ ($\vec{k}_{\parallel}$ being the parallel component to the surface of the wave vector $\vec{k}$ of the scattered electron) has the same energy dependence as the superstructure spot intensity from an ordered array of such adsorbates in an equivalent local adsorption geometry and of a surface reciprocal lattice vector equal to the same value of $\vec{k}_{\parallel}$. After this discussion one can understand that the only difference between a LEED and a DLEED pattern is just that the former has a lot less intensities to be considered and measured. Here we want to emphasize on a fact that a theoretician does not have to deal with. It is the difference in the degree of difficulty the intensity of a diffuse tiny, dim spot can be measured compared to the superstructure large, bright spot which completes the answer to the question we asked in the beginning of the section. One other profit that somebody gets from this reduction in data resolution is the increase in the available energy range; the upper limit can go as high as $400\,eV$. That in DLEED experiments would end up in disturbing effects from the much brighter Bragg spots and thermal diffuse scattering (this last one is a phenomenon present in both DLEED and LEED where the diffraction patterns are filled up with diffuse intensity from the scattering of the electrons off the surface atoms that vibrate. In the case of DLEED this diffuse intensity is added to the elastically scattered one resulting in a complete distortion of the data and the reconstructed images. On the other hand, in the case of

LEED the Bragg spots are much more brighter and distinguishable than the thermal diffuse intensity and render its existence unimportant for the holography methods. This is the reason that DLEED experiments take place in temperetures around $90\,K$ whereas for LEED the room temperature is just fine).

This small amount of data converts the ensemble from continuous to discrete. So, the first change that the algorithm has to undergo is the replacement of the integral over $\vec{k}_{\parallel}$ in (130) to a sum. One might think that since now we have reduced the number of data used in the algorithm we should investigate its reliability for small and large surface unit cells and set its limits. In this thesis we try to set its lower limit to $p(2 \times 2)$ reconstructions whereas Reuter *at al.* in a recently published paper[?] proved that it works well for $p(3 \times 3)$ unit cell of SiC(111). Of course the larger the new surface period, the more spots and hence the more data left for the algorithm and the more similar the situation becomes to the DLEED case. We should also mention the fact that the LEED pattern contains bright Bragg spots resulting from the scattering from the substrate atoms, the so-called integral order beams and less bright spots the result from the scattering between adsorbate and substrate atoms and are called fractional order beams (figure 74).

Before we finish with this section we should mention that in order to use our holographic method all we need is a beam-splitter atom that will provide us with a reference and an object wave, provided that any substrate reconstruction contributes relatively little to the DLEED pattern or superstructure spots. This has to be the only atom per superstructure unit cell that breaks the periodicity of the substrate lattice in order

to prevent intermixing of images centered on several such holographic reference wave sources. It is completely irrelevant whether these beam splitters are adsorbed atoms or atoms of the clean surface that have undergone reconstruction.

6.4   Elimination of the χ-function

The reader will have noticed by now that all the captions of the figures we presented in chapters 4 and 5 had the indication: "Reconstruction using the χ-function". In chapters 3 and 4 we had explained the reason that led us to suggest this function. We saw there that by inserting such a function into our algorithm we managed to rid of an important drawback; the structure factor, $S(\vec{q}_{\parallel})$, of the adsorbed atoms which for the case of diffuse LEED is an unknown quantity due to the lack of long-range order among the adsorbed atoms. The fact that the data is collected on a Cartesian reciprocal space grid allows the avoidance of the Bragg spots that carry only partial information about the positions of the adsorbates relative to the substrates. We have for the structure factor of the adsorbates.

$$S(\vec{q}_{\parallel}) = \sum_{n,j=1}^{N} e^{i\vec{q}_{\parallel} \cdot (\vec{r}_j - \vec{r}_n)} \tag{90}$$

where, $\vec{r}_j$ and $\vec{r}_n$ are the position vectors of the adsorbed atoms j and n respectively. These vectors are parallel to the clean surface. $\vec{q} = \vec{k} - \vec{k}'$, is the momentum transfer due to the scattering and we keep only the component which is parallel to the surface due to the dot product in the exponential of (90). Looking at (90) we can distinguish between three cases:
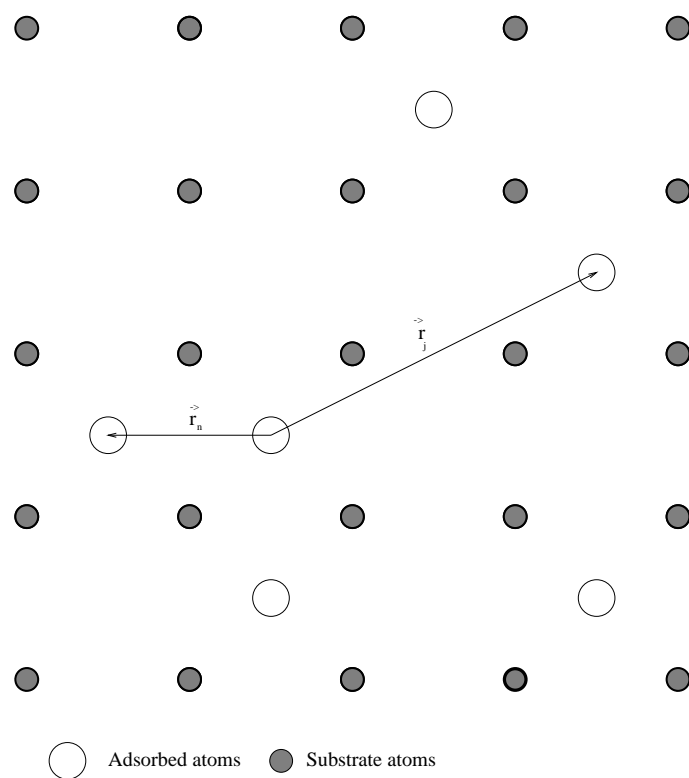
Figure 66: Random adsorption

1. When we have fully random adsorption on the clean surface, as figure 66 shows, the structure factor is equal to N. A simple calculation can show that:

$$
\begin{aligned}
S(\vec{q}_{\parallel}) &= \sum_{n,j=1}^{N} e^{i\vec{q}_{\parallel}\cdot(\vec{r}_n - \vec{r}_j)} \\
&= \sum_{n=j}^{N} e^{i\vec{q}_{\parallel}\cdot(\vec{r}_n - \vec{r}_j)} + \sum_{n \neq j=1,}^{N} e^{i\vec{q}_{\parallel}\cdot(\vec{r}_n - \vec{r}_j)} \\
&= N + 0 = N
\end{aligned}
\tag{136}
$$

the second sum being zero due to the all possible combinations of the $\vec{r}_n - \vec{r}_j$ vectors. Due to this factor the resulting DLEED patterns are just more intense versions of that from a single adsorbate.

2. In the case that we have partial order of the distribution of the adsorbates on the clean surface then the structure factor is a quantity which is difficult to be determined and it does not have a constant value. This unknown and varied value of S results in altering the diffuse diffraction intensities (but not uniformly as in the first case of the complete disorder) thus introducing extra structure to the DLEED pattern. We have shown in chapter 3 that if H_o is the DLEED intensity from only one adsorbate then that from all the adsorbates will be $H = H_o S$. In (134) S is function only of $\vec{k}_{\parallel}$. This enables it, as clearly can be seen in (93), to be common factor in both the numerator and the denominator and be canceled out, making χ structure factor-free, thus eliminating the unwanted aforesaid problems. We also discussed, in chapter 3, that the way we have constructed the χ-function enables us to avoid running into Bragg rods (look also at figure 37).

3. The third case is when we have fully ordered adsorption, as figure 67 shows. A
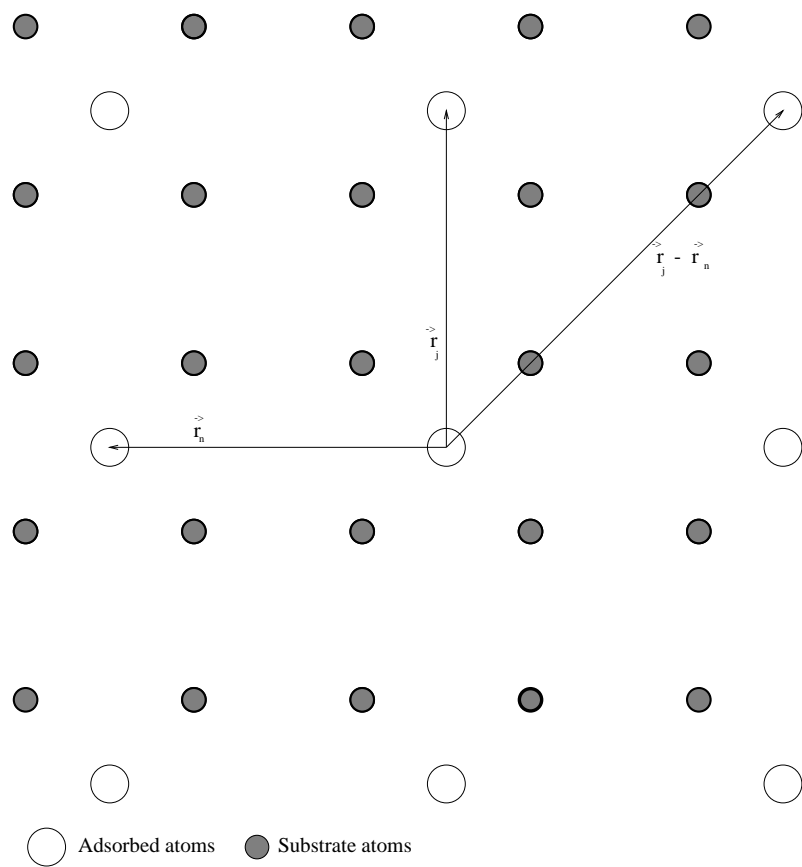
Figure 67: Ordered adsorption

large number of surface structures belong to this category, like the $c(2 \times 2)$ or the $p(2 \times 2)$ reconstruction of the clean surface or of adsorbates on it, the two structures we have been studying (O/Ni(001) and K/Ni(001)) belonging to the latter category.

Let us take a closer look at that third category. As figure 67 shows, all vectors $\vec{r}_j - \vec{r}_n$ indicate the position of an adsorbed atom. On the other hand $\vec{q}_\parallel$ is a reciprocal lattice vector and we know that the dot product of it with a vector like $\vec{r}_j - \vec{r}_n$ results into multiples of 2π, that is:

$$\vec{q}_\parallel \cdot (\vec{r}_j - \vec{r}_n) = 2\pi \times \text{integer} \tag{137}$$

With this in mind the sum in (90) can be calculated analytically, resulting in:

$$
\begin{aligned}
S(\vec{q}_\parallel) &= \sum_{j,n=1}^{N} \exp(2\imath\pi \times \text{integer}) \\
&= \sum_{n=1}^{n=N} \left(\sum_{j=1}^{N} \exp(2\imath\pi \times \text{integer}) \right) \\
&= \sum_{n=1}^{N} (N) \\
&= N \sum_{n=1}^{N} 1 \\
&= N \times N = N^2 \tag{138}
\end{aligned}
$$

From the above simple calculation we see that the structure factor is no longer such a quantity to take special precautions of, and automatically all the theory that gave birth to the χ-function can be ignored. It can be argued that we may not need to eliminate the structure factor any longer since it is a constant, but the enhancement of the interference terms between the reference and object waves in H by subtracting off

the H_{av} term might worsen the image reconstruction. This can be seen by the following thinking: The term H_{av} is a rough approximation of the self-interference terms R^*R, as the reader can recall from chapter 3. This term no longer contains any information about the phase of the reference wave and depends only on the atomic scattering factor which varies slowly over the backscattering hemisphere[?] (see also figure 33). Of course the O^*O terms have been ignored due to their very small value compared to $|R|^2$. The only terms that contain information about the substrate atoms relative to the adsorbate one are the two interference ones, that is, R^*O and RO^*. Since in our reconstruction algorithm we enter the diffraction intensities indirectly through the χ-function and since, as we said, H_{av} is only a crude approximation of the self-interference terms, it is clear that this way we cause a degradation of the input data. This may be a reasonable approximation for large data set, as it is with the DLEED diffraction patterns, where these deleterious effects are averaged out by the abundance of data. Yet, this is not as reasonable approximation for limited data, as it is with the $p(2 \times 2)$ patterns. Therefore we suggest that the modified form of the CORRECT algorithm (106) be:

$$B(\vec{r}) = \sum_{k_\parallel} \left[\sum_{k_\perp} K(\vec{k}, \vec{r}) H(\vec{k}) e^{-(\imath kr - k_\perp z)} \right] e^{\imath \vec{k}_\parallel \cdot \vec{r}_\parallel} \tag{139}$$

where the kernel K is defined in (105). But we still have to cope with the lack of information the self-interference terms carry and have to find a way to eliminate them. If one thinks, as we mentioned a few lines ago, that the these terms vary slowly they would be expected to cause distortions mainly in the part of the reconstructed image near its origin[?]. But near the origin we do not expect to find nothing else but the adsorbate atom. We therefore suggest that we ignore reconstructed intensities within a

small radius sphere around the origin ($\approx 0.5\,\text{Å}$).

6.5 The effect of the sampling interval in reciprocal space

The center of the CORRECT algorithm is a two-dimensional sum over $\vec{k}_\parallel$ which is an approximate double Fourier transform between the two-dimensional reciprocal and real space. It contains the summation over discrete values that are associated with the discrete intensity spots left by the constructive interference of the scattered electrons. From the mathematical point of view, this recording of the discrete values is called *sampling*. The spots that sample the diffraction pattern are located at evenly spaced intervals from each other. Taking into consideration the aforesaid features (that is, the discretely sampling and the evenly spaced intervals where this sampling takes place), we realize that we are coping with a mathematical phenomenon known as *aliasing*, associated with the sampling theorem[**?**]. To be more specific; let us assume that a continuous function is sampled at equal intervals Δ. The sampling theorem states that if this function, sampled at that interval, happens to be *bandwidth limited* to frequencies smaller in magnitude that a critical frequency f_c, *i.e.*, if its Fourier transform is zero outside the interval $(-f_c, f_c)$, then the function is *completely* determined by its samples. This critical frequency is called *Nyquist critical frequency* and is defined as:

$$f_c \;=\; \frac{1}{2\Delta} \tag{140}$$

or
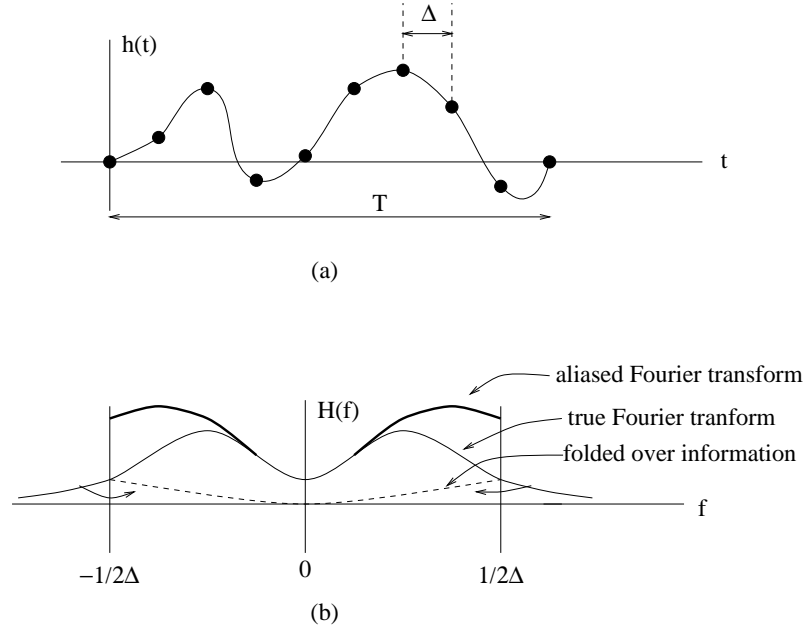
Figure 68: The sampling theorem and the aliasing phenomenon. (a) $h(t)$ is a function sampled at equal intervals Δ. (b) Its true and aliased Fourier tranform, $H(t)$.

$$f_c = \frac{2\pi}{2\Delta} \tag{141}$$

depending whether the exponential in the Fourier integrand contains the coefficient 2π or

not. One consequence of this theorem is that if a function is *not* bandwidth limited to less

that the Nyquist frequency, its Fourier transform within the interval $(-f_c, f_c)$ contains

information that belongs to frequencies outside the limit that the critical frequency sets.

What actually happens is that all the power spectral density that lies outside of the range

$-f_c < f < f_c$ is spuriously moved into the range. This phenomenon is what we called

earlier "aliasing" and a visualization of what happens can be seen in figure 68. In panel

(b) of this figure the reader can see both the true and the false Fourier transform of the

function of panel (a) which is sampled at equal intervals Δ. If the Fourier transformed

function was defined completely with the interval $(-1/2\Delta, 1/2\Delta)$ then the true and false transforms would have been coincided. However, in the case that this does not happen the transformed function within the critical frequency contains information from both within and without it. It looks as if the information outside has been folded over or aliased in the $(-f_c, f_c)$ space. Extrapolating what we have said above to our case, we understand that our algorithm, due to the aliasing phenomenon, will give rise to distorted reconstructed images. But, let us attempt to quantify the previous discussion.

In a LEED pattern from a $p(2 \times 2)$ superstructure, the reciprocal-lattice rows that include integer-order Bragg spots sample fractional-order spots at intervals of g, the magnitude of a substrate reciprocal lattice vector (rows labeled $0, \pm 1, \pm 2, \pm 3$ and ± 4 of figure 74). The rows that lie between them sample the fractional-order spots at spacings of $g/2$ (rows $\pm 1/2, \pm 3/2, \pm 5/2$ and $\pm 7/2$ in figure 74). Since only the fractional-order spots are included in the sum over $\vec{k}_\parallel$ in (139), we may assume an effective Δ of somewhat between these values. Taking $\Delta = g = 2\pi/a$ (where a is the length of a surface unit vector of the substrate lattice) and substituting into (140) or (141) we propose that the safe range of lateral validity of a the reconstructed image is somewhere between $\pm a$ and $\pm a/2$ from the adsorbate in directions of the real-space lattice vectors[?]. Fortunately, this limited region of validity does not prevent the recovery of the local environment of the prominent adatom or adsorbate on the surface in almost any imaginable case. Thus we suggest that the reduced sampling of diffraction data necessitated by the replacement of a continuous DLEED pattern by an array of superstructure spots does not lead to a breakdown of the algorithm (139), but merely limits the lateral range of the image.

6.6 Final results

In this section we are presenting the final results we are getting using the modified holographic algorithm (139) for both simulated and experimental LEED intensities.

6.6.1 DLEED 2×2 sampling

We will start from the point we had left off at the end of chapters 4 and 5. The reader should recall that there we had tried to reconstruct images using diffuse LEED diffraction patterns with a sampling of 2×2. Our attempt was disappointing, as one can recall by looking at figures 55, and 56, where the images were either heavily artifacted or unrecognizable. We repeated our calculations using diffraction patterns produced by our model program (see appendix B) with the same disappointing results (figure 63 and 64). At that point we had concluded that the algorithm were not working appropriately and needed modification.

In what it follows we present our new reconstructed images that came about after we had used the new modified CORRECT algorithm. We started off with our model program and continued on with the DLEED program of Pendry and Saldin[**?**]. Figures 69, 70, 71 and 72 show the reader the fine images we obtained.

6.6.2 Simulated LEED data from ordered adsorbates

Next we attempted to reconstruct images from realistic LEED data. First we tried to apply our method to simulated data. To do this we ran the *van Hove-Tong LEED* program that simulates a conventional LEED experiment for different structures[**?**]. We
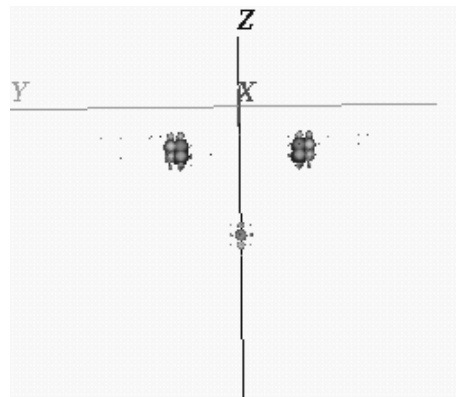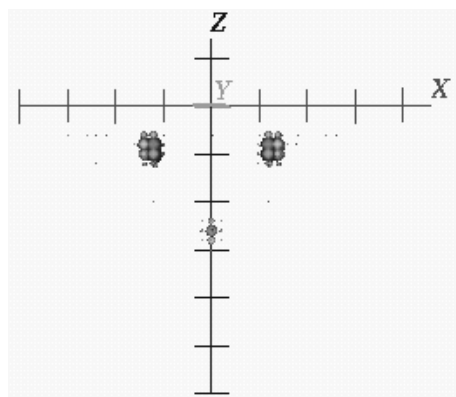
O/Ni(001)
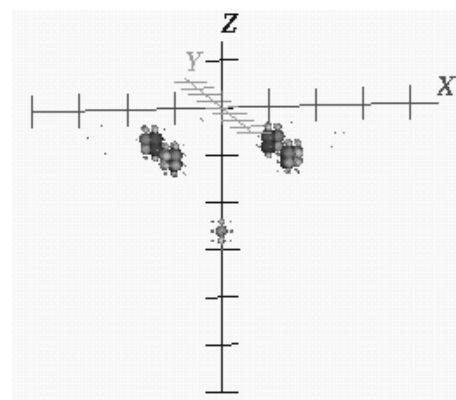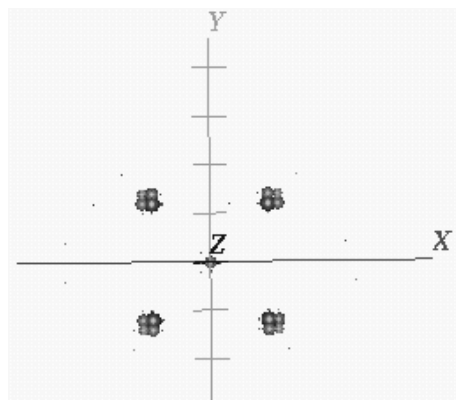
Figure 69: Reconstruction of O/Ni(001) structure from theoretically calculated DLEED diffraction patterns using the model program. Energy range: 113-235 eV, $C = 5.0\,a.u..$ No usage of the χ-function was made.
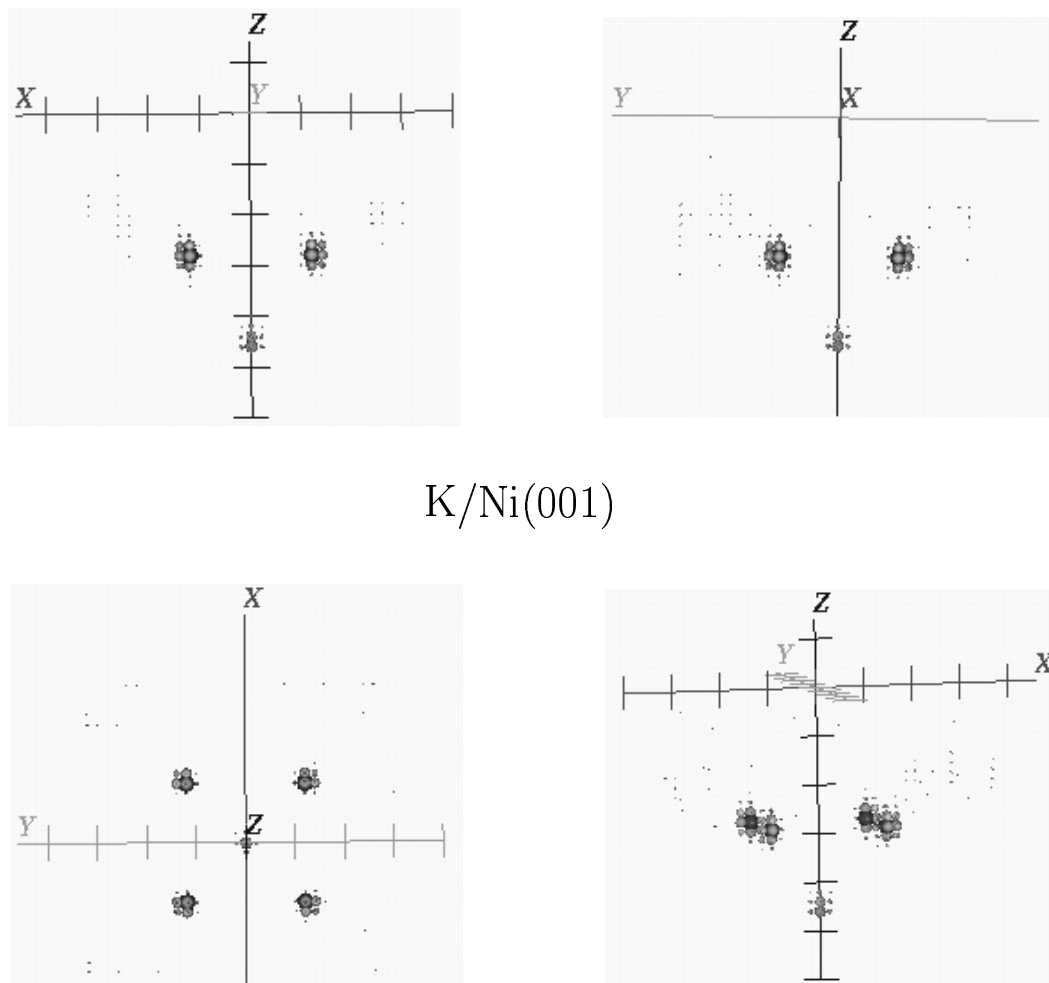
K/Ni(001)

Figure 70: Reconstruction of K/Ni(001) structure from theoretically calculated DLEED diffraction patterns using the model program. Energy range: 70-435 eV, $C = 25.5\,a.u.$. No usage of the χ-function was made.
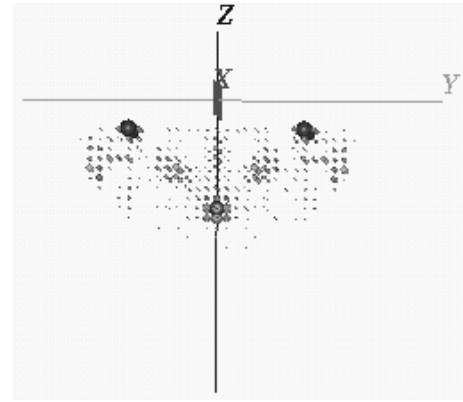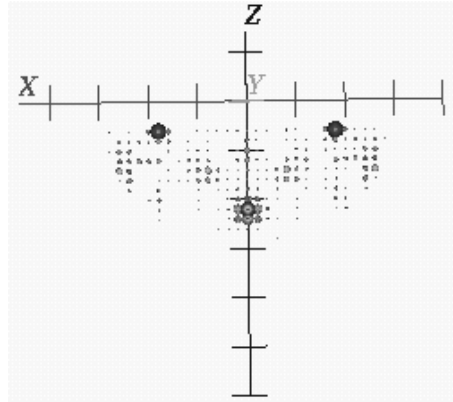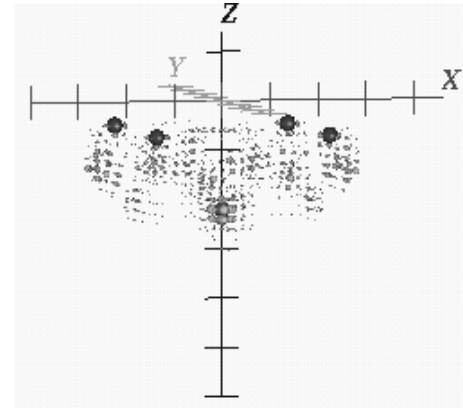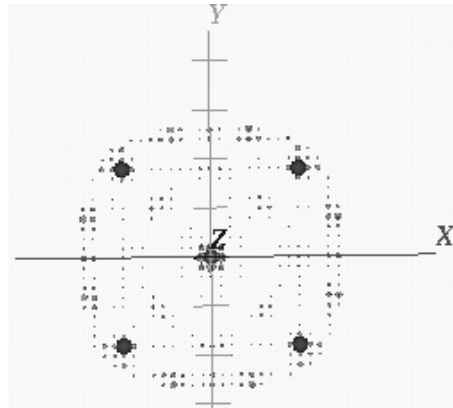
O/Ni(001)

Figure 71: Reconstruction of O/Ni(001) structure from theoretically calculated DLEED diffraction patterns. Energy range: 113-235 eV, $C = 1.0\,a.u.$. No usage of the χ-function was made.
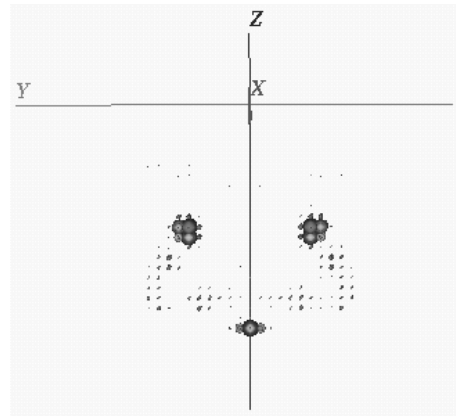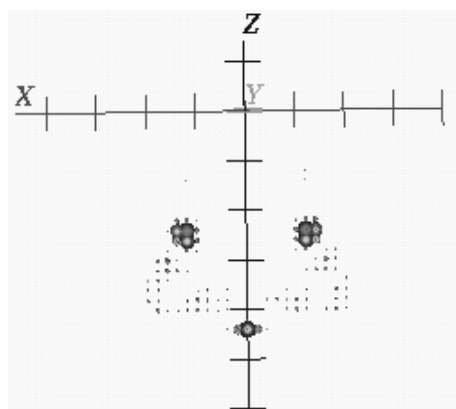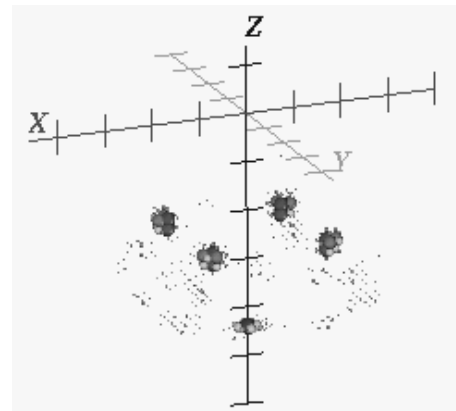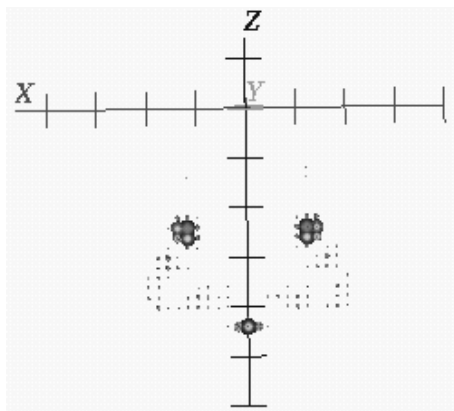
K/Ni(001)

Figure 72: Reconstruction of K/Ni(001) structure from theoretically calculated DLEED diffraction patterns. Energy range: 70-435 eV, $C = 1.1\,a.u.$. No usage of the χ-function was made.

○   Substrate layer

●   Adsorbate layer
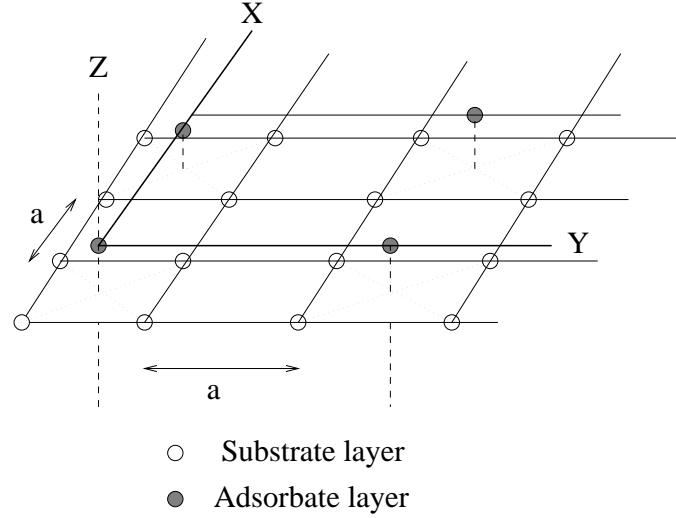
Figure 73: Geometry of a $p(2 \times 2)$ overlayer in hollow site on an fcc (001) surface. a is the surface lattice constant.

considered the fcc (001) substrate with a $p(2 \times 2)$ overlayer and we limited ourselves to hollow adsorption site (figure 73) and to normal electron incidence. We repeated our calculations for O/Ni(001)-$p(2 \times 2)$ and the artificial K/Ni(001)-$p(2 \times 2)$ (since the potassium over the clean surface of the nickel really reconstructs as $p(4 \times 2)$). We produced 25 diffraction patterns with energy range from $120.0 \, eV (4.41 \, a.u.)$ to $360.0 \, eV (13.24 \, a.u.)$ for both adsorbates. Each diffraction pattern contains 249 beams (69 integral-order and 180 fractional-order), as figure 74 shows. In order that the simulation was as close to the experiment as possible we limited our data used within a 50° polar semi-angle, which corresponds to the standard angular range of conventional electron detectors[?] and additionally had been shown to be the most appropriate in earlier holographic DLEED investigations [?].
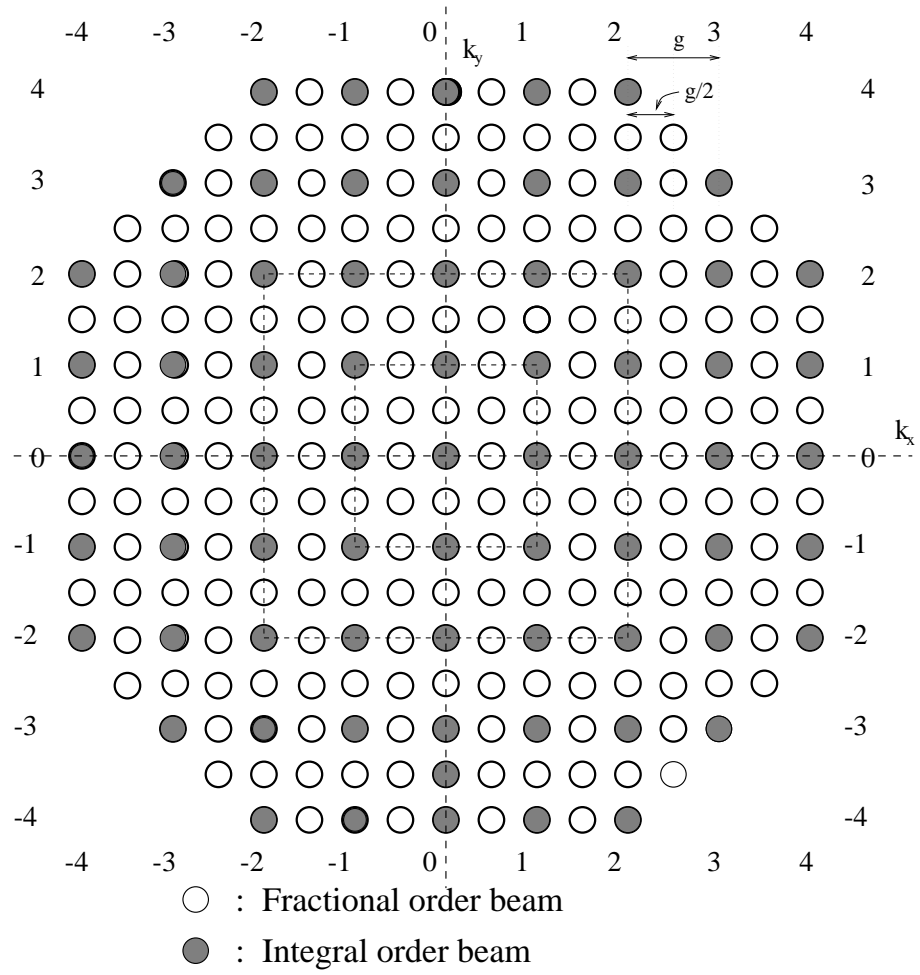
Figure 74: Reciprocal space pattern: Open circles represent integral-order beams, filled circles represent fractional-order beams

O/Ni(001)-$p(2 \times 2)$

Figure 75 clearly identifies the four-fold adsorption site of the oxygen on the clean surface of nickel. The oxygen is weak scatterer compared to the strong nickel. Thus one would expect distorted images since the beam splitter (O) in this case would not produce strong reference waves. The above figure proves that our algorithm works even in this case very well. The optimum C constant was found equal to $C = 1.05\,a.u.(0.56\,\text{Å})$. The atoms of the first layer appear displaced inwards. This is due to the simplicity of the kernel K at its present stage which is only a 0th approximation to the backscattering properties of the system[?].

K/Ni(001)-$p(2 \times 2)$

Although the potassium does not reconstruct as a $p(2 \times 2)$ but as $p(4 \times 2)$, nevertheless we wanted to test the validity of our method with this too[?]. We positioned K at the four-fold hollow site, $2.56\,\text{Å}$ above the surface of nickel. Figure 76 does not leave us with any doubt about the reliability of the CORRECT algorithm.

6.6.3   Experimental data

As a last step we try to invert experimental data of the O/Ni(001)-$p(2\times2)$ system. After standard crystal preparation, the Ni substrate was subjected to an exposure $2 \times 10^{-8}\,mbar$ of O for $60\,sec$ at $90\,K$. Subsequent annealing at $500\,K$ led to the formation of a sharp $p(2\times2)$ superstructure pattern. The measurement was performed using the standard Video-LEED system developed by the group of Klaus Heinz [?, ?] and included
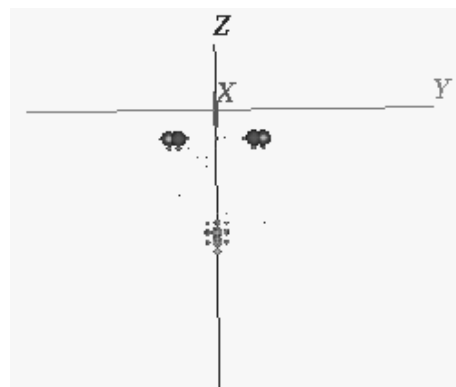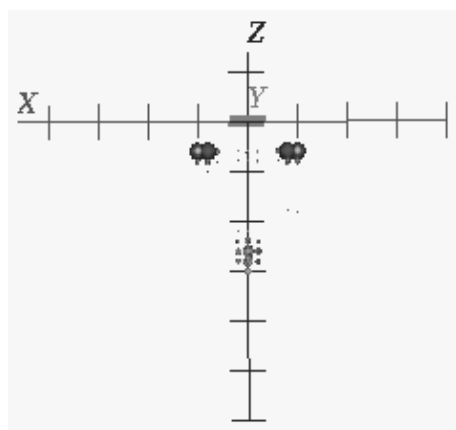
O/Ni(001)
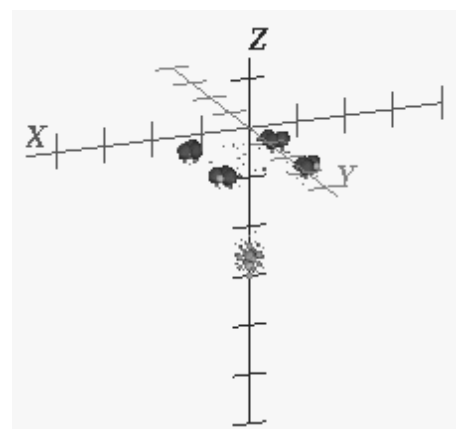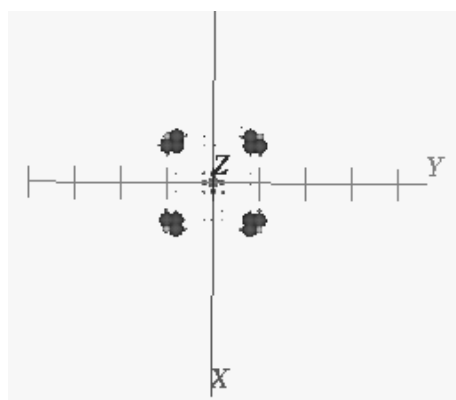
Figure 75: Reconstruction of O/Ni(001)-$p(2 \times 2)$ structure from 25 theoretically calculated LEED patterns ($120.0\,eV\,(4.41\,a.u.)$ to $360.0\,eV\,(13.24\,a.u.)$).
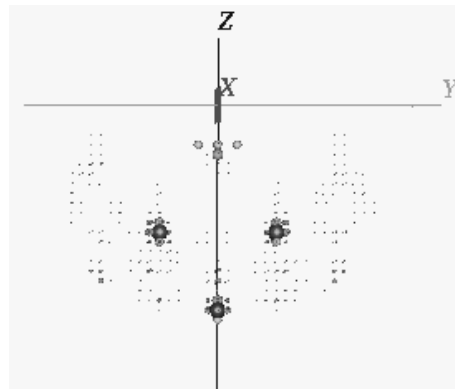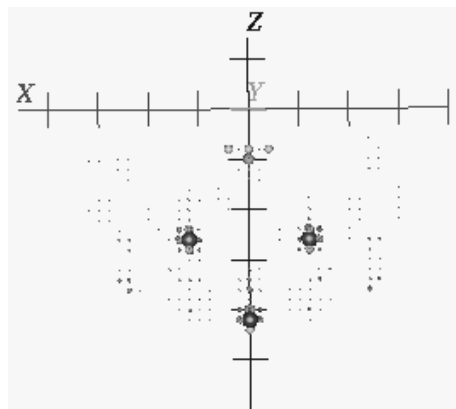
K/Ni(001)
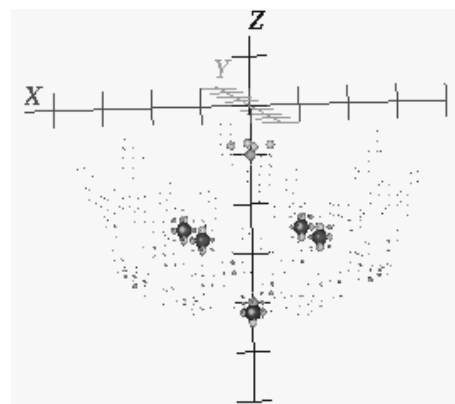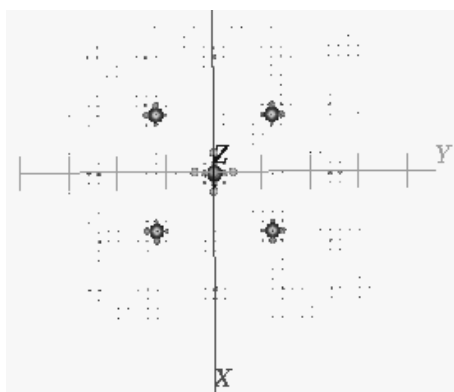
Figure 76: Reconstruction of K/Ni(001)-$p(2 \times 2)$ structure from 25 theoretically calculated LEED patterns ($120.0 \, eV \, (4.41 \, a.u.)$ to $360.0 \, eV \, (13.24 \, a.u.)$).

4-fold symmetry averaging according to the expected rotational symmetry of the diffraction pattern. The full data set comprises the 8 symmetry inequivalent fractional-order beams closest to specular reflection in the energy range $90 - 344\,eV$. Good agreement of this enlarged data set was found with the three fractional-order spot I-V curves used in the earlier quantitative LEED study [?]. Figure 77 shows the reconstructed local adsorption geometry. Although the experimental data set is smaller with respect to the total energy range and the total number of fractional-order beams, we nevertheless find essentially the same stability, accuracy and unambiguity of the image as described for the other data sets. Even on reducing the number of beams used to the 5 nearest to the (00) beam in the diffraction patterns, the image continued to reliably show the 4-fold hollow adsorption site with an only slightly degraded overall image quality.

This final result shows, that no particularly large data set needs to be measured to ensure a proper working of the reconstruction algorithm. Rather, it is the same I-V curves that are measured for a quantitative LEED analysis, that also provide the input to the holographic inversion. Ultimately, it is only this similarity of required data that can make holographic LEED a practically useful complement to the established quantitative LEED analysis at the present time.
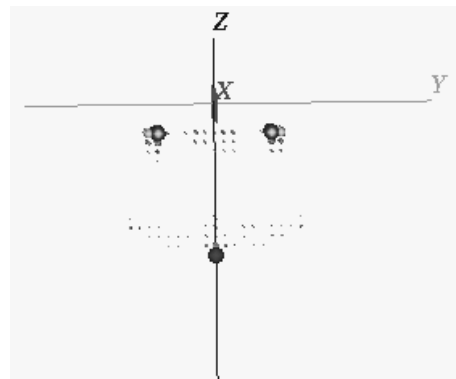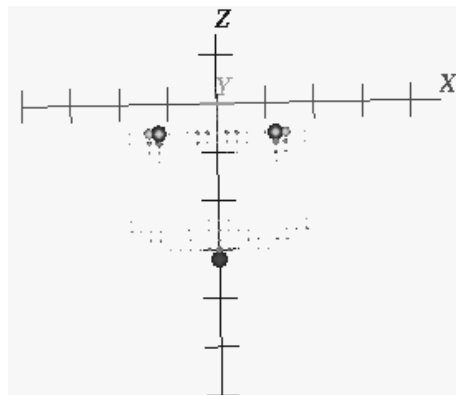
O/Ni(001)
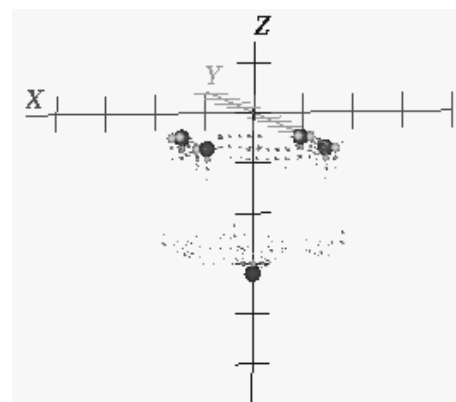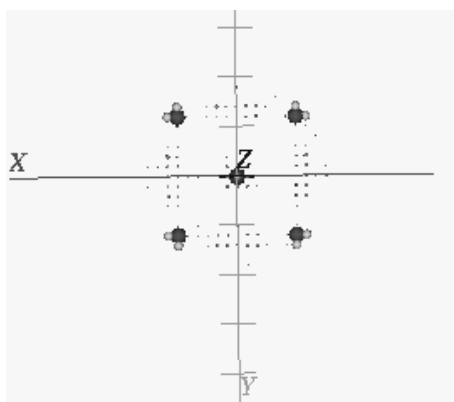
Figure 77: Reconstruction of O/Ni(001)-$p(2 \times 2)$ structure from 25 experimental LEED patterns $(120.0\,eV\,(4.41\,a.u.)$ to $360.0\,eV\,(13.24\,a.u.))$.

Chapter 7

Conclusions

Our main goal was to develop a method that will act as a guide to analytical LEED calculations. It is made clear from the first chapter that these calculations are time consuming and employ a trial-and-error scheme that mostly depends on the experience of the scientist and the power of computation equipment he has at his disposal. We remind ourselves what the LEED cycle is by looking at figure 1 of the introduction. The LEED pattern analyzer will have to start his investigation of the structure that is hidden behind it by assuming a tentative structure. This part of the investigation is extremely important and can dramatically affect the time that the search will take. It is understandable that if the choice of the trial structure is a poor one the whole cycle will start off on the wrong foot resulting in disappointing failures. Of course LEED is a method that so far has solved many simple and complicated surface structures and the people working on it are experts in picking the right trial structure. However, if we had a way to really visualize the object of our investigation and use that to kick

off the LEED cycle as shown in figure 1 we would be able to save enormous amounts of both computational and human time. It is exactly this aim that holographic LEED (h-LEED) promises to fill, at least with a certain common class of surface structures.

The development of this method was the main subject of this thesis. We did not try to solve any really unknown structure; the two systems we worked on, O/Ni(001) and K/Ni(001), have been solved years ago using conventional LEED methods [**?**, **?**, **?**, **?**, **?**, **?**, **?**, **?**, **?**, **?**]. But the idea behind this effort was consistent with the route any new surface method follows; that is, we test its ability to do real investigation by analyzing well known systems. Only when we exhaust it on as many such known systems as we can and see that it correctly produces the same results as other traditional methods do, are we then ready to look upon it closer and try to test it with an unknown system. Recently a paper by K. Reuter *at al.* published[**?**] in the Physical Review Letters, the first one where the solution of the (3×3) reconstruction of SiC(111) using h-LEED was announced. After this success we feel that the time has come to announce that h-LEED is a reliable surface method and it can be used in connection with conventional LEED and other methods for surface investigation. We saw the historical course the CORRECT algorithm followed before it reached the current form. As we have mentioned so many times and the reader will have surely realized by now, this algorithm is just the zeroth approximation of the method. It is subject to and will undergo changes. One basic reformation that ought to take place has to do with the kernel function ($K(\vec{k}, \vec{r})$). The numerator comprises of two terms. The second of them, which represents the scattering off the substrate atoms, at this point has been set equal to a constant, following the

LEED diffraction
pattern

"Black box" containing
the reconstruction program

3D holographic image
of the structure
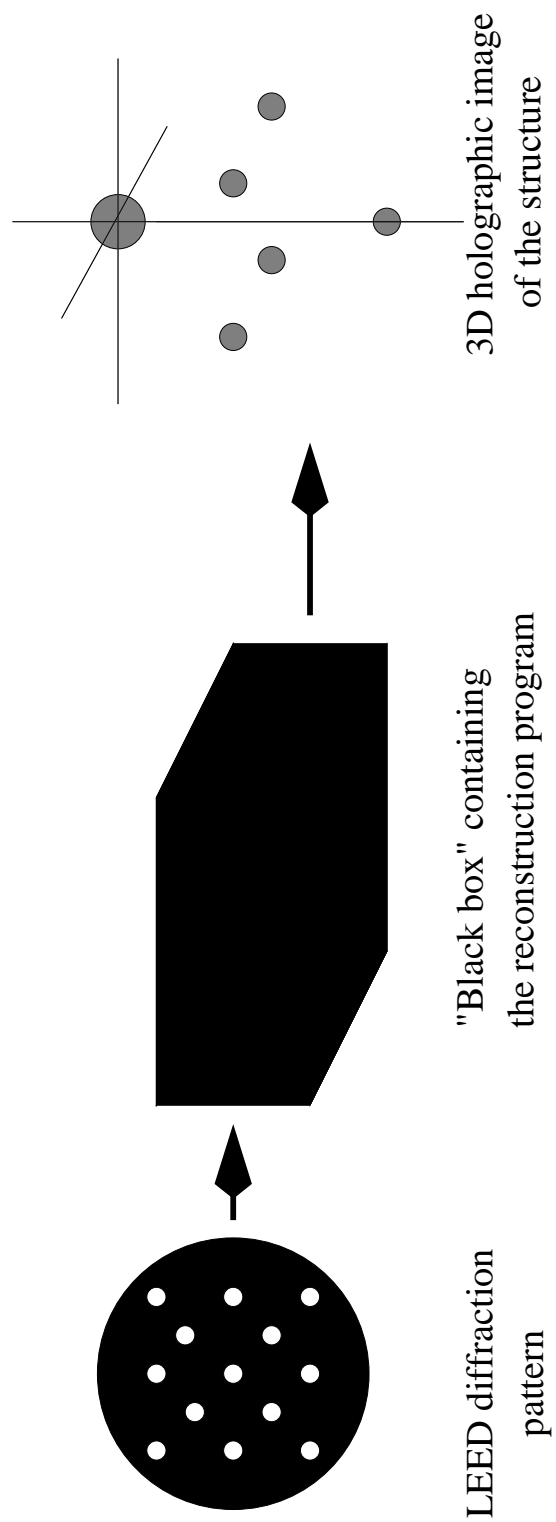
Figure 78: The future of h-LEED

argumentation in chapter 3. This obviously is not quite right. It is most likely that the scattering by the substrate atoms is under the influence of the energy of the incident electrons, fact that, in this initial stage of the algorithm, has been ignored. On the other hand, it is obvious from the two systems we have studied (O/Ni(001) and K/Ni(001)), that the value of this term depends on the structure. This observation has not been exploited as much. One other feature that we kept mentioning in this dissertation is the removal of the Bragg spots from the experimental diffraction patterns or their omission during the simulation of the experiment. These spots carry two different kinds of information. The first kind has to do with the substarte atoms that is not used from h-LEED. The other kind has to do with the adsorbates relative to the substrates, since some reference and object beams interfere constructively at exactly the positions of the Bragg spots. Unfortunately, at this moment we do not have a mechanism, a method that will isolate the former and release the useful for holography latter information. That is the reason we omit them completely. A future research, maybe another PhD thesis, will try to take the method one or more steps further by attempting to address both approximations we cited above. After such an investigation and development the CORRECT algorithm may be tested to more structurally complicated surfaces.

In one of the original papers, when DLEED holography was still in its baby cradle, Dr. Saldin was wondering: "Atomic-Resolution Electron Holography—A realization of Gabor's Dream?"[**?**]. Now we believe that the answer is more positive than ever before. We do not know when exactly it will happen but we feel that a day when a LEED pattern will be fed in a "black box" (figure 78) which will be able to output a 3D holographic
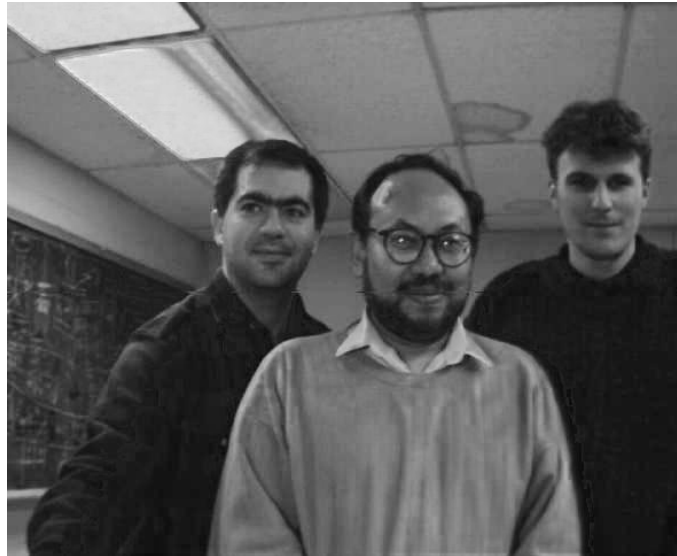
Figure 79: The h-LEED group, from right to left: Karsten Reuter, Dilano K. Saldin, John A. Vamvakas

image of the structure that produced the pattern is not too far away.

The three persons worked so that h-LEED becomes a reliable method are shown in figure 79.
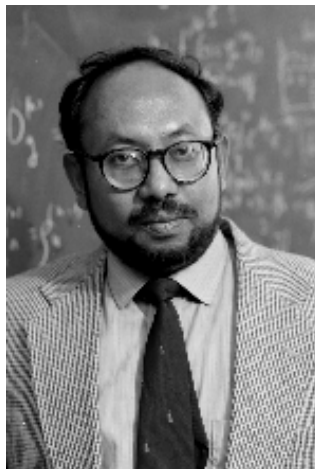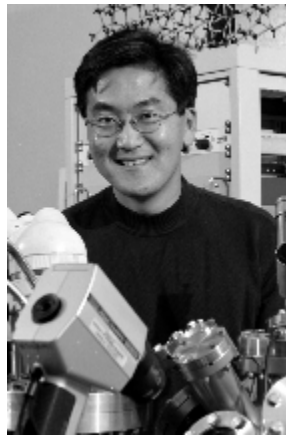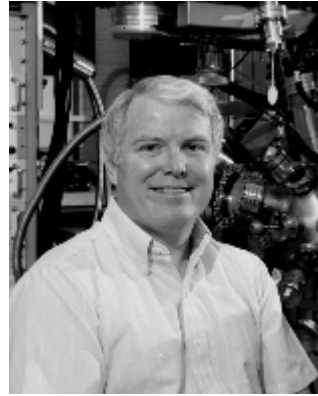
Figure 80: The PhD commitee; From left to right and from upper to lower: Marija Gajdardziska-Josifovska, Brian P. Tonner, Jun Nogami, Richard S. Sorbello, Dilano K. Saldin

Appendices

Appendix A

Calculation of the maximum value

of angular momentum, $\ell_{\max}$
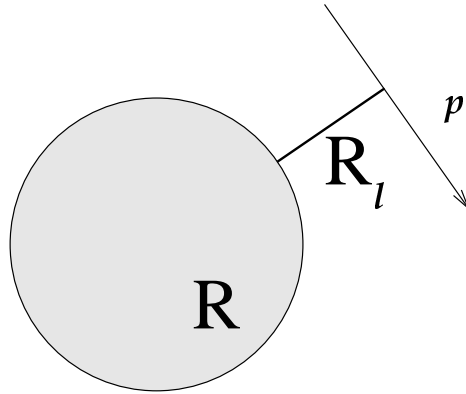
Figure 81: The classical trajectory of an electron approaches the ion-core no closer than a distance R_ℓ determined by the angular momentum. If R_ℓ is greater than the muffin-tin radius, R, the classical particle does not penetrate the potential

Following the elementary treatment from L.I. Schiff's "Quantum Mechanics"[?], we can think as follows: All the potential is confined in a sphere of radius R. Suppose there is a classical particle of angular momentum ℓ about the center of the ion core, and linear

momentum p. Then, at a distance R_ℓ from the center of the potential sphere its angular momentum will be given by:

$$pR_\ell = \ell\hbar \qquad (142)$$

According to classical Physics, if $R_\ell > R$ the particle will never see the potential as figure 81 shows. On the other hand, if the particle is treated quantum mechanically it will be able to penetrate into the classically forbidden region. But the more the classical laws are violated by this penetration the less probability there is of this happening. This means that when $R_\ell \approx R$ the electron will see only the outermost parts of the ion-core where the potential is weakest. Substituting in (142) a typical electron energy, $50\,eV$, say, which corresponds to a momentum of $3.95 \times 10^{-24}\,mKg/s$ and a typical muffin-tin radius of $1.25\,\text{Å}$, we will find a maximum value for the angular momentum:

$$
\begin{aligned}
\ell_{\max} &\simeq \frac{pR_\ell}{\hbar} \\
&\simeq \frac{3.95 \times 10^{-24} \times 1.25^{-10}}{1.05 \times 10^{-34}} \\
&\simeq 4 \qquad (143)
\end{aligned}
$$

Appendix B

The model program and its

accesories

B.1   The Simple DLeeD Program

The program *Simple DLeeD* (see B.2) calculates the diffuse LEED diffraction pattern for one energy at a time defined in line 11 as parameter *engy*. Actually this energy is fed into the program from a simple C-shell script (see B.6). When the pattern has been calculated for one energy (*energy*1, say) the script feeds the program with the next one (*energy*2) until all *engy* energies have been used up. The parameter NN in line 12 indicates which energy is calculated each time and takes values from 1 to *num*. Line 13 defines the number of the atoms used, $NATO$, the total number of energies, *num*, and the maximum value of the angular momentum, $l_{\max}$. The pattern calculated is a square matrix dimension $nkx \times nky$ in the reciprocal space with resolution dk, defined in line

15. *theta* and *phi* in line 16 indicate the incident angle.

After the declaration part (lines 19 through 26) the program starts reading in the data files (lines 30-61). It begins with the positions of the cluster atoms. File *cluster*, (B.3), contains that information. Following are the phase shifts of both the adsorbate and the substrate atoms contained in the files *ps.ads* and *ps.sub*. (B.4) shows a sample of the contents of a phase shift file. We need the phase shifts up to a maximum angular momentum $l_{\max}$. So, each energy is followed by the phase shifts in $radians$ corresponded to $0, 1, \ldots, l_{\max}$ angular momenta.

Lines 71 through 132 contain the main program. The two-dimensional reciprocal space is tiled up in a $nkx \times nky$ array. At each point of the array it calculates the instensity of four beams interfering there. These four beams are: (a) The first kind reference wave (calculated by the *reference* subroutine in line 86), (b) the second kind reference wave (calculated by the subroutine *reference_ primej* in line 93), (c) the first kind and (d) the second kind object waves (calculated by subroutines *objectj* and *object_primeji* in lines 97 and 106 respectively). The algorithm followed by the program has the form:

```
FOR ALL POINTS IN THE RECIPROCAL SPACE
      CALCULATE THE REFERENCE WAVE (REF)
      FOR EACH ATOM j OF THE CLUSTER
   CALCULATE THE SECOND REFERENCE WAVE (REFP)
   CALCULATE THE OBJECT WAVE (OBJ)
   CALCULATE THE SECOND OBJECT WAVE (OBPJ)
```

```
                  ADD THEM ALL UP (P = REF + REFP + OBJ + OBPJ)

     CALCULATE THE INTENSITY

     END
```

In line 117 the program determines the maximum value the calculated intensity has and uses it in line 123 to normalize the entire pattern.

A sample of the typical output is given in (B.5).

B.2   The code

```
 1   ccccccccccccccccccccccccccccccccccccccccccccccccccccccccccccccc

 2         PROGRAM Simple DLeeD

 3   ccccccccccccccccccccccccccccccccccccccccccccccccccccccccccccccc

 4   c     Author: John A. Vamvakas

 5   c     Author started writting it on: Thurday, August 22, 1996

 6   c     Last modification: Tuesday, November 26, 1996

 7   c     NOTE:   Dr. Xiang Chen helped the author with a number

 8   c         of useful observations. His contribution is

 9   c             greatly appreciated.

10   ccccccccccccccccccccccccccccccccccccccccccccccccccccccccccccccc

11         parameter(engy=0.0000)

12         parameter(NN=0)

13         parameter(NATO=5,num=30,lmax=9)

14         parameter(nkx=81,nky=81,dk=0.16698)
```

```fortran
15        parameter(pi=3.1415926535897931)

16        parameter(theta=3.*pi/4.,fi=0.0)

17        parameter(ik=8,ij=0)

18

19        character*70 dummy

20        complex ci,p,ref,refp,refpj,ob,obj,obp,obpji

21        complex del_ad(num,0:lmax+1),del_sb(num,0:lmax+1)

22        real ps_r(0:lmax+1),hankl(0:lmax),lgn_pl(0:lmax+1)

23        real kx,ky,k,k0x,k0y,k0z,k_prll

24        real pinte(nkx,nky),cluster(300,100)

25

26        ci=(0.0,1.0)

27

28  c Reads in cluster data from channel 4 (file: "cluster")

29

30        open(4,file="cluster",status="old")

31        do i = 1,11

32          read(4,3)dummy

33        enddo

34        read(4,1)or_id,or_x,or_y,or_z

35        do i=1,NATO

36          read(4,2)(cluster(i,j),j=1,7)

37        enddo
```

```fortran
38        close(4)

39

40  c Reads in phase shifts for substrate (atom type 2 in file
41  c "cluster") from channel 8 (file: "ps.sub")

42

43        open(8,file="ps.sub",status="old")
44        read(8,*)im

45

46  c Reads in phase shifts for adsorbate (atom type 1 in file
46  c "cluster") from channel 9 (file: "ps.ads")

48

49        open(9,file="ps.ads",status="old")
50        read(9,*)im

51

52        do n = 1,num
53           read(9,15)energy_ads,(ps_r(i),i=0,lmax)
54  do i=0,lmax
55    del_ad(n,i)=ps_r(i)+ci*0.0
56  enddo
57  read(8,15)energy_sub,(ps_r(i),i=0,lmax)
58  do i=0,lmax
59    del_sb(n,i)=ps_r(i)+ci*0.0
60  enddo
```

```
61          enddo

62

63  1       format(i5,f14.5,f10.5,f10.5)

64  2       format(i5,f14.5,f10.5,f10.5,f8.3,f6.1,i5)

65  3       format(a61)

66  15      format(6e12.5)

67          close(9)

68          close(8)

69

70

71          pmax=0.0

72          k = sqrt(2.*engy)

73          k0x = k*sin(theta)*cos(fi)

74          k0y = k*sin(theta)*sin(fi)

75          k0z = sqrt(k**2-k0x**2-k0y**2)

76          do iky = 1,nky

77            ky = dk*(iky-(nky-1)/2-1)

78           do ikx = 1,nkx

79             kx = dk*(ikx-(nkx-1)/2-1)

80             k_prll = sqrt(kx**2+ky**2)

81             ref = (0.0,0.0)

82             refp = (0.0,0.0)

83             ob = (0.0,0.0)
```

```fortran
84              obp = (0.0,0.0)
85              if (k_prll.le.k) then
86                call reference(lmax,engy,num,NN,del_ad,ref,
87      &                  k,kx,ky,k0x,k0y,k0z,lgn_pl,hankl)
88              do j = 1,NATO
89                 xj = cluster(j,2)
90                 yj = cluster(j,3)
91                 zj = -cluster(j,4)
92                 rj = cluster(j,5)
93                 call reference_primej(lmax,engy,num,NN,del_ad,
94      &                  del_sb,refpj,xj,yj,zj,rj,k,kx,ky,k0x,k0y,
95      &                  k0z,lgn_pl,hankl)
96                 refp = refp + refpj
97                 call objectj(lmax,engy,num,NN,del_ad,del_sb,
98      &                     obj,xj,yj,zj,rj,k,kx,ky,k0x,k0y,k0z,
99      &                     lgn_pl,hankl)
100                ob = ob + obj
101           do i = 1,NATO
102                  xi = cluster(i,2)
103                  yi = cluster(i,3)
104                  zi = -cluster(i,4)
105                  ri = cluster(i,5)
106  call object_primeji(lmax,engy,num,NN,del_ad,del_sb,
```

```fortran
107        &                  obpji,xj,xi,yj,yi,zj,zi,rj,ri,k,kx,ky,k0x,
108        &                  k0y,k0z,lgn_pl,hankl)
109                    obp = obp + obpji
110                  enddo
111                enddo
112              endif
113              p = ref + refp + ob + obp
114  c           p = ref + refp + ob
115  c           p = ref + ob
116              pinte(ikx,iky) = (cabs(p))**2
117              if (pinte(ikx,iky).ge.pmax) pmax = pinte(ikx,iky)
118            enddo
119          enddo
120          write(100,100)engy,theta,fi
121          write(100,101)ik,ij
122          do iky=1,nky
123            write(100,102)(pinte(ikx,iky)*990./pmax,ikx=1,nkx)
124          enddo
125          write(100,103)pmax
126  100     format(3f7.4)
127  101     format(2i3)
128  102     format(10f8.3)
129  103     format(e13.6)
```

```fortran
130

131       STOP

132       END ! PROGRAM Simple DLeeD

133 cccccccccccccccccccccccccccccccccccccccccccccccccccccccccccc

134 c                        SUBROUTINES                        c

135 cccccccccccccccccccccccccccccccccccccccccccccccccccccccccccc

136       subroutine reference(lmax,engy,num,NN,del_ad,ref,

137      &              k,kx,ky,k0x,k0y,k0z,lgn_pl,hankl)

138

139 c ''reference'' calculates the wave scattered off the adsorbate

140 c atom (Oxygen) in the form of spherical one. This information

141 c is borne by the atomic scattering factor ''f_ad'' calculated

142 c by the ''atosfac'' subroutine. ''10000.'' represents the

143 c distance of the sample from the detector and is arbitrary.

144 c The author chose this number to indicate that the distance

145 c between the sample and the detector compared to the

146 c interatomic ones within therein is infinate.

147

148       real engy,k,kx,ky,kz,k_prll,k0x,k0y,k0z,lgn_pl(0:lmax+1)

149       complex ci,del_ad(num,0:lmax+1)

150       complex ref,f_ad,hankl(0:lmax)

151

152       ci=cmplx(0.0,1.0)
```

```fortran
153

154          k_prll = sqrt(kx**2+ky**2)

155          kz = sqrt(k**2-k_prll**2)

156          costh = (kx*k0x+ky*k0y+kz*k0z)/(k**2)

157          call atosfac(costh,del_ad,engy,num,NN,f_ad,10000.,

158     &             lgn_pl,hankl,lmax)

159          ref = f_ad

160          return

161          end

162 cccccccccccccccccccccccccccccccccccccccccccccccccccccccccc

163          subroutine reference_primej(lmax,engy,num,NN,del_ad,

164     &       del_sb,refpj,xj,yj,zj,rj,k,kx,ky,k0x,k0y,k0z,

165     &       lgn_pl,hankl)

166

167 c ''reference_primej'' subroutine calculates the wave that has

168 c undergone one scattering off a substrate atom (Nickel) and

169 c another one off the adsorbate (Oxygen). These two

170 c scatterings appear through the ''f_sb'' and ''f_ad''.

171 c The term ''e_ik0rj'' contains the information about the

172 c phase difference between the wave traveling to the

173 c detector having been scattered off the adsorbate atom

174 c (the so-called reference wave) and this one.

175
```

```fortran
176        real engy,k,kx,ky,kz,k0x,k0y,k0z,k_prll,kdotr,k0dotr

177        real lgn_pl(0:lmax+1)

178        complex hankl(0:lmax)

179        complex ci,del_ad(num,0:lmax+1),del_sb(num,0:lmax+1)

180        complex refpj,f_ad,f_sb,e_ikrj,e_ik0rj

181

182        ci=cmplx(0.0,1.0)

183

184        k_prll = sqrt(kx**2+ky**2)

185        kz = sqrt(k**2-k_prll**2)

186        kdotr = xj*kx+yj*ky+zj*kz

187        k0dotr = xj*k0x+yj*k0y+zj*k0z

188        e_ikrj = cexp(ci*k*rj)

189        e_ik0rj = cexp(ci*k0dotr)

190        costh_s = k0dotr/(k*rj)

191        costh_a = kdotr/(k*rj)

192        call atosfac(costh_a,del_ad,engy,num,NN,f_ad,rj,
193      &          lgn_pl,hankl,lmax)

194        call atosfac(costh_s,del_sb,engy,num,NN,f_sb,rj,
195      &          lgn_pl,hankl,lmax)

196        refpj = f_ad*f_sb*(e_ikrj/rj)*e_ik0rj

197        return

198        end
```

```fortran
199   ccccccccccccccccccccccccccccccccccccccccccccccccccccccccccccccc

200         subroutine objectj(lmax,engy,num,NN,del_ad,del_sb,obj,

201        &          xj,yj,zj,rj,k,kx,ky,k0x,k0y,k0z,lgn_pl,hankl)

202

203   c ``objectj'' calculates the wave that (having been scattered off

204   c the adsorbate atom first) scatters off the substrate atom.

205   c The ``e_ikr'' is the phase difference between the refernce wave

206   c and this one.

207

208         real engy,k,k_prll,kx,ky,kz,k0x,k0y,k0z,kdotr

209         real lgn_pl(0:lmax+1)

210         complex hankl(0:lmax)

211         complex ci,del_ad(num,0:lmax+1),del_sb(num,0:lmax+1)

212         complex obj,f_ad,f_sb,e_ik0rj,e_ikdotr

213

214         ci=cmplx(0.0,1.0)

215

216         k_prll = sqrt(kx**2+ky**2)

217         kz = sqrt(k**2-k_prll**2)

218         kdotr = xj*kx+yj*ky+zj*kz

219         e_ik0rj = cexp(ci*k*rj)

220         e_ikdotr = cexp(-ci*kdotr)

221         costh_s = kdotr/(k*rj)
```

```fortran
222          costh_a = (xj*k0x+yj*k0y+zj*k0z)/(k*rj)
223          call atosfac(costh_a,del_ad,engy,num,NN,f_ad,rj,
224      &            lgn_pl,hankl,lmax)
225          call atosfac(costh_s,del_sb,engy,num,NN,f_sb,rj,
226      &            lgn_pl,hankl,lmax)
227          obj = f_ad*f_sb*(e_ik0rj/rj)*e_ikdotr
228          return
229          end
230 cccccccccccccccccccccccccccccccccccccccccccccccccccccccccccccccc
231          subroutine object_primeji(lmax,engy,num,NN,del_ad,del_sb,
232      &              obpji,xj,xi,yj,yi,zj,zi,rj,ri,k,kx,ky,
233      &              k0x,k0y,k0z,lgn_pl,hankl)
234
235          real engy,k,kx,ky,kz,k0x,k0y,k0z,k_prll
236          real kdotri,k0dotrj
237          real lgn_pl(0:lmax+1)
238          complex hankl(0:lmax)
239          complex ci,del_ad(num,0:lmax+1),del_sb(num,0:lmax+1)
240          complex obpji,f_ad,f_si,f_sj,e_ikrj,e_ik0rj,e_ikri
241          complex e_ik0dotrj,e_ikdotri
242
243          ci=cmplx(0.0,1.0)
244
```

```fortran
245        k_prll = sqrt(kx**2+ky**2)

246        kz = sqrt(k**2-k_prll**2)

247        k0dotrj = k0x*xj+k0y*yj+k0z*zj

248        kdotri = kx*xi+ky*yi+kz*zi

249        ridotrj = xi*xj+yi*yj+zi*zj

250        costh_sj = k0dotrj/(k*rj)

251        costh_si = kdotri/(k*ri)

252        costh_a = ridotrj/(ri*rj)

253        e_ikrj = exp(ci*k*rj)

254        e_ikri = exp(ci*k*ri)

255        e_ik0dotrj = exp(ci*k0dotrj)

256        e_ikdotri = exp(-ci*kdotri)

257        call atosfac(costh_a,del_ad,engy,num,NN,f_ad,ri,

258     &           lgn_pl,hankl,lmax)

259        call atosfac(costh_sj,del_sb,engy,num,NN,f_sj,rj,

260     &           lgn_pl,hankl,lmax)

261        call atosfac(costh_si,del_sb,engy,num,NN,f_si,ri,

262     &           lgn_pl,hankl,lmax)

263        obpji = f_ad*f_si*f_sj*(e_ikrj/rj)*(e_ikri/ri)*

264     &           e_ik0dotrj*e_ikdotri

265      return

266      end

267 cccccccccccccccccccccccccccccccccccccccccccccccccccccccccccccccccc
```

```fortran
268          subroutine atosfac(costh,del,engy,num,NN,f,r,
269     &                    lgn_pl,hankl,lmax)
270
271  c ``atosfac'' calculates the
272  c atomic scattering factors. ``lgn_pl'' and ``hankl'' stand
273  c for Legandre Polynomials and coefficient Hankel Functions
274  c respectively. ``costh'' is the cosine of the angle of
275  c scattering. ``del'' is the phase shift.
276  c ``engy'' is the energy of the incident electron.
277  c ``f'' is the scattering factor given out by the subroutine.
278  c ``r'' is the distance the electron travels before its next
279  c scattering or before it reaches the detector.
280
281          real engy,lgn_pl(0:lmax+1),k
282          complex ci,f,del(num,0:lmax+1),hankl(0:lmax)
283
284          ci=cmplx(0.0,1.0)
285
286  c Calculate the Legendre polynomials
287
288          lgn_pl(0)=1.0
289          lgn_pl(1)=costh
290          do l=1,lmax-1
```

```fortran
291          pp=(2.0*float(l)+1.0)*lgn_pl(l)*lgn_pl(l)

292          qq=float(l)*lgn_pl(l-1)

293          lgn_pl(l+1)=(pp-qq)/(float(l)+1.0)

294       enddo

295

296  c Atomic scattering factor with coefficient of the Hankel

297  c function

298

299       hankl(0)=(1.0,0.0)

300       k=sqrt(2.*engy)

301       hankl(1)=1.+ci/(k*r)

302       do l=1,lmax-1

303          hankl(l+1)=hankl(l-1)+float(2*l+1)*ci/(k*r)

304     &          *hankl(l)

305       enddo

306

307  c Atomic scattering factor

308

309       f=(0.0,0.0)

310       do l=0,lmax

311          f=f+(2*l+1)*cexp(ci*del(NN,l))*sin(del(NN,l))

312     &           *lgn_pl(l)*hankl(l)

313       enddo
```

```
314        f=f/k

315        return

316        end
```

B.3   The atoms coordinates input file

```
1      =============================================================

2      I.D; 1-Adsorbate, 2-Substrate

3      r(au) = sqrt(x**2 + y**2 +x**2)

4      r(A) = r(au) * 0.529

5      theta = (from topview) the angle between the +x axis and

6        the line connecting the atom type 1 and atom

7        type 2. Atom type 1 sits at the center of the

8        coordinate system.

9      =============================================================

10     I.D        x(au)      y(au)      z(au)    r(au)   r(A)   theta

11     =============================================================

12      1        0.00000   0.00000   0.00000

13      2        2.35177   2.35177   1.54958   3.669   1.9    45

14      2       -2.35177  -2.35177   1.54958   3.669   1.9   225

15      2       -2.35177   2.35177   1.54958   3.669   1.9   135

16      2        2.35177  -2.35177   1.54958   3.669   1.9   315
```

B.4 Phase shifts input file sample

Each set of phase shifts comprises two lines. The first number of the first line indicates the energy in *Hartrees*. The rest are the phase shifts for angular momenta $\ell = 0, 1, 2, \cdots, 10$.

```
0.73500E+00 0.11172E+01 0.14147E+01 0.13700E-01 0.40000E-03 0.00000E+00
0.00000E+00 0.00000E+00 0.00000E+00 0.00000E+00 0.00000E+00 0.00000E+00
0.91880E+00 0.10080E+01 0.15840E+01 0.23000E-01 0.80000E-03 0.00000E+00
0.00000E+00 0.00000E+00 0.00000E+00 0.00000E+00 0.00000E+00 0.00000E+00
0.11025E+01 0.91540E+00 0.16643E+01 0.34800E-01 0.15000E-02 0.00000E+00
0.00000E+00 0.00000E+00 0.00000E+00 0.00000E+00 0.00000E+00 0.00000E+00
0.12863E+01 0.83460E+00 0.17018E+01 0.49200E-01 0.24000E-02 0.10000E-03
0.00000E+00 0.00000E+00 0.00000E+00 0.00000E+00 0.00000E+00 0.00000E+00
0.14700E+01 0.76280E+00 0.17174E+01 0.66100E-01 0.37000E-02 0.20000E-03
0.00000E+00 0.00000E+00 0.00000E+00 0.00000E+00 0.00000E+00 0.00000E+00
0.16538E+01 0.69800E+00 0.17212E+01 0.85100E-01 0.53000E-02 0.30000E-03
0.00000E+00 0.00000E+00 0.00000E+00 0.00000E+00 0.00000E+00 0.00000E+00
0.18376E+01 0.63910E+00 0.17184E+01 0.10620E+00 0.73000E-02 0.40000E-03
0.00000E+00 0.00000E+00 0.00000E+00 0.00000E+00 0.00000E+00 0.00000E+00
0.20213E+01 0.58500E+00 0.17118E+01 0.12910E+00 0.98000E-02 0.60000E-03
0.00000E+00 0.00000E+00 0.00000E+00 0.00000E+00 0.00000E+00 0.00000E+00
0.22051E+01 0.53510E+00 0.17030E+01 0.15340E+00 0.12600E-01 0.90000E-03
0.00000E+00 0.00000E+00 0.00000E+00 0.00000E+00 0.00000E+00 0.00000E+00
```

```
0.23888E+01 0.48870E+00 0.16932E+01 0.17890E+00 0.16000E-01 0.12000E-02
```

....

....

....

B.5   Sample of a typical output

The first line contains information about the energy in *Hartrees* (first number) and the angles of incidence (θ and ϕ). The next line idicates the usage of 8×8 grid of data per Brillouin zone. The body of the output contains the intensities that are written out as arrays of 81×81 (81 groups of 81 intensities per group). The last line gives the maximum intensity.

```
 2.5726 2.3562 0.0000

  8   0
```

....

....

....

```
0.000    0.000    0.000    0.000    0.000    0.000    0.000    0.000    0.000    0.000

0.000    0.000    0.000    0.000    0.000    0.000    0.000    0.000    0.000    0.000

0.000    0.000    0.000    0.000    0.000    0.000    0.000    0.000    0.000    0.000

0.000    0.000    0.000 491.468 437.913 328.743 236.230 186.085 173.245 178.377

182.626 178.377 173.245 186.085 236.230 328.743 437.913 491.469   0.000    0.000

0.000    0.000    0.000    0.000    0.000    0.000    0.000    0.000    0.000    0.000

0.000    0.000    0.000    0.000    0.000    0.000    0.000    0.000    0.000    0.000

0.000    0.000    0.000    0.000    0.000    0.000    0.000    0.000    0.000    0.000

0.000
```

```
0.000 0.000    0.000    0.000    0.000    0.000    0.000    0.000    0.000    0.000

0.000 0.000    0.000    0.000    0.000    0.000    0.000    0.000    0.000    0.000

0.000 0.000    0.000    0.000    0.000    0.000    0.000    0.000    0.000    0.000

0.000 668.060 832.539 712.252 489.275 293.272 192.238 196.470 269.379 350.169

384.326 350.169 269.379 196.470 192.238 293.272 489.275 712.252 832.539 668.060

0.000    0.000    0.000    0.000    0.000    0.000    0.000    0.000    0.000    0.000

0.000    0.000    0.000    0.000    0.000    0.000    0.000    0.000    0.000    0.000

0.000    0.000    0.000    0.000    0.000    0.000    0.000    0.000    0.000    0.000

0.000

.............................................................

.............................................................

.............................................................

0.479733E+00
```

B.6 The C-shell script

This script has been developed to automatize the feeding of the main program with energies.

```
1  #!/usr/bin/csh

2  #

3  set old_eng = 0.0000

4  @ old_indx = 0

5  @ indx = 1

6  foreach energy (energy1 energy2 ... energyeng 0.0000)

7          ex - dld2.f << EOF
```

```
 8         12s/$old_eng/$energy

 9         13s/$old_indx/$indx

10          w

11          q

12  EOF

13  set old_eng = "$energy"

14  f77 dld2.f

15  a.out

16  /usr/bin/mv fort.100 fort.$indx

17  @ old_indx = $indx

18  @ indx++

19  if ($indx > 37) then

20     @ indx = 0

21  endif

22  end
```

John A. Vamvakas

Title of Dissertation

Holographic LEED: A direct method for surface crystallography

Place and Date of Birth

Piraeus, Greece,   December 16, 1963

Degrees

University of Wisconsin-Milwaukee,   1994, M.S.

University of Patras, Greece,   1987, B.S.

Publications

- **Holographic LEED: A review of recent progress**, D.K. Saldin, X. Chen, J.A. Vamvakas, M. Ott, H. Wedler, K. Reuter, K. Heinz and P.L. de Andrés; *Surface Review Letters*, **4**, 991 (1997). Invited paper, Proc. 5th International Conference on the Structure of Surfaces, Aix-en-Provence, France, July 1996.

- **Influence of the data base and algorithmic parameters on the image quality in holographic diffuse LEED**, K. Reuter, H. Wedler, M. Ott, K. Heinz, J. A. Vamvakas, X. Chen and D.K. Saldin, *Physical Review B*, **55**, 5344 (1997).

- **Holographic methods for X-ray and electron crystallography**, D.K. Saldin, V.L. Shneerson, J.A. Vamvakas and D.L. Wild, *Micron*, **55**, 321 (1997).

- **Extending DLEED holography to small ordered superstructures: modifications and limits**, K. Reuter, J.A. Vamvakas, D.K. Saldin, V. Blum, M. Ott, H. Wedler, R. Döll and K. Heinz, *Physical Review B*, in press.

- **Holographic electron diffraction from surfaces: conjuring 3D atom images from Bragg spots**, K. Reuter, M. Ott, V. Blum, H. Wedler, K. Heinz, J.A. Vamvakas and D.K. Saldin, *Science*, to be submitted.

Presentations

- Presentation on "Reconstruction of atomic adsorption sites on surfaces by holographic LEED" on American Physical Society 1996 March Meeting, Saint Louis, Missouri

- Oral presentation in "Holographic LEED: A Direct Method for Surface Crystallography" on UWM Laboratory of Surface Science 3rd Annual Student Symposium, April 27, 1996, University of Wisconsin-Milwaukee

- Oral presentation on "Influence of the date base algorithmic parameters on the image quality in holographic diffuse LEED" on American Physical Society 1997 March Meeting, Kansas City, Missouri

- Presentation on "Holographic reconstruction of atomic adsorption sites from fractional-order LEED spots" on American Physical Society 1998 March Meeting, Los Angeles, California

- Poster on "Holographic LEED: A Direct Method for Surface Crystallography" on Microscopy of Surfaces and Interfaces; April 26, 1996, UWM, Milwaukee, Wisconsin

Professor Dilano Kerzaman Saldin   Date